TU Delft

Master Thesis

Efficient Support structure design for variation of environmental parameters within an offshore windfarm

Author:
Anirudha Pandit
Student No: 4234529

Supervisor:
Dr. Ir. Michiel Zaayer

Applied Science
Sustainable Energy Technology
Delft University of Technology

28-Aug-2014

TU Delft Delft University of Technology

Delft University of Technology
Department of
Aerospace Engineering

The undersigned hereby certify that they have read and recommend to the Faculty of Applied Sciences (TNW) for acceptance a thesis entitled

Efficient Support structure design for variation of environmental parameters within an offshore windfarm

by

Anirudha Pandit

in partial fulfillment of the requirements for the degree of
Master of Science Sustainable Energy Technology

Supervisor:	Dr. ir. Michiel Zaayer
Readers:	Prof. dr. Gerard van Bussel
	Dr. ir. Niels Diepeveen

Abstract

The offshore wind industry is growing fast, but the cost of wind energy is still high. There is a need for improvement in several areas. One of them is support structure cost. This cost can be reduced if support structures are designed tailored to their local environment. The thesis focuses on the development of simplified procedure to design multiple support structures for a wind farm.

Within the thesis, the offshore wind support structure design process is studied. From this study, important design steps are listed out and simplification is carried out for those steps. The simplification is carried out for the IEC design load cases, natural frequency, grout length, penetration length, yielding and buckling constraints. To implement the simplified models, a Python based design tool is improved. In the simplified design process data obtained form the reference location design is used to design other support structures of the wind farm. The simplified design is carried out only for the main design drivers which are obtained from the reference location. As dimensions obtained from the simplified design are not same as detailed design, a method of correction factors is employed to obtain the final dimensions of the support structures.

The effectiveness of the simplified process is tested by performing a case study and by analysis of its response to the changes in environmental parameters. The absolute accuracy is in the range of 0-6%. This is found to be sufficient to support the accuracy of the simplified design process.

Acknowledgement

I would like to express my gratitude towards some people who have helped me and without their assistance this thesis would not have been possible.

I consider myself fortunate to have Dr. ir. Michiel Zaayer as my supervisor. Without his support, attention and guidance I would not have achieved what I have achieved. I have learned a lot form you. The bi-weekly meetings and valuable discussions have helped me to tailor my work and report. Your endless devotion in providing feedback helped me to bring this thesis to a higher level.

Furthermore, I would like to thank Prof. dr. Gerad J.W. van Bussel and Dr. ir. Bierbooms for their support, guidance and detailed comments and discussions during the thesis work and intermediate progress meeting. I am grateful towards Dr. E. Lourens for helping me to solve Ansys problems. I am thankful to Dr. Niels Diepeveen for accepting my request and valuable discussion.

I would like to thank my friends for their enthusiasm and help during the thesis period. Finally, I would like to thank my family for supporting me to achieve my goal.

Contents

List of Figures

List of Tables

Abbreviations

ALS	Accidental Limit State
API	American Petroleum Institute
BEM	Blade Element Momentum
DLC	Design Load Cases
DNV	Det Norske Veritas
DUWIND	Delft University Wind Energy Research Department
EWEA	European Wind Energy Association
ECM	Extreme Current Model
ECD	Extreme Coherent gust with Direction change
EDC	Extreme Direction Change
EOG	Extreme Operating gust
ESS	Extreme Sea State
ETM	Extreme Turbulence Model
EWLR	Extreme Water Level Range
EWH	Extreme wave height
EWM	Extreme Wind Model
EWS	Extreme Wind Shear
FEM	Finite Element Method
FLS	Fatigue Limit State
GL	Germanischer Llyod
GROW	Grouted Joints for Offshore Wind Turbine Structures
GUI	Graphical User Interface
GWEC	Global Wind Energy Council
IEC	International Electrotechnical Commission
JIP	Joint Industry Project

KC	Keulegan-Carpenter
LPC	Levelised Production Cost
MSL	Mean Sea Level
NDM	Non Dimensional Model
NCM	Normal Current Model
NSS	Normal Sea State
NTM	Normal Turbulence Model
NWLR	Normal Water Level Range
NWH	Normal Wave Height
NWP	Normal Wind Profile
OOFEIA	OFELIA Offshore Foundations Environmental Impact Assessments
RWH	Reduced wave height
RNA	Rotor Nacelle Assembly
SSS	Severe Sea State
SWH	Severe Wave Height
SLS	Serviceability Limit State
SCF	Stress Concentration Factors
ULS	Ultimate Limit State
VOWS	Violent Overtopping by Waves at Seawalls

Chapter 1

Introduction

1.1 Wind energy

For the last 150 years fossil fuels have been used as a primary supply of energy. Resources of fossil fuels are limited on human time scale and are depleting at a faster rate than ever before. The energy consumption of the world is projected to increase by 56% by 2040 [8], mostly because of the increasing demand from developing countries like India, China and Brazil and increase in the population growth. Current proven coal, oil and gas reserves would only last for 112, 46 and 54 years respectively with the current rate of production [8]. Use of fossil fuels cause environmental hazards and negative effects on human health. Additionally, fossil fuels are non renewable on human time scale and their price depends upon the political stability in oil producing countries. Renewable energy not only conserves the environment but also makes countries energy independent. There is an urgent need for transition from fossil fuels to renewable energy.

At the end of the nineteenth century, the first electricity generating wind turbine was installed in Denmark. In the 1940, first megawatt capacity wind turbine was installed in the USA. The growth of wind energy has always fluctuated with the price of fossil fuels. But the 1970's oil crisis rekindled the interest in the wind energy and the concept of wind farm was introduced [9].

1.1.1 Wind energy development

Since the start of the 21^{st} century, use of wind energy is intensifying especially in Europe, USA, China and India. A size of the wind turbines has grown from 50 kW to 6 MW capacity. Increase in the capacity of wind turbines has also brought new engineering and design challenges. But it has also helped to reduced the Levelised Production Cost (LPC) of wind farms. Wind farms are generally divided into onshore and offshore, depending upon their location. According to GWEC [10] and EWEA [11] in the year 2012:

- Worldwide annual market and cumulative capacity growth of wind energy was 10% and 19% respectively
- Total worldwide installed capacity was 282,482 MW
- Wind energy in Denmark met 25.6% of total electricity consumption
- 5.3% of EU's electricity demand is provided by wind energy
- 192,000 jobs created in the EU alone and expected to generate 600,000 more jobs by 2020

The wind energy has met with public anger. Issues such as landscape pollution, noise pollution, flickering effects, bird deaths and subsidy from tax payer's money are some of the biggest concerns.

1.1.2 Offshore wind energy

Offshore wind energy can solve most of the problems faced by the wind energy industry. Higher and steadier energy production can be achieved because of the stronger and steadier winds. As offshore wind farms are away from residential areas, problems like noise pollution, visual disturbance and land availability can be avoided. But offshore wind farms have their own problems, such as harsh environment, higher loads on structures, large installation and maintenance costs. Despite of tough conditions, offshore wind energy is increasing rapidly. According to the report of EWEA [12]:

- 5GW of total capacity was installed in the EU by the end of 2012.

- 58000 jobs were created in 2012
- Offshore wind energy represents 10% of total wind energy installed (2012 end)
- By 2030, offshore wind capacity would reach 150GW meeting 14% of EU's electricity demand
- UK tops the offshore wind energy market with 458 MW installed capacity in 2012 followed by Denmark, Germany and Belgium

Growth in offshore wind energy is largely due to the EU requirement to meet renewable energy targets. As the offshore wind industry is gaining momentum, more and more wind farms are being built in deeper water depths. In 2012, average water depth and distance to shore for offshore wind farms were 22m and 29km respectively [1]. Fig. 1.1 gives better understanding of the current trend.

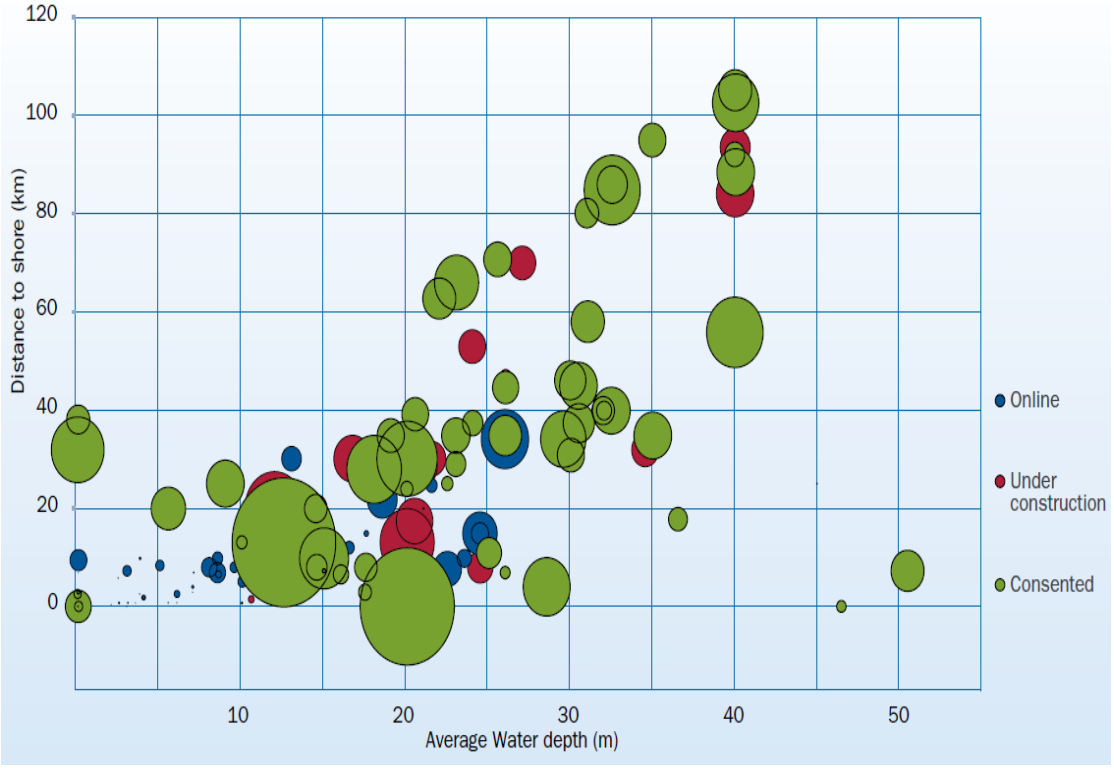

FIGURE 1.1: Average water depth and distance to shore for online, under construction and consented wind farms (Bubble size represents capacity of wind farm)[1]

Most of the developments are happening in the North Sea region, as it enjoys shallower water depths compared to other seas in the EU area. Fig. 1.2 gives percentage breakdown of consented wind farms by the sea basin.

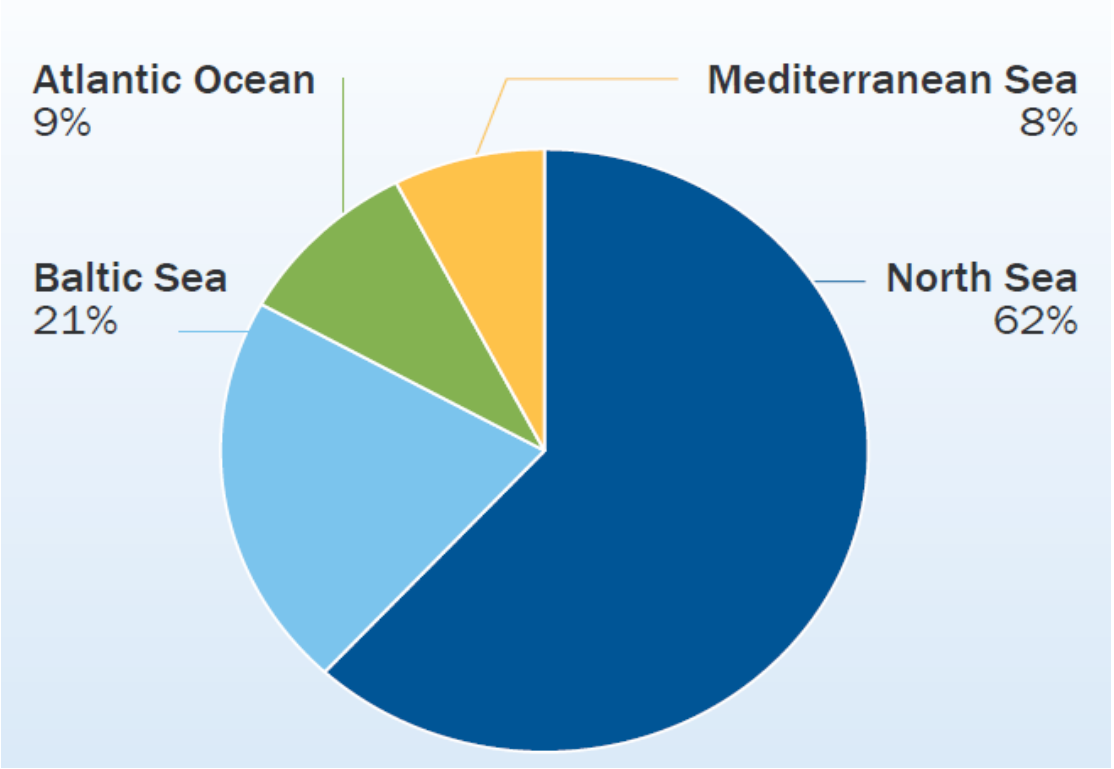

FIGURE 1.2: Share of consented wind farms by sea basin.[1]

1.1.3 Offshore support structures

During initial years, experience from the oil and gas sector was used to design and install offshore wind support structures. Various types of offshore support structures are available in the wind industry. Fig. 1.3 depicts support structures relevant to the offshore wind energy.

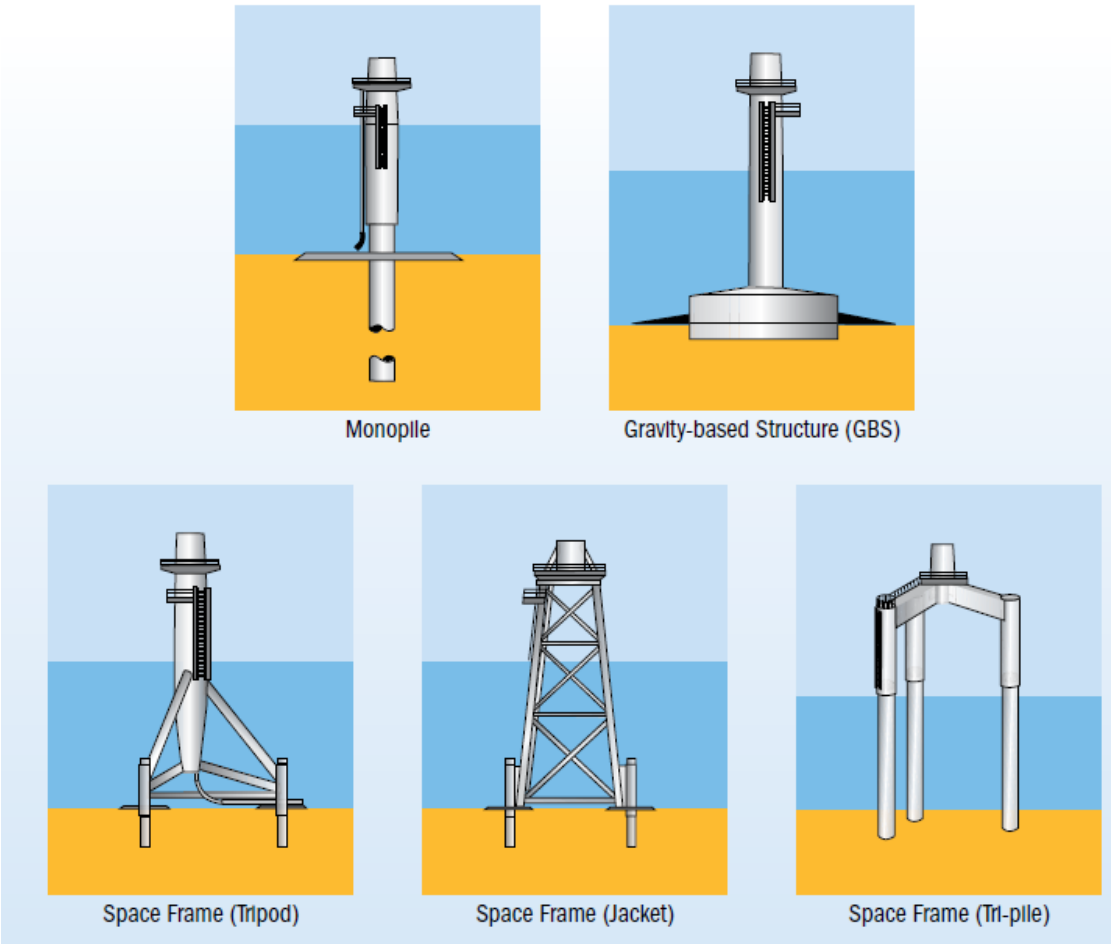

FIGURE 1.3: Offshore wind farm support structures.[1]

The monopile foundation is the most commonly used structure in the offshore wind industry. Main reason behind the use of monopile, is the ease of construction and installation. The monopile is also known as a foundation of the support structure. The transition piece connects the monopile and turbine tower. Fig. 1.4 shows the percentage market share and number of foundations installed for each support structure type.

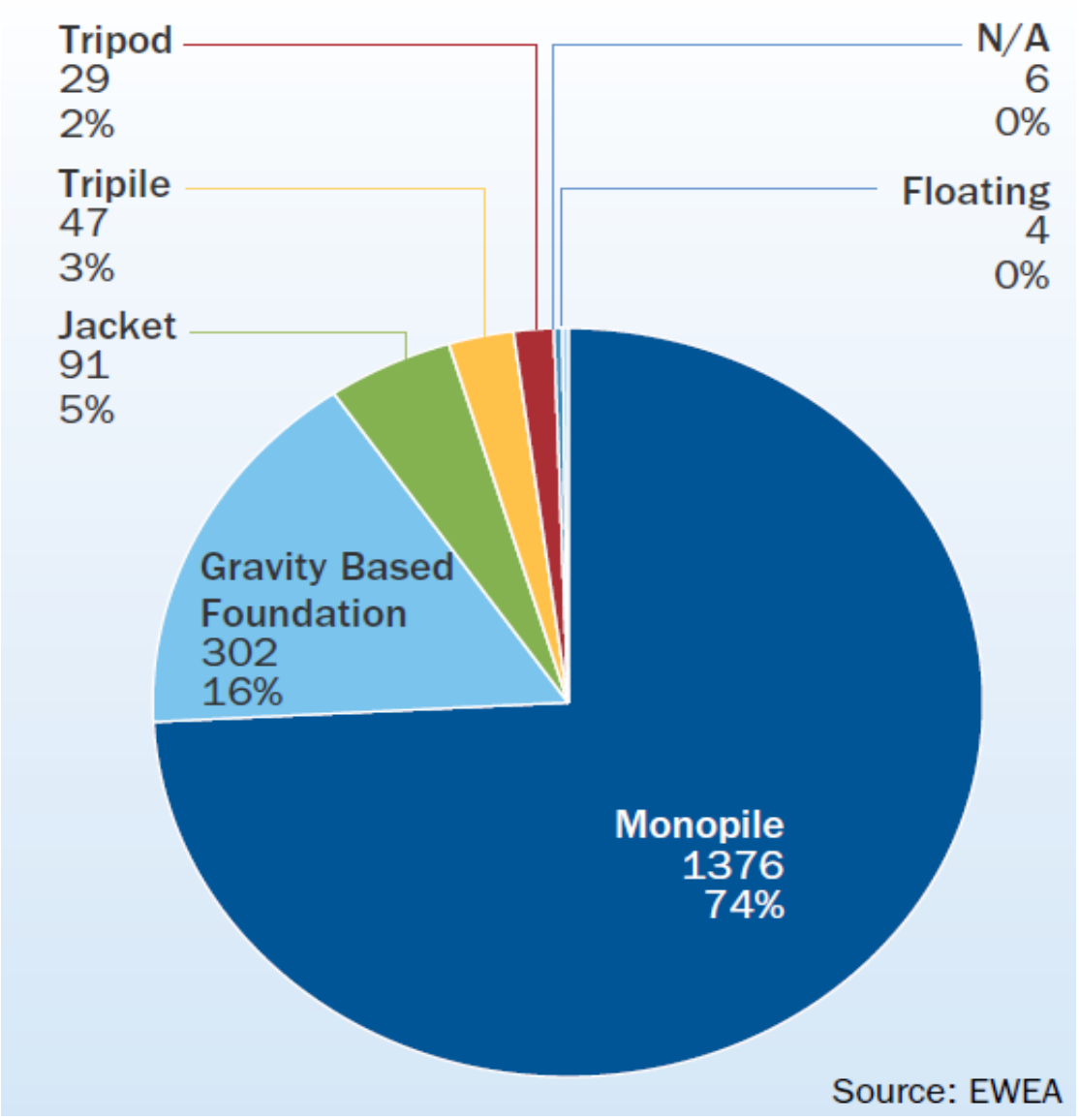

FIGURE 1.4: Share of support structures for wind farms at the end of 2012.[1]

Fig. 1.5 gives the overview of an offshore wind turbine with monopile as the support structure.

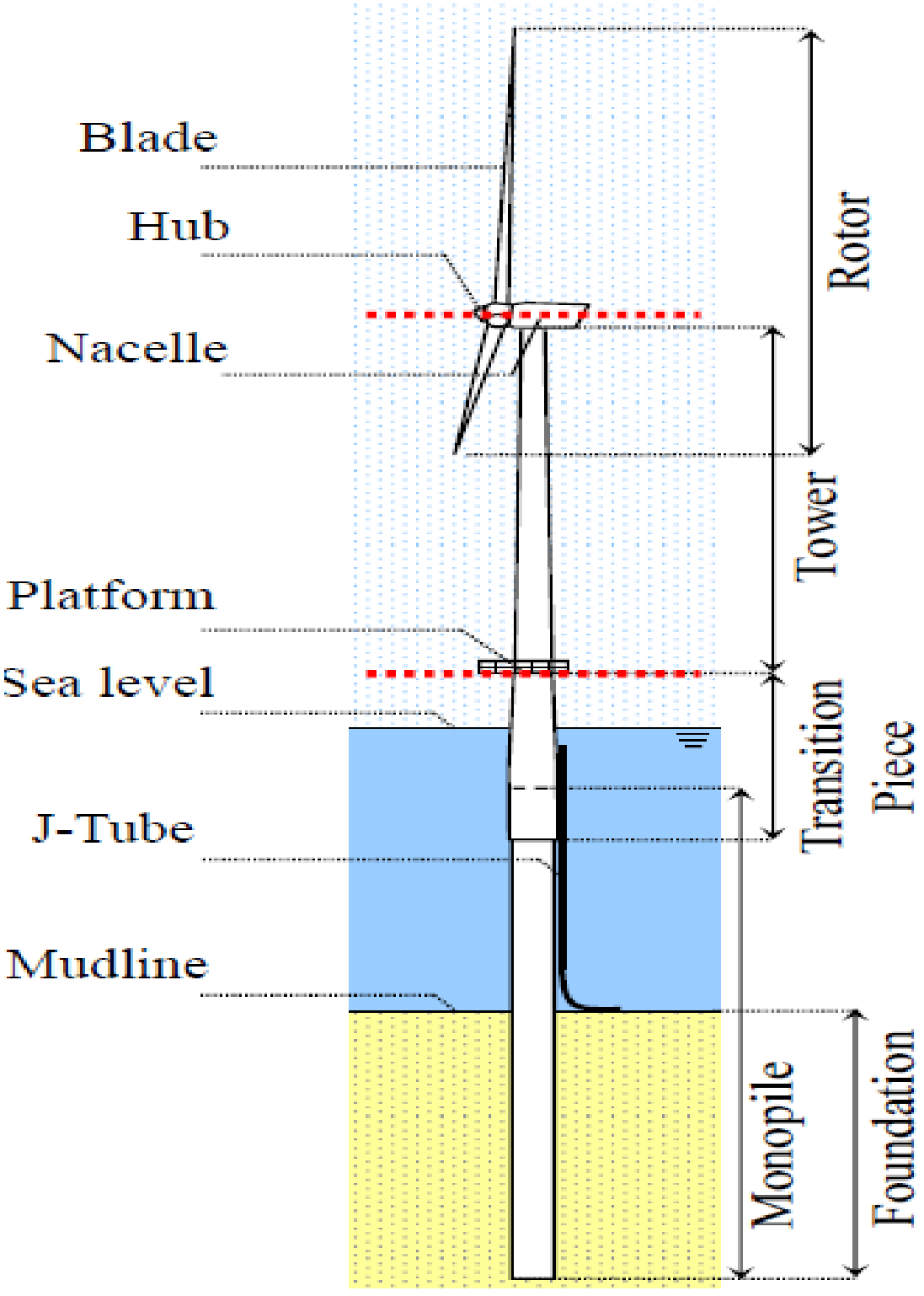

FIGURE 1.5: Monopile support structure nomenclature.[2]

1.2 Motivation

Main concerns for offshore wind farm developers are cost and time. The cost of a support structure is directly related to its mass and the time required to manufacture and install it. The support structure design is a very complex and time consuming process. Offshore wind farm developers design one or two support structures for an entire wind farm. This is due to the complexity of the design process. These support structures are designed for the largest possible loading conditions. The largest loads are experienced at the deepest water depth within the wind farm. To satisfy the structural stability of all wind turbines installed, all support structures have to be designed for the deepest water depth. This increases the total capital cost of the support structure.

Fig. 1.6 shows the capital cost breakdown of an offshore wind farm. The offshore support structure cost component is 27% of the total project cost. This cost can be reduced if individual support structures are tailored to the local environmental conditions for each wind turbine.

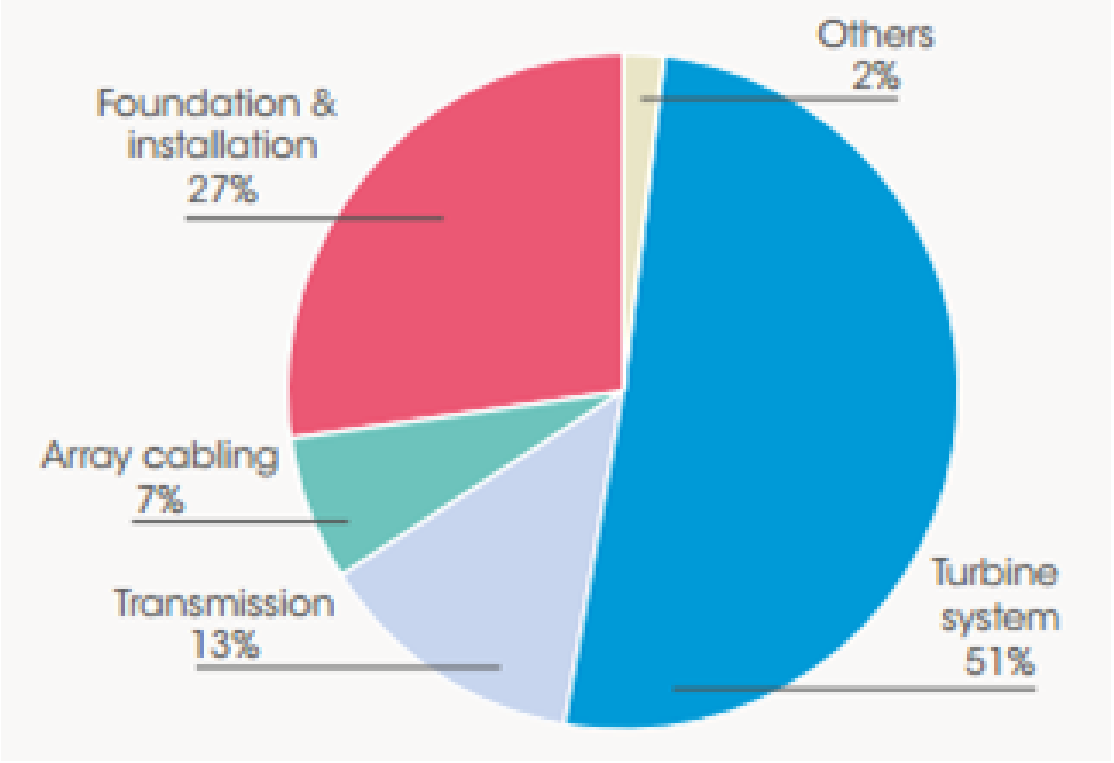

FIGURE 1.6: Capital cost breakdown of a large offshore wind farm.[3]

Each support structure is required to be certified. Various certification bodies are involved in this process ranging from international to national level. From the support structure design point of view "Project Certification" is very important [13]. The certification process needs to be kept in mind while designing the support structure. From Fig. 1.4 it is evident that most of the wind farms have employed monopiles as support structures. Most of the new consented wind farms are in water depths of 10-40m and will also employ monopile [14]. Therefore main focus of this study is on monopile support structures. Carrying out the design process for each support structure is a tedious task. Therefore there is a great need for the simplification of the design process. Main aim of the simplification process is to design multiple support structures for an entire offshore wind farm in minimum possible time. In order to explore this field, an MSc thesis project is defined within the wind energy research institute (DUWIND) of the Delft University of Technology. The certification process is kept in mind during the development of the simplified design process.

1.3 Thesis objective

Considering the interest and need of the project, the following objective can be defined: *"Develop a simplified design process for an offshore wind support structure with a monopile as a foundation unit, which uses results of the reference detailed design support structure to design the rest of the support structures of the wind farm."*

1.4 Approach

The aim of the thesis is to simplify a support structure design process to design multiple support structures within an offshore wind farm. The focus point of the thesis is the development, usefulness and practicality of the proposed method. Two basic activities are development and testing of the proposed technique. Studies from different disciplines are carried out to develop the new design method. These disciplines are offshore hydrodynamics, soil-structure interaction, structural mechanics and aerodynamics.

The followed approach can be broken down in five steps. First, a detailed study of the existing design process is carried out to understand the process. Then, from this

study a method is proposed to solve existing time consuming activities. The next step is concerned with the integration of multiple disciplines to develop a model for implementation of the proposed method. This is the most important step in the design process. Later, based on the previous step, a design tool is improved to implement and evaluate the proposed method. For this step, a design tool developed by Michiel is used as a base[15]. The last step is about conclusions from the evaluation of the existing method and recommendations for future work.

1.5 Scope of the thesis

Effort is made to incorporate all parts and design requirements of the support structure. However due to the limited availability of time, only important areas are covered. The list containing applicability and limitations of the thesis is given below:

- The thesis study is only valid for support structures having a monopile as a foundation unit
- The proposed simplification is not valid for the area with ice ridges or ice sheets
- The simplification is not carried out for secondary steels of the support structure
- The soil model is developed for sandy soils. The developed soil model is not applicable for areas prone to seismic activities and clay containing soil
- This study is useful for site specific design assessment of "Project Type" certification
- Simplification is carried out for the Ultimate Limit State (ULS), penetration length, grout stability and natural frequency analysis.
- Fatigue simplification is not performed

1.6 Organization of the report

This thesis is divided into six chapters. The thesis starts with the study of the support structure design procedure. Chapter 2 gives the detailed insight into the support

structure design. This chapter begins with the steps a designer needs to follow to design the support structure. Next, each step is described in detail and their importance from the designing point of view is explained. In Chapter 3, the improvements made in the Michiel's software in order to implement the simplification process are explained. This chapter also explains the constraints modelling and its application on the design variables, application of correction factors and selection of reference location.

In Chapter 4 simplified models of aerodynamic and hydrodynamic loading, IEC load cases, structural and grout stability, natural frequency, penetration length are explained. Assumptions made to achieve the simplification are also listed down in each section. Chapter 5 begins with the case study. The response of the simplification process to environmental variables is checked. Dimensions obtained from the simplified method and the detailed method are compared to asses the effectiveness of the simplified process. Conclusions and recommendations are discussed in the last chapter, Chapter 6.

Chapter 2

Detailed design Process of offshore wind support structure

2.1 Introduction

This chapter begins with the explanation of the support structure design process. Next, each step of the design process is explained in detail. Fig. 2.1 depicts the one of the possible ways of designing offshore wind turbine support structures. It is an iterative process.

The support structure design starts with the gathering of environmental data. The environmental data consists of wind data, met ocean data and soil data. The environmental data and the turbine data affect the support structure design most. The first step in the design process is to determine hub height and platform level of the support structure. These are determined using water level, wave height and rotor diameter data. The next important step is to determine the allowable natural frequency range for the support structure based on the turbine's rotational speed range and a wave spectrum. Based on this allowable natural frequency range, a target natural frequency is set with an appropriate safety margin. Based on the target natural frequency, diameter and the wall thickness of the support structure are calculated.

The transition piece internal diameter is calculated based on the monopile diameter and grout thickness. The turbine tower top diameter is constrained by the yaw bearing

diameter. The turbine tower is divided into different sections because of manufacturing limitations. The turbine tower thickness varies from bottom to top. With this geometry, extreme loads on the support structure are determined.

Using extreme load case, the penetration length of the foundation should be determined. For the offshore support structure both lateral and axial stability of the foundation should be checked. Generally, the lateral stability is the governing factor for the support structure penetration length [16]. Next, a structural stability check should be performed for the extreme load case. If the structural stability check fails, then the wall thickness of the support structure should be increased. The natural frequency will get affected with the increase in the thickness. A check should be performed for the natural frequency after changing the thickness. Before finalizing the design, a fatigue check should also be performed.

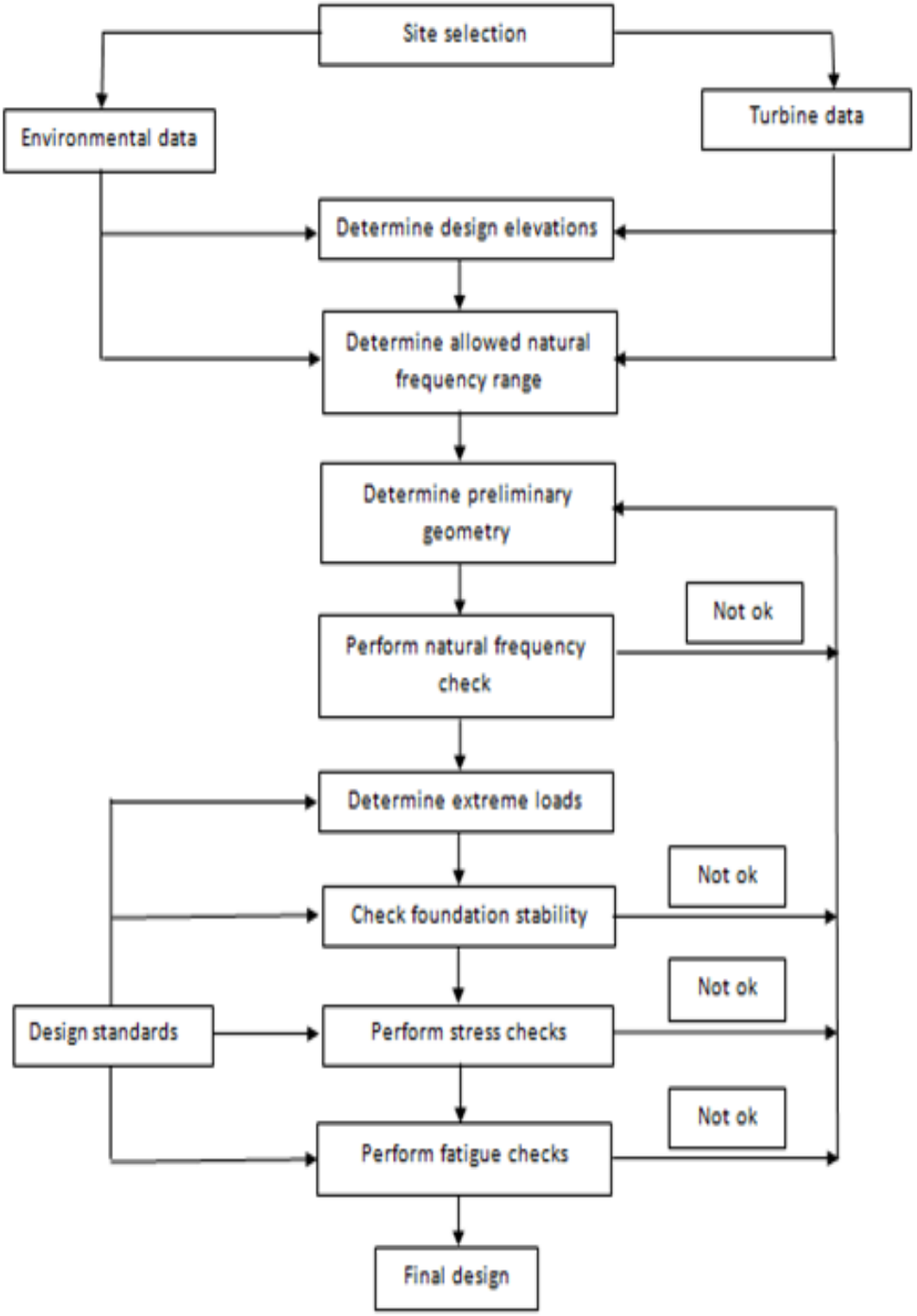

FIGURE 2.1: Offshore wind support structure design process.

2.2 Metocean data

Good quality metocean data is very important for the support structure design. This reduces uncertainties in the design process . The metocean data consists of the atmospheric temperature range, ice loading, wind, waves, currents, water level, salinity, water temperature range, marine growth, seismic activity, soil data, air and water densities, sea bed characteristics, shipping activities, existing and future pipeline and cables routes.

The atmospheric temperature range, salinity, water temperature range affect material properties over the years. Salinity causes corrosion in the structure which decreases its load carrying capacity. Changes in temperature levels causes thermal stresses in the structure. This affects the ULS and fatigue life of the structure. Wind, wave and current values and directions determine the extreme hydrodynamic loading on the structure and fatigue damage. The marine growth, J-tube, anodes add extra axial load and also increase the effective diameter of the monopile which eventually increases the hydrodynamic loading. Increase in the diameter and roughness of the cylinder cause vortex formation at lower Reynold's number where normally no vortex shedding occurs [17]. The axial and floating ice loading contribute to axial and lateral loads respectively and influence the aerodynamic drag coefficient. Water levels determine the platform level. Soil data is important for the foundation stability. The penetration length of the foundation depends on the soil properties [5].

2.3 Wind turbine

A turbine plays the important role in the support structure design. From the design point of view turbine capacity, rotor diameter, Rotor Nacelle Assembly (RNA) mass and eccentricity, operational rotor speed, turbine tower dimensions and mass are important parameters. The turbine capacity influences the maximum thrust force. RNA mass and eccentricity, turbine tower dimensions and mass play an important role in the natural frequency calculation of the support structure. The eccentricity of the RNA mass gives additional moment on the support structure. The operational rotor speed of the turbine determines the 1P and 3P frequency range. The rotor diameter is used in the hub height calculation. The control system determines the response of the turbine to wind speed and direction variation.

2.4 Design elevations

The first step in the design process of the support structure is to determine the hub height and platform level. Based on the environmental data, turbine data and regional government requirements, platform and hub height are determined. Both, the platform and hub height are important from the design process perspective. The thrust load and aerodynamic moment are dependent on the hub height. The boat landing and flange connection between turbine tower and transition piece are located at the platform level. The platform height should be sufficient to avoid slamming forces from the waves.

The hub height is determined by the platform level, blade clearance and rotor diameter. The blade clearance is the distance between the platform and the lowest position of a blade tip. This distance should be sufficient to allow safe access to the platform for personnel and equipment and can also depend upon local regulations. The center of gravity of the nacelle mass is dependent on the hub height. It has an impact on the natural frequency of the structure and should be determined in the beginning of the design process. Fig. 1.5 indicates the various design levels for a monopile support structure.

2.5 Natural frequency

The natural frequency of the support structure has major effect on its dynamic behavior. If the natural frequency of the support structure is near the excitation frequency, the structure will undergo resonance. This causes higher stresses in the support structure which affects the structural stability. Therefore, it is importance to have natural frequency of the support structure different from the excitation frequencies. The support structure gets excited by wave energy and rotational frequencies of wind turbine, 1P and first several frequencies that are multiples of the number of rotor blades. For example, three bladed turbine, 3P, 6P, 9P...are important from structural desin point of view. For two bladed turbine these are 2P, 4P, 6P ....etc. For three bladed turbine 1P and 3P frequency ranges are represented by boxes in Fig. 2.2. The wave energy spectrum is represented by a curve in the diagram. The first natural frequency of the offshore wind turbine is represented by a straight line. The objective is to avoid the natural frequency of the support structure from coinciding with 1P, 3P range and wave energy spectrum.

The structure is known as a stiff-stiff, soft-stiff and soft-soft if its natural frequency is higher than 3P, in between 1P and 3P and lower than 1P respectively. The natural frequency of the support structure should not be in the soft-soft region as the wave energy spectrum is present in the soft-soft region and the structure will also have large deflections. For the support structure to have natural frequency in the stiff-stiff region, it is required to make it too bulky which is not economical. The best design option is to have natural frequency of the support structure in the soft-stiff region [18] [5][19]. The natural frequency of the support structure should be kept near the lower bound of the soft-stiff range. This is recommended so as to achieve structural stability with the minimum mass of the support structure.

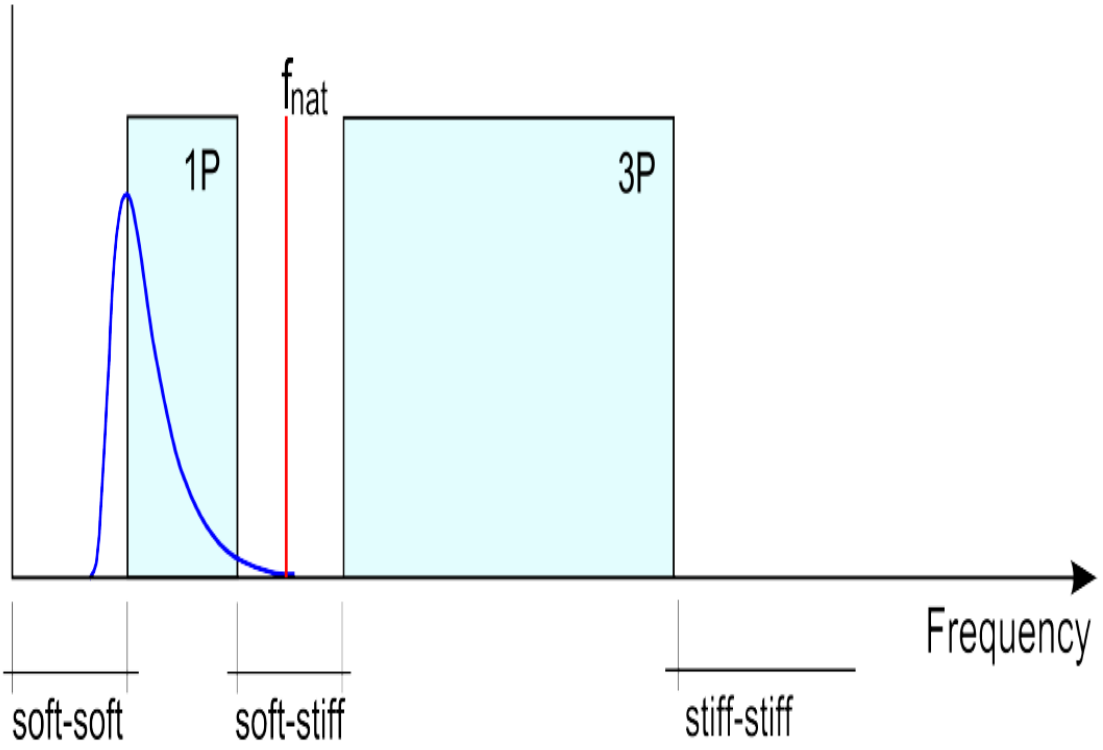

FIGURE 2.2: Allowable natural frequency range diagram.[4]

Real fluids always have some viscosity therefore flow around the structure slows down and gives rise to boundary flow phenomena. This generates vortex induced vibrations in the structure. If the structural natural frequency matches with the vortex shedding frequencies, large vibrations can occur. This analysis should also be performed before finalizing the dimensions of the support structure.

2.6 Hydrodynamic loads

2.6.1 Wave kinematics

Wind is the main driver behind sea waves. There is a continuous transfer of energy from wind to water. At one point waves travel at the same speed as the wind and thereafter there is no transfer of energy form wind to sea. This sea state is known as "fully developed" [20]. Formation of waves depends upon the wind speed, fetch, wind duration and water depth at the site. If the time or fetch is smaller than required to form a "fully developed" sea state then the sea state is known as "partially developed".

Waves generated by wind are mainly classified in two categories, sea and swell waves. Sea waves are generated by the local wind field. The waves are short crested and highly irregular in nature. When these waves propagate out of the area in which they were generated, they are known as swell. Swell waves can propagate longer distances. Swells are more regular and round crested.

In an offshore wind farm, water depth and bathymetry changes from location to location and this affects wave properties such as wave height, group speed and wavelength [21]. When the wave profile is not parallel to the sea bed profile then crest in the shallower region moves slower than in deeper water. This causes to change the direction of propagation of the wave crest. It is known as wave refraction. As the wave propagates and reaches the shore it becomes steep and unstable. With the increase in the steepness of the wave, velocity of the wave particles also increases. The wave starts to break when particle velocity becomes greater than the wave velocity.

Wave spreading affects the wave particle horizontal velocity. This reduces the forces on the support structure. Wave spreading is affected due to the shoaling, refracting, wave height, local bathymetry and location. DNV allows reduction in velocity and acceleration by up to 20% for directional and non-breaking waves. The wave spreading factors for the North Sea are in the range of 0.73 to 0.96 [22]. Wave spreading analysis at the location should also be carried out. A recent study conducted by the University of Hanover at FINO 1 offshore platform showed that wave spreading reduces the fatigue damage by around 30% [23].

The wave force depends on the inertia and drag coefficients. The inertia and drag coefficients depend upon the shape of the structure, Reynolds number, Keulegan-Carpenter (KC) number, MacCamy-Fuchs number, material defects, marine growth and roughness number [24] [25]. Interested readers can read about inertia and drag coefficients in detail from [25].

2.6.2 Currents

Sea currents are mainly generated by the forces of tides, wind, Coriolis force of earth rotation, salinity and temperature difference at a particular location. Local bathymetry also plays an important role in the current velocity. The current velocity is generally highest at locations where the tidal difference has a high value. The current velocity affects the wave speed, waves travel faster with the current. Wave theories predict wave speed relative to the current. The wave period measured by an instrument is Doppler shifted. The second main effect of current is the additive effect it has on horizontal wave particle velocities. To determine wave particle velocities it is necessary to know the current speed[26].

The current velocity variation over time is relatively small compared to the wave and wind variation [4]. It is therefore common to assume the sub-surface current velocity to be constant in design calculations. When current interacts with the structure its flow gets obstructed. This causes overall reduction in current velocity. This is known as current blockage. The EU project OFELIA (Offshore Foundations Environmental Impact Assessments) demonstrated 10-20% reduction in wave height and current speed behind the monopile [27]. The obstruction due to the structure creates a horseshoe vortex in front of the structure, vortex shedding at the lee-side of the pile and contraction of the streamline at the sides of the pile. This increases the sediment transport capacity which leads to the scour [28]. Current can also cause vortex-induced vibration which might affect the structural stability.

2.7 Tides

The sea level varies with time. Main drivers of these variations are earth's rotation and sun and moon's gravitational pull. A storm surge and local bathymetry also affect the

sea level on some occasions. The tidal height affects the platform level of the support structure. After installation of the monopile, water level inside it remains constant but outside water level changes from time to time. This generates circumferential stress in the pile. This affects ULS and Fatigue Limit State (FLS) of the structure.

2.8 Wind loads

The wind velocity varies with time, direction and height. Wind speed is mainly dependent on the Coriolis force due to the earth rotation, pressure gradient and terrain roughness. Wind speed increases with height and this phenomenon is known as wind shear. Wind loads on the structure are affected due to the thrust force, turbulence intensity, drag etc.

2.8.1 Turbulence intensity and wake

The turbulence intensity is defined as the standard deviation of time varying wind speed divided by the mean wind speed based on 1-minute average data [29]. The turbulence intensity is directly proportional to the roughness of the terrain and inversely proportional to the altitude. The turbulence intensity for an offshore site has a low value compared to an inland site as the surface roughness of sea is very low.

Wind farms contain a number of turbines. This gives rise to wakes. The wake reduces the wind speed for the downwind turbines. The layout of the wind farm plays a major role in the wake formation. Wake effects not only reduces the power production but also increases loading on the turbine. Wake effects in the wind farm increase the total turbulence intensity. This effect has to be included in the design calculation. For further explanation of turbulance intensity, wake formation and models refer to [30][31] [32][33][34][35].

2.9 Stress concentration factor and Factor of safety

The support structure surface is not a smooth surface over the length. It has welded joints, flange connections, discontinuities etc. This raises the stress level at a particular

location. This has adverse effects on the fatigue life and structural stability. Design standards specify stress concentration factors (SCF) for different situations. The stress calculated for different loading conditions needs to be multiplied by the stress concentration factors.

There are some uncertainties present in the structural design like [36]:

- Composition of material and the effect of variation in properties.
- Effect of corrosion, wear.
- Validity of mathematical models used to represent reality.

The uncertainties can be taken care of by applying a factor of safety. The allowable design quantity should be divided by the factor of safety. The design quantity can be load carrying capacity, material properties etc.

2.10 Stability of structures

A phenomena of slender member bending laterally abruptly from its longitudinal position due to compression is known as buckling [37]. When a column is subjected to bending, axial compression it undergoes compression. If the loading reaches the critical value, the column becomes unstable and buckles. The buckling limiting strength depends upon various factors like boundary conditions, member dimensions, material properties, imperfections, residual stresses etc.

The tendency of the structure to buckle locally before overall failure is called local buckling. The local buckling creates distortion in the cross section of the structure. The local buckling reduces the load carrying capacity of the structure due to reduction in the strength. The buckling of the structure is characterized based on the slenderness ratio. For higher slenderness ratios with high thickness (D/t>10) value column generally buckles globally. For higher slenderness rations with smaller thickness value column might buckle locally. For smaller slenderness ratios the column fails due to yielding. The yield criteria should also be checked for the structural stability.

The torsional loading occurs in the structures due to eccentricities involved in the lateral loading. The source of eccentric loading is mainly due to the turbulence intensity, yaw

misalignment etc. The torsional buckling criteria should also be checked before finalizing the support structure dimensions.

2.11 Foundation stability

The soil data consists of soil layers and properties of soil at a particular site. Soil is generally divided into sand and clay type. Based on its properties, sand is divided into loose, medium, dense and very dense sand. The friction angle, sub unit weight, unit skin friction, unit bearing pressure are important properties of the sand. For clay, submerged unit weight, strain for 50% stress and undrained shear strength are important properties. The unit skin friction and unit bearing pressure are used for the axial stability check of the support structure.

Over the project life support structure is subjected to cyclic loading. This impacts the soil properties over the years. The site investigation and analysis of soil has to be carried out to get clear understanding. The support structure is subjected to cyclic wind and hydrodynamic loading. The penetration length must be sufficient to provide lateral and axial stability.

A pile has a tendency to form a plug. Raines observed that a plugged pile behaves like a close ended pile [38]. The tendency to form a plugged pile vary directly and inversely with the penetration depth and internal diameter [39]. Paikowsky and Whitman claimed that the possibility of plugging is greater once the ratio of penetration length to pile diameter is greater than 20 in dense sand [40]. The axial load carrying capacity of the plugged pile consists of external shaft and end bearing resistances. For an unplugged pile, axial capacity depends upon internal and external shafts and annulus resistance. Piles installed in dense sand tend to plug more than those installed in loose sand. The support structure settlement analysis should be performed for the project site. Fig 2.3 gives an example of both a plugged and an unplugged pile case.

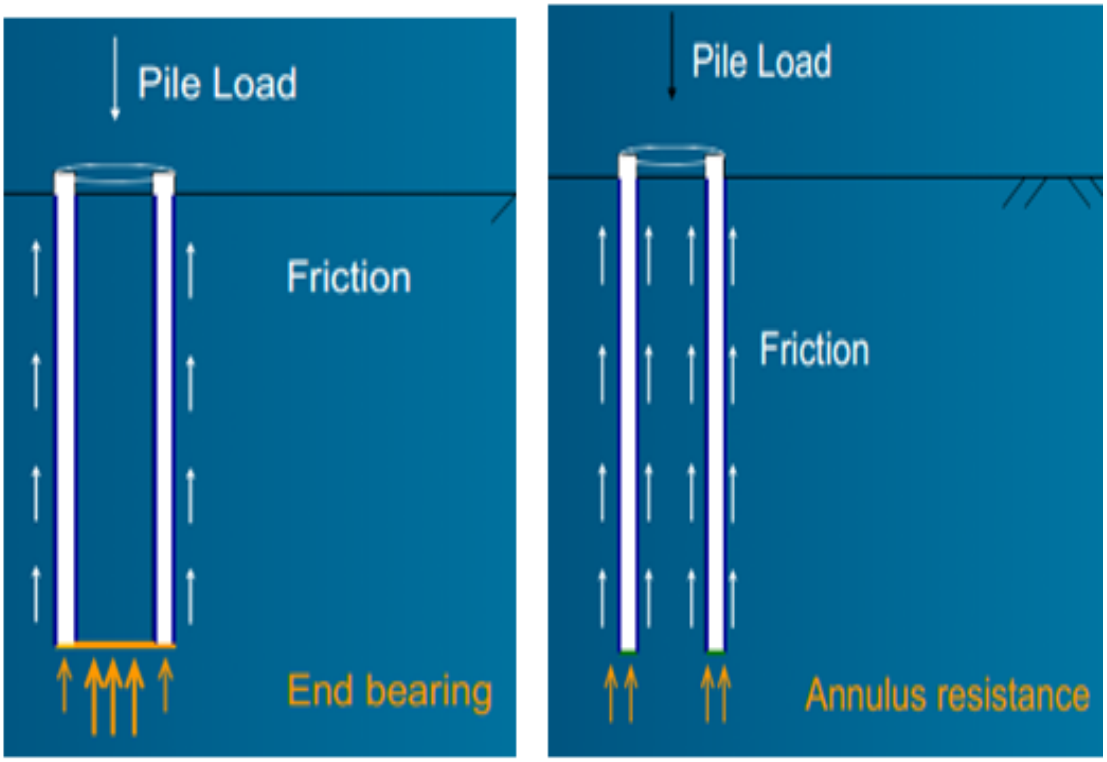

FIGURE 2.3: Plug and unplug pile.[5]

2.12 Grout stability

The grouted connections are used to transfer the loads and connect the transition piece to monopile. Since 2009, slippage is observed in the grouted connection for many offshore wind farms. To study its reasons and mitigation methods a JIP (Joint Industry Project) named GROW (Grouted Joints for Offshore Wind Turbine Structures) by DNV, GL and various industry partners is carried out [41] [42].

Dynamic bending, torsion and axial loading are the main types of loading experienced by the grouted connections. Generally it is assumed that the effect of hoop stresses are not significant for the grouted connections. The axial capacity of the grout depends upon the surface irregularities, surface roughness and tolerances between grout and steel. During initial loading grout capacity depends upon both surface roughness and tolerances. Over the time period bonding capacity between grout and steel deteriorates and after some time bond between grout and steel slips. After the slippage, the grout capacity only depends upon the tolerances and radial stiffness. The slenderness ratio

of the transition piece and monopile also plays an important role in the grout stability. The high slenderness ratio causes the ovalisation of the structure and this leads to the gap formation between grout and steel. The abrasive wear of sliding surfaces between steel and grout should also be considered in the design process. The rate of wear is proportional to the bending moment and contact pressure. The torsional capacity of grout depends upon the resistance to sliding and tolerances in the connection.

The main findings of the JIP suggest to use cylindrical shape piles with shear keys for monopile and transition piece overlap or conical shape steel shells. The reasons for these suggestions are:

- Reduced interface shear capacity with the increasing diameter of the connections in combination with a low long-term effective resistance between the steel and grout surfaces for loads that exceed the bond/sliding friction capacity.
- Lack of requirements as to minimum tolerances.

The capacity of the grout reduces with the number of dynamic load cycles. The installed shear keys add to the shear force capacity of the grout. On the other hand, limited axial settlements can be achieved by using a conical shape pile section. The largest torsional capacity is achieved for smaller cone angles. The stresses generated due to settlement can be avoided by using cylindrical rings at the end of the grouted connection. The overlap between monopile and transition piece has some part of the section below sea level. It is important to avoid the ingress of water as this affects the fatigue capacity and may lead to the cracking of the grout.

2.13 Fatigue

Varying stresses smaller than the yield stress can cause failure of the structure. This phenomenon is known as fatigue. This is because the stress at the failure site is higher than the calculated stress due to the imperfections in the material, manufacturing and associated stress concentration factors. Existing cracks can grow or new cracks can develop with a varying load. After several cycles a large crack can cause a failure and collapse of the structure [43]. There are various methods to determine fatigue damage, readers can refer to [44][45][46]. Here, only the S-N curve method is explained. The

S-N curve is a graph with stress (S) on the Y-axis and the number of cycles (N) of the particular stress the structure can withstand on the X-axis. The support structure has different geometries for different locations. The support structure has some part in the air and some in water. The selection of the S-N curve depends on these details.

The user of the S-N curve should have information about the number of cycles for which the load would be applied. For offshore structures the applied load is a combination of hydrodynamic and aerodynamic loads with no specific frequency. Stresses for fatigue damage are determined from time signals of loading. This approach requires large time vs stress records to describe random loading processes. To overcome this problem the Rail-flow counting technique can be used. The Rain-flow technique gives the number of cycles a particular stress level has occurred. With stress levels, number of cycles and S-N curve, the fatigue damage of the structure can be found out using the Palmgren-Miner rule. According to the Palmgren-Miner rule, fatigue damage is equal to the ratio of number of cycles for which a load is applied to the number of specified cycles for that particular load on the S-N curve. The total damage is the summation of all the damages for all stress levels. The total damage should be less than unity to prevent the failure of the support structure. The Palmgren-Miner rule can be summarized as:

$$D = \sum \frac{n_i}{N_i} \tag{2.1}$$

where,

D	Fatigue damage	[-]
n_i	number of load cycles	[-]
N_i	allowed number of load cycles	[-]

Chapter 3

Simplified design application

3.1 Introduction

In the previous chapter, a detailed design of an offshore wind support structure with a monopile as a foundation is illustrated. At the start of this chapter an overview of steps a designer has to follow for the application of simplified design process are presented. The design driver constraint modeling is explained later. Next, design variables involved in the simplification process are listed down. In the end, calculation of correction factors and selection of reference location is clarified.

A Python based design tool developed by Michiel is used as a starting point for the application of the simplified design method. The hub height, platform level, transition base level, grout annulus and turbine tower length calculations are kept unchanged from his design tool [15].

For the application of the simplified design process, the GUI (Graphical User Interface) and support structure module are modified and improved. In this tool, the user has to give inputs for environmental and turbine parameters, and design driver values of the reference location. The buckling or yielding can be a design driver for the turbine tower and transition piece thickness, while for monopile it can be natural frequency, yielding or buckling. The buckling constraint consists of global, local and torsional buckling. The simplified models for the natural frequency, grout, yielding and buckling are explained in chapter 4.

3.2 Application of simplified design process

The objective of the simplification process is to design multiple support structures tailored to their local environments in minimum possible time. Fig. 3.1 shows the application and flow chart of the simplified design process. The square box with curved edges is the final outcome of the simplified design process.

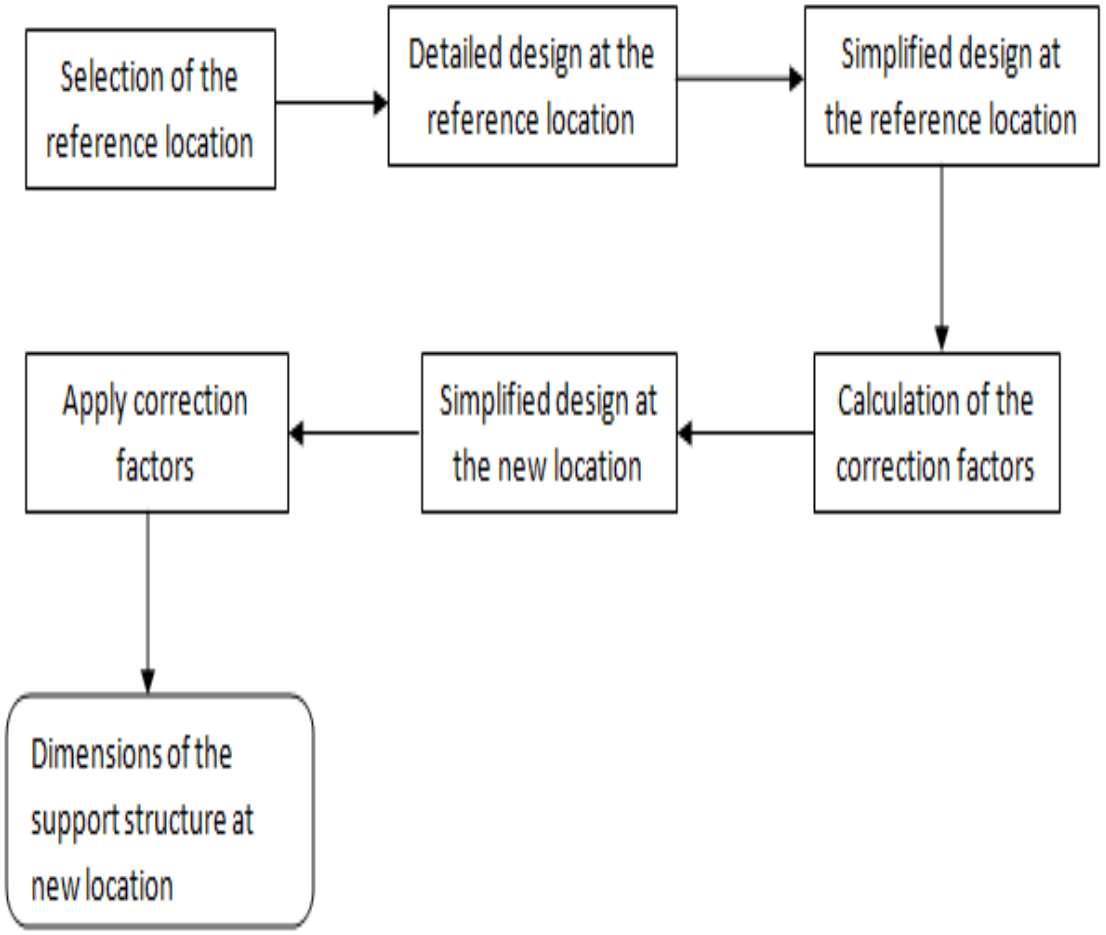

FIGURE 3.1: Overview of the simplification process.

The first step is the selection of the reference location. The method of selection of the reference location is explained in the section 3.7. The next step is to carry out a detailed design of the support structure at the reference location. The design driver and their values for each section of the support structure should be identified. In step 3, design drivers and their values obtained from the detailed design and the environmental conditions of the reference location should be given as an input to the design tool. The support structure dimensions obtained from simplified models are output of the tool.

The next step is the calculation of the correction factors. The explanation of the need, definition of the correction factors and dimensions for which correction factors need to be found out are mentioned in the section 3.6.

Next, the step number 5 is the simplified design at a new location within a wind farm where a support structure needs to be designed. The environmental values corresponding to the new location and design driver values of the reference location should be given as an input to the design tool. The dimensions obtained from the design tool should be multiplied by the corrections factors to get the final dimensions of the support structure at the new location.

Now, for another location within a wind farm, design can directly start with the step number 5. It highly unlikely to change the turbine within a wind farm. Therefore turbine data remains the same for the reference and new location.

3.3 Constraint modelling

The main constraints addressed in this thesis are natural frequency, yielding and buckling. The goal of the constraint modelling is to find the dimensions of the support structure for a given simplified model.

Eq. 3.1 gives the constraint modelling function:

$$f = g(x) - C \tag{3.1}$$

where,

f	root finding function	[-]
$g(x)$	simplified model function	[-]
x	design variable	[m]
C	constraint value	[-]

For this project Brentq root finding method is used. Brentq method is the application of secant method which uses inverse quadratic extrapolation. It is also known as the van

Wijngaarden-Deker-Brent method. For more information on Brentq method interested reader can refer to literature [47][48][49].

For the application of this method f must be a continuous and sign changing function between the design variable interval x. The variable x has upper and lower bounds. The design variable interval x is explained for each section of the support structure in section 3.4. A simplified design model function, $g(x)$, calculates the value of the simplified model for a variable x.

The function f converges when the root is known to lie within the defined value. This defined value is known as xtol in Brentq code. The value of x for which the function f converges is taken as the final value of the dimension. For the diameter, grout length and penetration length calculations xtol is taken as 0.01m, while for thickness calculations it is taken as 0.0001m.

After designing the support structure at the reference location, the main design drivers and their values for monopile, transition piece and turbine tower are known. This design driver value is C. The user has to give the design driver values as an input for each section of the support structure.

The design driver values for the grout is obtained from the DNV standard. The function f of the grout length is given by Eq. 4.40. The penetration length is calculated using Eq. 4.35 and 4.36. The larger of the two values is taken as the final penetration length. The functions f of the penetration length are Eq. 4.35 and 4.36. The function f for yielding, torsional , global and local buckling are Eq. 4.21, 4.23, 4.24 and Eq. 4.25 respectively.

In Eq. 4.36, 4.35 and 4.40 the function on the left hand side of the negative sign is g(x) and on the right hand side constraint C.

3.4 Design Variables

As stated earlier, the design variables in the simplification problem are thickness and diameter of the support structure. Offshore support structures consists of different sections, turbine tower, transition piece and monopile. Each section is represented by the top and bottom diameter and thickness. For transition piece and monopile have constant diameters and thickness value over the length.

3.4.1 Monopile

For monopile, diameter is the only design variable. The monopile diameter is determined by satisfying the buckling, natural frequency or yielding constraint depending upon the main design driver at the reference location. For buckling constraint the design driver can be the global, local or torsional buckling.

The thickness of the monopile is related to its diameter. This is done to avoid buckling during pile driving. This recommendation is given by the API standard [6]. Eq. 3.2 gives the relation between monopile diameter and thickness:

$$t = 0.00635 + 0.01 D_m \tag{3.2}$$

where,

t	thickness of monopile	[mm]
D_m	diameter of monopile	[mm]

For the buckling constraint, it is assumed that the maximum stress occurs at the mudline. The hydrodynamic loads are determined using the monopile diameter for parts below the transition piece bottom, while the transition piece diameter is used for parts above the transition piece bottom. For parts of the structure above mean sea level (MSL) the aerodynamic loads are determined, while hydrodynamic loads are determined for the transition piece and monopile below MSL.

For root finding problem Brentq method is applied. Brentq function has to be a sign changing function. As lower diameter value results in the higher design driver value and higher diameter results in the lower design driver values, making f a sign changing value. Most of the monopiles have values of the diameter in the range of 3-7m. Therefore the interval for the tried diameter in Brentq code is fixed to 1-10m.

The penetration length is found using Blum model. For the penetration length, length is varied to satisfy the Blum criteria. The interval for the tried penetration length in Brentq code is fixed to 1-100m. The monopile top is decided by the overlap length:

$$M_{top} = l_{overlap} + TP_b \tag{3.3}$$

where,

M_{top}	monopile top level wrt MSL	[m]
$l_{overlap}$	overlap length	[m]
TP_b	transition piece base wrt MSL	[m]

The monopile length is determined by summing up the penetration length, overlap length, difference between the transition piece base bottom and mudline:

$$M_l = p_l + l_{overlap} + TP_b - mudline \tag{3.4}$$

where,

M_l	monopile length	[m]
$l_{overlap}$	overlap length	[m]
$mudline$	mudline wrt MSL	[m]
p_l	penetration length	[m]

3.4.2 Transition piece

For the transition piece only thickness is the design driver. The diameter of the transition piece is calculated by summing up the monopile diameter, grout thickness and transition piece thickness. The thickness is determined by the buckling or yielding constraint. The user has to give input value for the targeted buckling or yielding value. The bottom of the transition piece level is also kept same (6m above the seabed or below the lowest water elevation, whichever of the two is lowest) as Michiel's calculation [15]. The diameter of the transition piece is given by:

$$D_{tp} = D_{mp} + 2 * t_g + 2 * t_s \tag{3.5}$$

where,

D_{tp}	transition piece diameter	[m]
D_{mp}	monopile diameter	[m]
t_g	grout thickness	[m]
t_s	transition piece thickness	[m]

To determine the thickness of the transition piece, loads on the transition piece have to be known. The outer diameters of the turbine tower and transition piece should be known to calculate the hydrodynamic and aerodynamic loads. For the axial load calculation, turbine tower thickness of each section should be known. But the thicknesses of the turbine tower sections depend on the moment of resistance offered by the section. The transition piece diameter is set equal to turbine tower base diameter. Therefore initial guess of the transition piece diameter is made to determine the turbine tower base diameter and loads on the structure. The method adopted for the calculation of turbine tower thicknesses is described in section 3.4.3.

The ratio of the diameters of monopile and transition piece of the detailed design at the reference location is used for the initial guess of the transition piece diameter. Based on this initial guess, the turbine tower thicknesses are determined. Now, the loads on the transition piece are known. Using these loads, the transition piece thickness is calculated. With this new thickness, new transition piece diameter is obtained. After this, an iterative method is applied till the difference between previous and current result for the transition piece diameter is less than 0.01m. Fig. 3.2 depicts the design algorithm for the the transition piece diameter calculation.

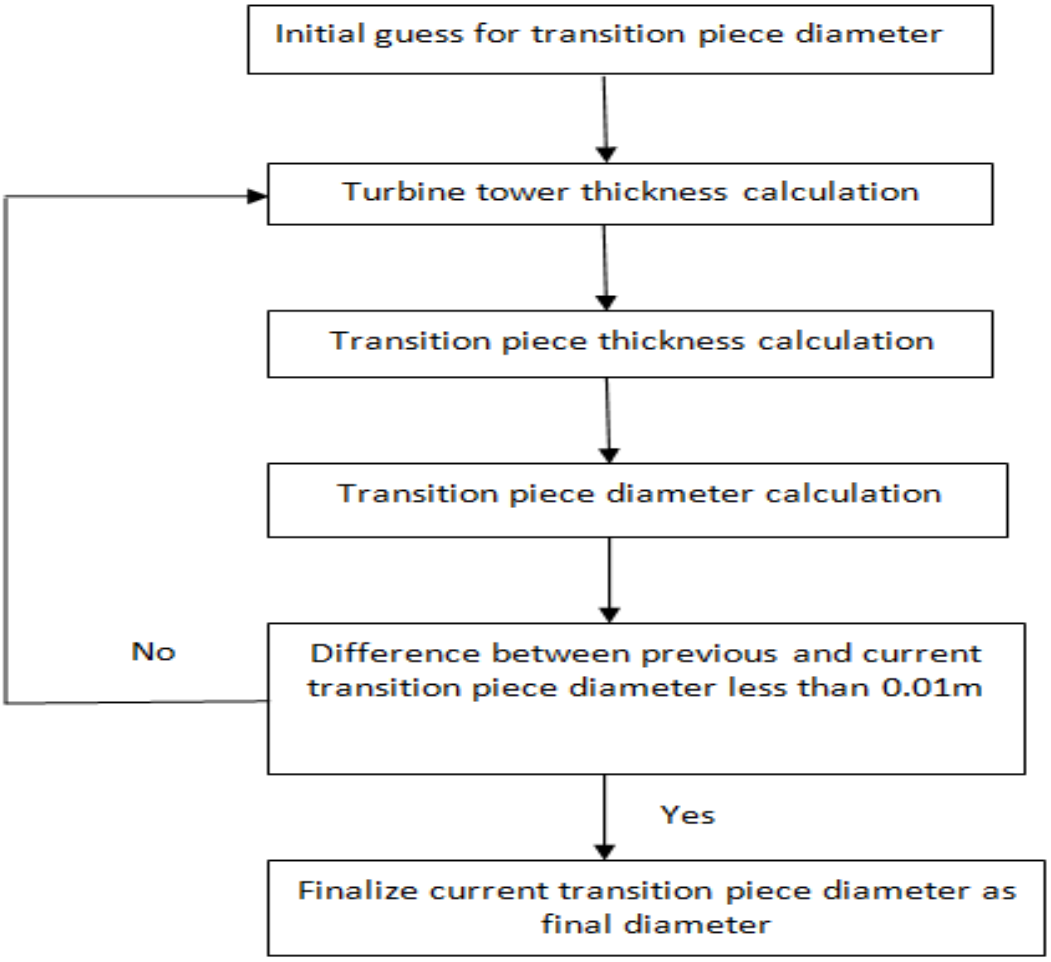

FIGURE 3.2: Algorithm for the transition piece diameter calculation.

The maximum stress is assumed to occur at the lowest section. This is because of the larger lever arm, axial load and higher localized stress due to transition piece and grout interaction. The buckling and yielding criterion is checked at the base of the transition piece. The interval for the tried thickness in Brentq code is fixed to 0.001-1m.

3.4.3 Turbine tower

The turbine tower bottom diameter is set equal to the transition piece diameter. The turbine tower top diameter is set equal to the yaw bearing diameter. This helps to transfer loads effectively from one part to another. The diameters of the intermediate sections are scaled linearly. Each section of the turbine tower has a constant thickness. The thickness is the design variable for the turbine tower. The tower wall thickness per section of the tower is determined by the buckling or yielding constraint. The

evaluation is performed at the base of the each section. The Brentq method is applied for the thickness calculation. The interval for the tried thickness in Brentq code starts at 0.001m and ends at the radius of the section. The RNA mass and aerodynamic loads are known at the top section. Therefore the design of the thickness starts from the top section of the tower. This helps to determine the accurate gravity loads for lower sections.

3.4.4 Grout

Only two parameters, grout length and thickness can be varied to alter the capacity of the grout. The grout thickness is governed by the installation constraint. Therefore overlap length is used as a design variable [50]. The grout thickness is set equal to 100mm [15]. Recent experiments performed at the university of Hannover and Oldenburg demonstrated that grouted connections subjected to bending loads can have an overlap length (grout length) equal to 1.25 times of monopile diameter and this ratio can be reduced if shear keys are used. But DNV has suggested to use overlap length to pile diameter ratio of 1.5. For the certification approval, overlap length obtained from Eq. 4.40 is compared with 1.5 times the pile diameter and the maximum of the two is taken as the final overlap length. For the calculation of the overlap length Brentq method is applied. Generally, an overlap length is in the range of 1.3 to 1.6 times the monopile diameter. Therefore the interval for the tried overlap length in Brentq code is fixed to 1-20m to make f a sign changing function.

3.5 The simplified method algorithm

Fig. 3.3 gives the algorithm of the simplified design method.

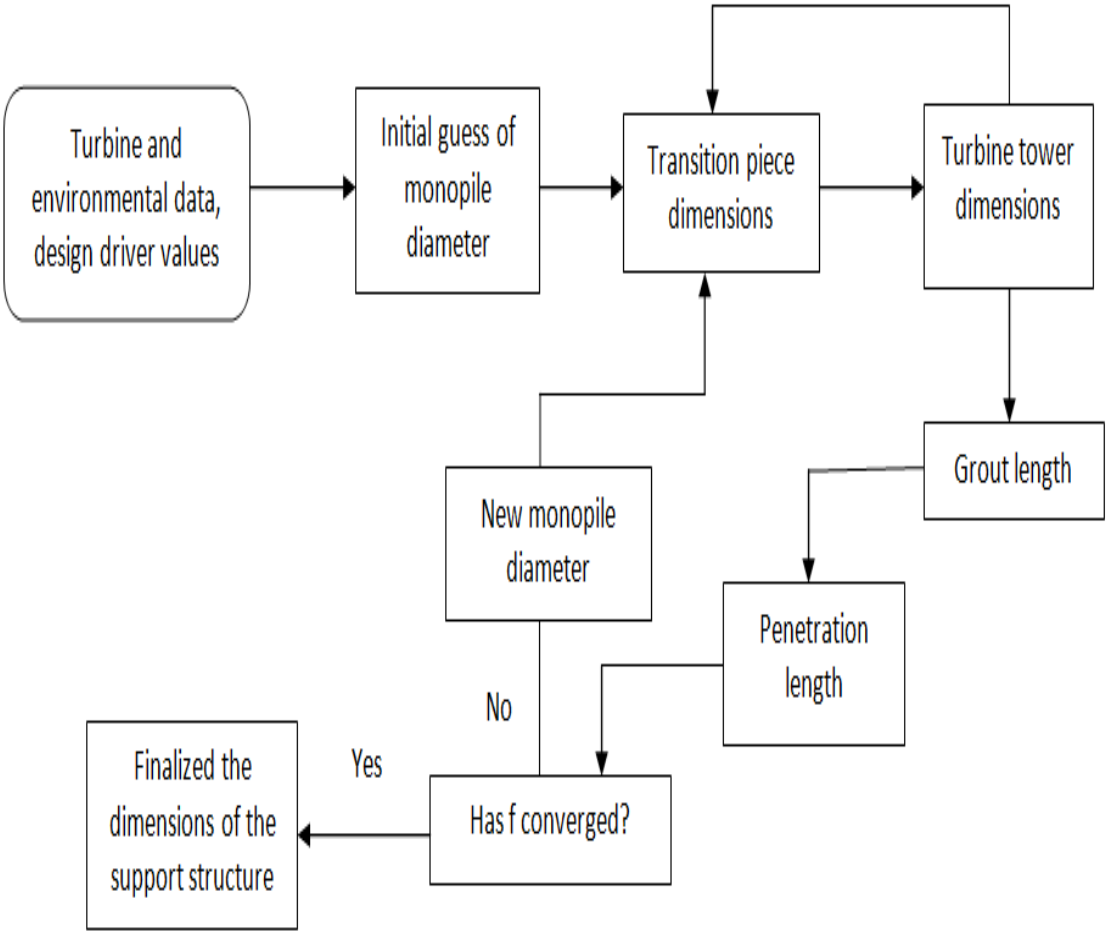

FIGURE 3.3: Algorithm of the simplified design process.

The transition piece dimensions, penetration length and grout length are directly dependent on the monopile dimensions. The turbine tower dimensions depend upon the transition piece diameter, hence indirectly related to the monopile diameter. Therefore the monopile diameter is taken as a starting point in the simplified design algorithm. The inter-relation between monopile dimensions and grout and penetration length can be understood by reading sections 4.7 and 4.8.

Now, once a designer has given inputs, the simplified design process starts with the lower bound of the monopile diameter in Brentq code. Next the thickness of the monopile is calculated. The relation between monopile diameter and thickness is given in the section 3.4.1. The next step is the calculation of the transition piece and turbine tower dimensions. These dimensions are interdependent. An iterative loop is used for the transition piece and turbine tower calculation. The iterative loop logic is explained

in the section 3.4.2. Next, grout and penetration lengths are calculated. Finally, the function f is checked for the convergence. If f converges then dimensions are finalized and if not then the new monopile diameter is chosen based on Brentq code and iteration is continued till f converges.

Table 3.1 gives the idea of on what basis variables are calculated. The term KBE corresponds to Knowledge Based Engineering. The KBE can be the direct formula, manufacturing constraints or engineering judgment.

TABLE 3.1: The summery of design variables calculation method.

Parameter	Method
Monopile diameter	Brentq code
Monopile thickness	KBE
Transition piece thickness	Brentq code
Transition piece diameter	KBE
Turbine tower base diameter	KBE
Turbine tower thickness	Brentq code
Turbine tower top diameter	KBE
Grout length	Brentq code
Grout thickness	KBE
Penetration length	Brentq code

3.6 Correction factors

For the design of the support structure simplified models are applied. These models do not represent the true nature of the design. Dimensions obtained from these models are different from the detail designed. The correction factors are applied to compensate for this. A correction factor is the ratio of a detailed design parameter to a simplified design parameter at the reference location.

The correction factors should be found out for the monopile diameter, penetration length, transition piece thickness and turbine tower thickness of each section. The monopile thickness is related to its diameter therefore once the monopile diameter is

corrected its thickness can be found out from the corrected diameter. The transition piece diameter is dependent on its thickness therefore once the thickness is corrected diameter can be found out using the corrected thickness. The correction factors are not found out for the turbine tower bottom and top diameter. As turbine tower top and bottom diameter are equated to the yaw bearing and transition piece diameter respectively. The correction factors used for this project are found out by:

$$C_f = \frac{D_n}{S_n} \tag{3.6}$$

where,

C_f	Correction factor
D_n	detailed design quantity
S_n	simplified design quantity
n	section of the support structure

3.7 Selection of the reference location

The basic assumption in the application of the correction factors is that the correction factors are independent of environmental variable. In reality, correction factors are dependent upon various parameters and these parameters change from location to location. This phenomena influences the selection of reference location within the wind farm. The variation in water depth and turbulence intensity within a wind wind farm has the largest impact on the support structure design. The reference location should be chosen at an intermediate water depth or a location with an intermediate turbulence intensity value or combination of both to minimize the error. The layout of the wind farm affects the turbulence intensity and water depths in which support structures will be placed. Therefore an engineering judgment should be made for the selection of the reference location.

Chapter 4

Simplification of the design process

4.1 Introduction

In the previous chapter, the simplified design process is explained. The main time consuming activities in the detailed design process are simulations required to perform for different Design Load Cases (DLC). Therefore a simplified method is proposed for the DLC. The formulation of simplified models for the wind loads, hydrodynamic loading, natural frequency, foundation and grout stability are carried out in this chapter.

4.2 Loads on the structure

In this section simplification of hydrodynamic and aerodynamic load are carried out.

4.2.1 Hydrodynamic loading

4.2.1.1 Wave kinematics

The determination of hydrodynamic loading is important step in the design process. A sea state is generally defined by the significant wave height and wave period. There are different wave theories available to describe the wave particle motion. The stokes theory

is most widely used. The Stokes wave theory assumes that the wave is incompressible and irrotational at all times. The two dimensional wave flow is derived based on the application of Laplace equation. Stokes also assumed that the waves are periodic and symmetric. The wave surface height is calculated based on even Fourier components which is an expansion of an infinite series. The series is truncated at order n. Depending upon the value of n, the wave theory is known as Stokes n^{th} order theory. The computational time increases with the order of Stokes theory.

The Stokes theory is based on the assumption that waves are not very steep. The Stokes wave theory is useful when the water depth to wavelength ratio is greater than 1/8 or 1/10. But in shallower water depths cnoidal wave theory is more satisfactory. For Stokes theory to be applicable in shallow water, wave amplitude is required to be very small which is unrealistic [51]. Cnoidal theory is not applied in engineering practice extensively as it uses Jacobian elliptical functions and integrals. This makes cnoidal theory cumbersome and time consuming [52].

As stated in the section 1.2, the aim of this thesis is to simplify the design process. Therefore 1st order Stokes theory is applied. For n=1, Stokes wave theory is known as linear wave theory. The linear wave theory is applied to represent the wave kinematics. Eq. 4.1 of the wave profile is described with MSL (Mean Sea Level) as a starting point [53]:

$$\eta = 2\zeta \sin(\omega t - k_{wave} x) \tag{4.1}$$

where,

λ_{wave}	wavelength	[m]
k_{wave}	wave number ($2\pi/\lambda_{wave}$)	[m^{-1}]
ω	wave frequency	[rad/s]
d	water depth	[m/s]
t	time	[s]
η	instantaneous water surface elevation	[m]
ζ	wave amplitude	[m]
x	distance traveled from starting point in horizontal direction	[m]

Kinematics of horizontal water particles for different water depth range is described by Eq. 4.2, 4.3 and 4.4 with z varying from 0 to $-d$. Waves are differentiated based on depths into shallow water, intermediate water and deep water waves [53]. For shallow water depth ($d/\lambda < 0.05$):

$$\begin{aligned} u(x,z,t) &= \frac{\zeta\omega}{kd}\sin(\omega t - k_{wave}x) \\ \dot{u}(x,z,t) &= frac\zeta\omega^2/kd\cos(\omega t - k_{wave}x) \end{aligned} \tag{4.2}$$

For intermediate water depth ($0.05 < d/\lambda < 0.5$):

$$\begin{aligned} u(x,z,t) &= \zeta\omega\frac{\cosh(k_{wave}(z+d))}{\sinh(k_{wave}d)}\sin(\omega t - k_{wave}x) \\ \dot{u}(x,z,t) &= \zeta\omega^2\frac{\cosh(k_{wave}(z+d))}{\sinh(k_{wave}d)}\cos(\omega t - k_{wave}x) \end{aligned} \tag{4.3}$$

For deep water depth ($d/\lambda > 0.5$):

$$\begin{aligned} u(x,z,t) &= \zeta\omega e^{kz}\sin(\omega t - k_{wave}x) \\ \dot{u}(x,z,t) &= \zeta\omega^2 e^{kz}\cos(\omega t - k_{wave}x) \end{aligned} \tag{4.4}$$

where,

u	wave particle velocity	[m/s]
$\dot{u}$	wave particle acceleration	[m/s^2]

4.2.1.2 Current

To find out the load due to the current on the support structure, the relation between the current velocity and water depth needs to be established. As stated in section 1.2, aim of the thesis is not only to simplify the design process but also to satisfy the certification requirements. For the current modelling the IEC-614003 design standard is followed [54]. The IEC design standard has specified two models for the relation between current and water depth.

- The power law profile.

- The linear profile.

The power law profile is for the application of sub surface currents and linear profile for wind generated near surface currents. The wind generated current linearly decreases with water depth and vanishes at 20m water depth. The wind generated current is used for Normal Current Model (NCM) and wind and subsurface currents are used for Extreme Current Model (ECM).

The power law and linear profiles are represented by Eq. 4.5 and 4.6 respectively:

$$U_{ss}(z) = U_{ss}(0)(\frac{z+d}{d})^{\frac{1}{7}} \tag{4.5}$$

$$U_w(z) = U_w(0)(\frac{1+z}{20}) \tag{4.6}$$

where,

$U_{ss}(z)$	extreme current velocity at depth z	[m/s]
$U_{ss}(0)$	current velocity at sea surface	[m/s]
$U_w(0)$	wind generated current velocity at sea surface	[m/s]
$U_w(z)$	wind generated current velocity at depth z	[m/s]

The wind generated current velocity is given by:

$$U_w(0) = 0.01V_{10m} \tag{4.7}$$

where, V_{10m} is the wind speed at 10m. The current speed should be multiplied by the probable current blockage factor at location before giving input in the design tool.

4.2.1.3 Wave loading

A number of assumptions are made for simplification of hydrodynamic loads:

- Marine growth is neglected.
- The motion of the support structure is ignored.

- C_m and C_d values are kept constant over the time scale of the project and for different water depths.

The Morison equation is widely used to calculate hydrodynamic loads on the offshore support structure. Wave loads on the support structure can be calculated by combining Morison equation and wave particle kinematics. A structure is subjected to current loading along with wave loading. The drag term of Morison's equation contains a velocity term. Therefore current velocity is incorporated in the hydrodynamic drag load. The Morison equation is as follows[55] [6]:

$$\begin{aligned} f_{Morison}(x,z,t) &= f_d(x,z,t) + f_i(x,z,t) \\ f_d(x,z,t) &= 0.5 C_{hd} \rho_{water} D(|u(x,z,t) + U_c|)(u(x,z,t) + U_c) \\ f_i &= 0.25 C_m \rho_{water} \pi D^2 \dot{u}(x,z,t) \\ m_i &= \int_{-d}^{0} f_i(z+d)dz \\ m_{hd} &= \int_{-d}^{0} f_d(z+d)dz \end{aligned} \tag{4.8}$$

where,

$f_{Morison}$	total hydrodynamic force	[N/m]
f_d	hydrodynamic drag force	[N/m]
f_i	hydrodynamic inertia force	[N/m]
C_{hd}	hydrodynamic drag coefficient	[-]
C_m	inertia coefficient	[-]
rho_{water}	density of water	[kg/m^3]
D	diameter of structure	[m]
U_c	current velocity	[m/s]
m_i	moment due to inertia load	[N-m]
m_{hd}	moment due to hydrodynamic drag load	[N-m]

The total hydrodynamic load on the support structure is the summation of drag and inertia loads. Inertia and drag loads are out of phase by 90°. This signifies that the maximum hydrodynamic load is not equal to either maximum drag or inertia load rather it is combination of both loads. Eq. 4.9 gives the total hydrodynamic load due to inertia

and drag loads:

$$F_{tot} = max(F_i cos(wt - kx) + F_d sin(wt - kx)|sin(wt - kx)|)$$
$$M_{tot} = max(m_i cos(wt - kx) + m_{hd} sin(wt - kx)|sin(wt - kx)|) \tag{4.9}$$

where,

F_{tot}	total hydrodynamic force	[N]
M_{tot}	total hydrodynamic moment	[N-m]

The C_m and C_d values should include the wave spreading factor.

4.2.1.4 Breaking waves loading

When the ratio of wave height to water depth or wave height to wave length reaches a particular value, waves start to break. For shallow and intermediate water depths the breaking wave limit is $H/d > 0.78$ and for deep water $H/\lambda_{wave} > 0.14$ [56][57]. Breaking waves induce large slamming loads on the support structure. The probability of breaking waves needs to be assessed at the wind farm location before starting the design process. Wagner and Von Karman have worked on the calculation of breaking wave force [58]. Recent studies performed under the framework of VOWS (Violent Overtopping by Waves at Seawalls) has come up with an intuitive formula for the breaking wave moment prediction [59]. The moment due to breaking wave force depends on the equivalent pressure point of the breaking force. The force and moment due to breaking of waves is given by [13]:

$$F_b = \lambda \eta_b C_s R \rho_{water} u^2$$
$$m_b = F_b(d + 0.43 H_{mo}) \tag{4.10}$$

where,

f_b	breaking wave force	[N]
C_s	slamming coefficient	[-]
λ	curling factor	[-]
η_b	maximum water surface elevation at breaking point	[m]
m_b	moment due to breaking wave	[N-m]
H_{mo}	wave height	[m]

Wagner showed that the value of the slamming coefficient depends upon the time and it varies from 0 to 2π. For the ULS case, extreme loading is of importance and the GL suggests to use a slamming coefficient of 2π. There is no consensus about the value of the curling factor. Goda and Wiegel estimated the value of the curling factor to be 0.4 and 0.5 respectively. Recent experiments performed by Wienke showed the mean value of curling factor of 0.46. The GL has specified the value of the curling factor as 0.5 which is used[13]. To get more idea about breaking wave phenomena and recent work, interested readers can read [60] [61] [62].

4.2.2 Hydrostatic loads

Tides, waves and storm surge change the water level at the site. This gives rise to additional circumferential hydrostatic loading. Depending upon the water level difference between inside and outside of the support structure, hydrostatic pressure will be compressive or tangential. For the simplified hydrostatic loading model, it is assumed that during the installation sea level was at MSL and throughout the project life the water level inside the support structure remains at MSL. The probability of occurring highest wave height and water level is highest during the storm condition. The difference between water level at any level below MSL is:

$$\Delta H = HAT + 0.55H_w + h_{stormsurge} \tag{4.11}$$

where,

HAT	Highest astronomical tide	[m]
H_w	wave height	[m]
$h_{stormsurge}$	positive storm surge	[m]
Δh	water level difference between inside and outside of monopile	[m]

The stress due to hydrostatic loading is given by:

$$P = \frac{\rho_{water} g \Delta h R_s}{t_s} \tag{4.12}$$

where,

g	acceleration due to gravity	[m/s^2]
R_s	radius of the section	[m]
t_s	thickness of the section	[m]

The hydrostatic stress is considered during the transition piece and monopile dimensions calculation.

4.2.3 Aerodynamic loads

The aerodynamic loads are affected by the turbulence intensity, yaw misalignment, thrust, wind shear, loss of electric network etc. This section explains the simplification of the aerodynamic loads.

4.2.3.1 Drag loading

The turbine tower and section of transition piece above the sea level are subjected to the drag load. Before calculation of the drag load, the variation in the wind speed with height is discussed.

The wind speed increases with height. Two models are primarily used to describe the wind shear effect, the power law and logarithmic profile [19]. The IEC design standard

describes the wind shear effect by power law profile. Eq. 4.13 describes the wind shear effect:

$$V_x = V_r(\frac{z}{z_{ref}})^{\alpha} \tag{4.13}$$

where,

V_x	velocity at height x w.r.t. MSL	[m/s]
V_r	velocity at reference height	[m/s]
z_{ref}	reference height	[m]
z	height above MSL	[m]
α	Power law coefficient	[-]

Eq. 4.14 gives the drag loading on the support structure due to wind:

$$\begin{aligned} f_d &= \int_{Z_{hub}}^{Z_{hub}-h} 0.5 C_d D(x) \rho_{air} V(x)^2 dx \\ m_d &= \int_{Z_{hub}}^{Z_{hub}-h} 0.5 C_d \rho_{air} D(x) V(x)^2 (x-h) dx \end{aligned} \tag{4.14}$$

where,

f_d	drag force	[N]
m_d	moment due to drag force	[N-m]
C_d	drag coefficient	[N]
ρ_{air}	air density	[kg/m^3]
h	height w.r.t. MSL at which force and moment required	[m]
$D(x)$	diameter at height x	[m]

4.2.3.2 Hub and torque loading

The wind turbine produces electricity by converting kinetic energy of the wind. The conversion of wind energy into electricity gives rise to the thrust force. Generally the simplified Blade Element Momentum (BEM) theory is used to represent the thrust force on the wind turbine support structure. In the simplified theory, ideal thrust coefficient

for corresponding wind speed is used to represent the wind loading. But this simplification does not take into account the turbulence intensity, yaw misalignment, idling/-parked condition, fault occurrence etc. This results in wrong loading on the structure. It is not possible to calculate the torque on the support structure using this simplified theory. For this reason another method is proposed to simplify the aerodynamic loads. The turbulence intensity in the thesis stands for the longitudinal turbulence intensity otherwise specified.

The thrust/hub load is considered as a point load at the hub height. For some DLC, the IEC mentions the yaw misalignment and electrical grid loss. The the variation of the yaw misalignment within a wind farm is unpredictable. Therefore for the simplification process variation in the yaw misalignment is not considered. In other words, if at the reference location a design load case with particular yaw misalignment value is the design driver then at other locations same vale of yaw misalignment is considered.

The variation in the turbulence intensity within a wind farm can reasonably be predicted. Therefore the load variation with the turbulence intensity is considered in the simplification process. The torque on the structure depends upon the lateral force and its eccentricity with the neutral axis along the y-axis. The variation in the torque along the structure is very less and is neglected in the simplification. Among various environmental parameters, the turbulence intensity has the highest influence on the torque value. Therefore as long as the turbulence intensity is same between the reference location and other locations within a wind farm, the torque value at other location is taken equal to the torque value of the reference location.

For the effect of change in the turbulence intensity a designer will have to perform some extra simulations. The step wise procedure is given below:

1. Identify the design driver load case for the reference location
2. Repeat the load case with 4 or 5 different turbulence intensities, do not change other parameters
3. During each run note down the lateral force (F_x) and torque (M_z) at the hub height
4. Plot graphs between F_x vs turbulence intensity and M_z vs turbulence intensity and extrapolate it for other turbulence intensities

5. At new location, F_x and M_z can be found out using the graphs

To understand the effect of turbulence intensity on the load, consider a cylinder in a turbulent flow. The wind load F can be given by,

$$\begin{aligned} F &= \frac{C_d}{2}\rho_{air}AV^2 \\ V(t,z) &= V(z) + v(t,z) \end{aligned} \tag{4.15}$$

where,

$V(z)$	mean wind speed at height z w.r.t. MSL	[m/s]
$v(t,z)$	standard deviation of turbulent wind speed fluctuation	[m/s]
$V(t,z)$	actual wind speed at height z w.r.t. MSL	[m/s]

The Eq. 4.15 can be expanded to,

$$\begin{aligned} F &= \frac{C_d}{2}\rho_{air}D(V^2 + 2Vv + v^2) \\ &\text{after time averaging} \\ F &= \frac{C_d}{2}\rho_{air}DV^2(1 + 2I_t + I_t^2) \end{aligned} \tag{4.16}$$

where I_t is turbulence intensity. The graph of $(1 + 2I_t + I_t^2)$ is approximately a straight line for I_t between 0 to 0.4, which is the area of interest for designers.

For aerodynamic loading the user has to give inputs for y-intercept, coefficients of 1st and 2nd degree of generated graph and turbulence intensity value at the location in the design tool. If the load-turbulence intensity follows a straight line then 2nd degree coefficient should be keep zero. The moment (m_t) due to thrust load is given by,

$$m_t = f_x(Z_{hub} - h) \tag{4.17}$$

4.2.4 Combine hydrodynamic and aerodynamic loading

The wind and wave direction can be different and some design load cases ask to consider wind-wave directionality [54]. Therefore, the total load on the structure is given by:

$$\begin{aligned} F_{final} &= (F_{tot} + F_b)cos(\theta) + f_d + F \\ M_{final} &= m_t + m_d + (m_b + m_i + m_{hd})cos(\theta) \end{aligned} \tag{4.18}$$

where,

θ	angle between wave and lateral direction	[degree]
F_{final}	combined hydrodynamic and aerodynamic force	[N]
M_{final}	combined hydrodynamic and aerodynamic moment	[N-m]

The wave-current directionality is not considered.

4.3 Design load cases (DLC)

The IEC has mentioned several load cases for ULS. For each load case the IEC has mentioned specific wind, wave, current and water level conditions. The current modelling is explained in the section 4.2.1.2. The wind speed, wave height and water level modelling is explained in this section. For each DLC a partial safety factor is specified. The loads obtained from the simplification are multiplied by the partial safety factor of 1.35 and 1.1 for normal and abnormal situation respectively [54]. The buoyancy force and gravity loads are multiplied by 0.9 and 1.1 respectively [54].

4.3.1 Wind speed modelling

The power law profile (Eq. 4.13) is applicable for the Normal Wind Profile(NWP),Normal Turbulence Model (NTM), Extreme Direction Change (EDC) and Extreme Turbulence Model (ETM) without any change. For Extreme Wind Model (EWM), the reference wind speed is multiplied by 1.3 and 1.04 in Eq. 4.13 to get the extreme 50 and 1 year wind speeds. For Reduced Wind Model (RWM), the reference wind speed is multiplied

by 1.1 and 0.88 in Eq. 4.13 to get the reduced 50 and 1 year wind speeds. For Extreme Operating gust (EOG), the gust speed is given as an input by the designer. The wind speed is $V_h + 0.74V_{gust}$. For Extreme Coherent gust with Direction change (ECD), the wind speed is taken equal to $V_h + V_{cg}$ where V_{cg} is coherent gust specified in the IEC standard [32]. For Extreme Wind Shear (EWS) wind speed is taken equal to:

$$V_{EWS} = V_h - 2\frac{z - z_{hub}}{D}(2.5 + 0.2 * \sigma\beta\frac{D}{\Lambda}) \tag{4.19}$$

where,

σ	standard deviation in wind speed	[m/s]
β	constant (6.4)	[-]
Λ	longitudinal turbulence scale	[m]
z	height above MSL	[m]
α	Power law coefficient	[-]

The wind speed calculated from these models is used in the calculation of the drag load.

4.3.2 Wave height modelling

For the Normal Sea State (NSS), Normal Wave Height (NWH), Severe Sea State (SSS) and Extreme Sea State (ESS) the wave height and period is determined from the met ocean data. For the Extreme Wave Height (EWH) model, 50 and 1 year wave heights are calculated by multiplying 50 and 1 year extreme significant wave heights by 1.86. For Reduced Wave Height (RWH), 50 and 1 year wave heights are calculated by multiplying 50 and 1 year extreme significant wave heights by 1.1. For Severe Wave Height (SWH) a designer has to give wave height input corresponding to SSS. The SWH is calculated by multiplying the SSS by 1.86.

4.3.3 Water level modelling

For water level data the IEC has mentioned three models. The hydrostatic head (water level) is chosen based on the given DLC. If DLC has specified to use MSL model then

the water level difference between inside and outside monopile is taken zero. If DLC mentions to use Normal Water Level Range (NWLR) model then in Eq.4.11, 1 year extreme values are used. If DLC mentions to use Extreme Water Level Range (EWLR) model then 50 year extreme values are used in Eq. 4.11.

4.3.4 Implemented design load cases

In IEC design standard a number of load cases are mentioned [54]. The simplification of the wave and aerodynamic loading has enabled to implement the following ULS load cases:

TABLE 4.1: The implemented design load cases

Power production
Power production plus occurrence of fault
start up
Normal shut down
Emergency shut down
Parked
Parked plus fault condition

The user is required to give design load case number as an input in the design tool[1]. The ULS loads are determined based on the static response only.

4.4 Stress concentration factors

The DNV standard is followed for stress concentration factors modelling [63]. The stress concentration factors are applied at locations where dimensions change abruptly. For the application of the stress concentration factors, it is assumed that the welds are single sided girth welds with full penetration. The misalignment due to manufacturing tolerances is unknown. The DNV has addressed this issue in its equation. Eq. 4.20

[1]For alpha-numeric DLC, an alphabet should be replaced with a number corresponding to its position in the English chart. For eg. DLC 6.1a should be written as 6.11.

gives the stress concentration equation.

$$SCF = 1 + \frac{3e}{t}$$
$$e = \text{min of} \begin{cases} 3mm \\ 0.2t \end{cases} \tag{4.20}$$

where,

e	misalignment	[mm]
t	thickness of the section	[mm]

The SCF is applied at the bottom of each section of the turbine tower and between transition piece and grout at the transition piece base. No SCF is applied at the mudline.

4.5 Structural stability

For the ultimate strength of the structure, yielding and buckling checks are performed. The material factor specified by respective design standard is used. Following items are neglected for the simplification:

- Secondary steel items like platform weight, J-tube, flanges etc.
- Effect of axial and lateral ice loading, marine growth

4.5.1 Yield criterion

The von misses stress criteria is used for the yield strength.

$$\frac{\sqrt{\sigma_x^2 + \sigma_y^2 - \sigma_x\sigma_y + 3\tau^2}}{\frac{\sigma_{yield}}{\gamma_m}} - C = 0 \tag{4.21}$$

where,

σ_x	stress in longitudinal direction	[N/m^2]
σ_y	stress in lateral direction	[N/m^2]
τ	stress due to torsion	[N/m^2]
σ_{yield}	yield limit of the material	[N/m^2]

4.5.2 Buckling

In this section simplification of the buckling design procedure is handled. For this project the GL design standard is consulted for the buckling calculation.

4.5.2.1 Torsional buckling

For torsional buckling GL standard suggests to use NORSOK n-004 for D/t $<$ 120 and API-LRFD for 120$<$D/t $<$ 300 design standards:
Equation for API-LRFD:

$$\frac{\tau_t}{F_v} - C = 0 \tag{4.22}$$

where,

τ_t	maximum torsional shear strength	[N/m^2]
F_v	nominal shear strength	[[N/m^2]

Equation for NORSOK n-004:

$$\begin{aligned} \frac{\frac{M_{sd}}{M_{RedRd}}}{\sqrt{(1.4 - \frac{V_{sd}}{V_{Rd}})}} - C = 0 \quad \text{for} \frac{V_{sd}}{V_{Rd}} \geq 0.4 \\ \frac{M_{sd}}{M_{RedRd}} - C = 0 \quad \text{for} \frac{V_{sd}}{V_{Rd}} < 0.4 \end{aligned} \tag{4.23}$$

where,

V_{sd}	maximum beam shear stress	[N/m^2]
V_{Rd}	maximum torsional shear strength	[N/m^2]
M_{sd}	nominal shear strength	[[N/m^2]
M_{RedRd}	maximum beam shear stress	[N/m^2]

4.5.2.2 Global buckling

An equation for global buckling is given by:

$$\frac{N_d}{\kappa N_p} + \frac{\beta_m M_d}{M_p} + \Delta n - C = 0 \tag{4.24}$$

where,

N_d	design load	[N]
N_p	plastic tip resistance	[N]
κ	reduction factor for flexural buckling	[-]
M_p	plastic resistance moment	[N-m]
M_d	design moment	[N-m]
β_m	moment coefficient	[-]

4.5.2.3 Local buckling

An equation for the local buckling criterion is given by:

$$(\frac{\sigma_x}{\sigma_{xu}})^{1.25} + (\frac{\sigma_\phi}{\sigma_{\phi u}})^{1.25} - C = 0 \tag{4.25}$$

where,

σ_x	design axial stress	[N/m^2]
σ_{xu}	ultimate axial buckling stress	[N/m^2]
σ_ϕ	design circumferential stress	[N/m^2]
$\sigma_{\phi u}$	ultimate circumferential buckling stress	[N/m^2]

For further clarification consult the GL offshore wind turbine design standard [13]. The turbine tower is made up of sections and each section has a different thickness value. The highest stress is at the bottom of the each section. The overall highest moment on the support structure is at the mudline. The buckling check is performed at the mudline, the bottom of the transition piece and the bottom of each section of the turbine tower.

4.6 Natural frequency

For simplification of the natural frequency a number of assumptions are made:

- Thickness of the turbine tower at intermediate sections is scaled linearly
- Soil stiffness is calculated using API standard [6]
- Secondary steel items like platform weight, J-tube, flanges etc. are neglected
- Grout is not included in the calculation

4.6.1 FEM Modeling

The support structure is represented by a beam and each element of the support structure is defined by two nodes. In the implemented model each discretized section has a length of 1m. For the overlap section of transition piece and monopile, wall thickness is taken equal to the summation of transition piece, monopile and grout thicknesses. The diameter of the overlap area is set equal to transition piece diameter. Each discretized section is considered of cylindrical shape. The monopile and transition piece have constant diameter and thickness. The turbine tower of the support structure has a tapered geometry with varying thickness. For the turbine tower, the diameter of each section is taken equal to the bottom diameter.

4.6.2 Mass and stiffness matrix

In this section a finite element models of the support structure and soil stiffness are explained.

4.6.2.1 Beam element matrices

There are different theories postulated for beam elements, the Euler-Bernoulli theory and the Thimoshenko theory. The Euler-Bernoulli beam theory is the oldest theory and it determines vertical and lateral deflection of the element. The Euler-Bernoulli beam theory assumes that beam axis always remain normal to neutral axis even after bending. The shear effect is neglected in the Euler-Bernoulli beam theory. The Euler-Bernoulli beam theory under predicts the deflections and over predicts the natural frequencies [64]. The Euler-Bernoulli beam theory is applicable and gives good results for beams with length to thickness ratio greater than 20. The offshore wind support structures are considered as slender structures and have diameter to thickness ratios greater than 20 at each section. Therefore Euler-Bernoulli beam theory is applied in this thesis. The mass (M) and elastic stiffness (K_e) matrices are:

$$M = \frac{\rho_m A_s l}{420}\begin{bmatrix} 156 & 22l & 54 & -13 \\ & 4l^2 & 13l & -3l^2 \\ & & 156 & -22l \\ sym & & & 4l^2 \end{bmatrix}$$
$$K_e = \frac{EI}{L^3}\begin{bmatrix} 12 & 6l & -12 & 6l \\ & 4l^2 & -6l & 2l^2 \\ & & 12 & -6l \\ sym & & & 4l^2 \end{bmatrix} \tag{4.26}$$

where,

ρ_m	density of material	[kg/m^3]
A_s	element area	[m^2]
l	element length	[m]
E	modulus of elasticity	[kg/m^2]
I	second moment of area	[m^4]

The offshore wind turbine is loaded axially with RNA. When the beam element is loaded axially, the interaction between the axial force and the lateral deformation of the structure needs to be included in the analysis. These effects are known as P-Δ effects. For

slender structures like wind turbines, axial load affects the structural stiffness and in turn affects the natural frequency [65]. The geometrical stiffness matrix (K_g) is given as:

$$K_g = -P \begin{bmatrix} 1.2/L & 0.1 & -1.2/L & 0.1 \\ & 2L/15 & -0.1 & -L/30 \\ & & 1.2L & -0.1 \\ sym & & & L/15 \end{bmatrix} \tag{4.27}$$

where, P is the RNA mass.

4.6.2.2 Soil stiffness model

To calculate the natural frequency and structural stability of the structure a FEM of soil is included. Different soil modeling methods are available. Most models are differentiated based on the linear and non linear spring model. For this project a linear spring model is used to minimize the computational time [66]. The most used method is the Winkler approach because of its simplicity [67]. But it is also the least accurate model, since it neglects the shear capacity of the soil [68]. In this approach soil is modeled as a linear lateral spring. For non linear spring models readers can refer to [69][70]. The soil stiffness model is added to the support structure stiffness model. The soil spring is attached to a beam element at each node:

$$K_s = kl \begin{bmatrix} \frac{13}{35} & \frac{11}{210}l & \frac{9}{70} & \frac{-13}{420}l \\ & \frac{1}{105}l^2 & \frac{13}{420}l & \frac{-1}{140}l^2 \\ & & \frac{13}{35} & \frac{-11}{210}l \\ sym & & & \frac{-1}{105}l^2 \end{bmatrix} \tag{4.28}$$

where, k is the soil stiffness and has unit N/m. Soil stiffness changes with the depth and soil layer. The API design standard is followed for the calculation of the soil stiffness. Eq. 4.29 gives the value of soil stiffness at particular soil depth H:

$$k = \text{min of} \begin{cases} (C_1 H + C_2 D)\gamma H \\ C_3 D \gamma H \end{cases} \tag{4.29}$$

where,

C_1, C_1, C_3	coefficients	[-]
H	soil depth	[m]
D	foundation diameter	[m]
γ	sub unit weight	[kg/m^3]

Coefficients C_1, C_2 and C_3 depend upon friction angle and are determined from Fig. 4.1.

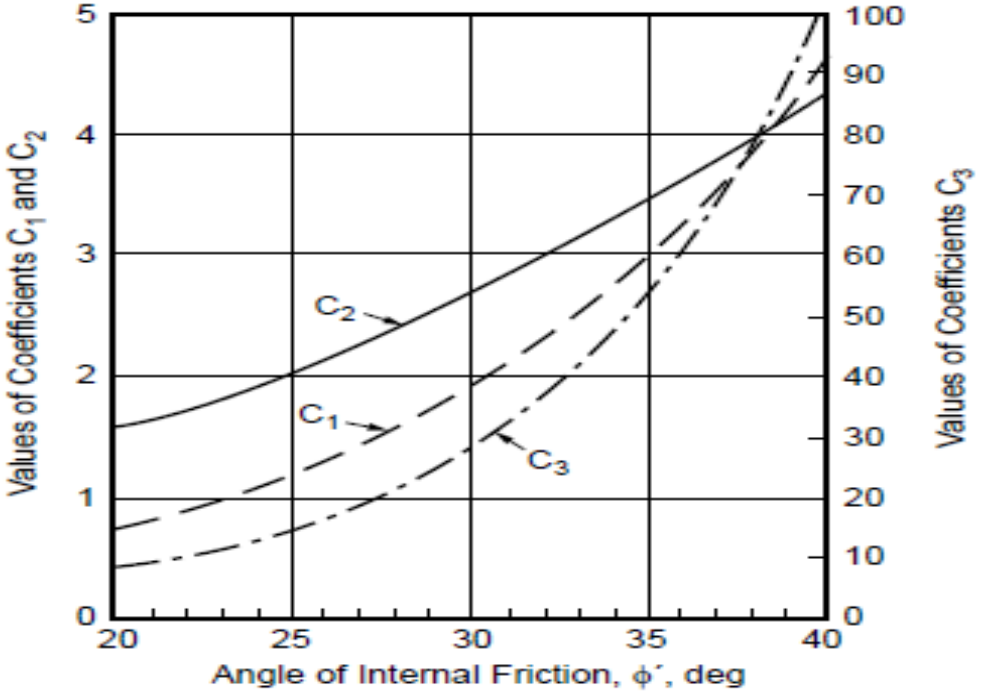

FIGURE 4.1: Stiffness coefficients as a function of friction angle.[6]

The final stiffness matrix consists of elastic, geometric and soil matrices:

$$K = K_e + K_g + K_s \tag{4.30}$$

The simplified model of offshore support structure is shown in Fig. 4.2. The t, n and k in the figure represent the element, node and soil spring stiffness.

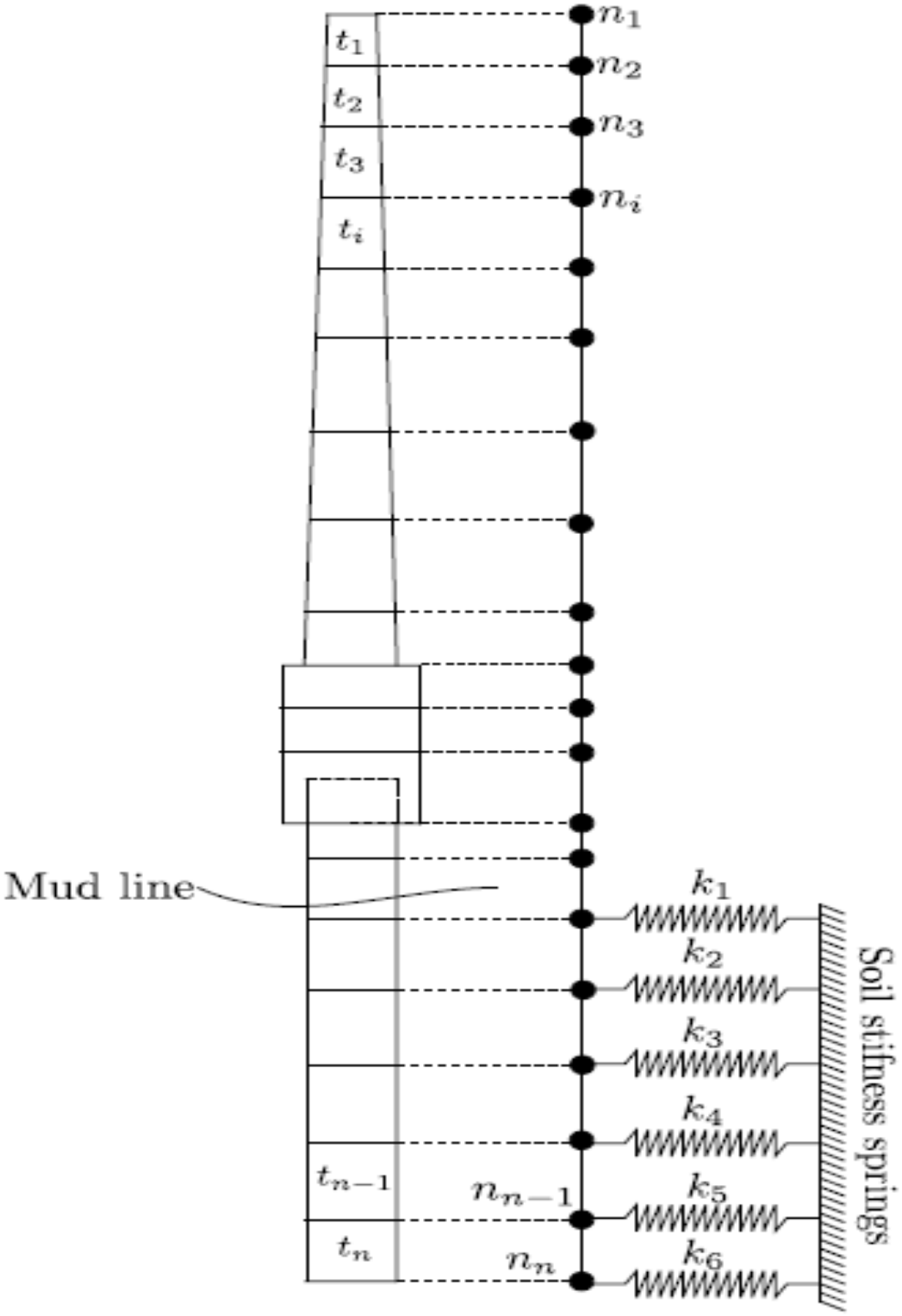

FIGURE 4.2: FEM of offshore wind turbine support structure.[7]

4.6.3 Natural frequency calculation

The dynamic equilibrium equation for the support structure is given by:

$$M_g\ddot{q} + K_g q = 0 \tag{4.31}$$

Using the eigenvalue problem the first natural frequency of the structure can be found out using 4.32:

$$M_g w^2 - K_g = 0 \tag{4.32}$$

where M_g and K_g are global mass and stiffness matrices and w is the diagonal matrix containing eigenfrequencies. For calculation of the global mass and stiffness matrix refer to [71]. The lowest eignfrequency is the natural frequency of the structure.

4.7 Foundation stability

For calculation of penetration length the loads are divided by the bearing capacity factor of 0.8 after application of partial safety factor [6].

4.7.1 Axial stability

For the axial stability a criterion specified in the API design standard is used [6]. In the simplification model both plugged and unplugged models are developed. The ultimate bearing capacity is a resistance offered by the pile to the axial loading. Eq 4.33 gives the ultimate bearing capacity of the pile:

$$Q_d = Q_f + Q_p = fA_s + qA_p \tag{4.33}$$

where,

Q_d	ultimate bearing capacity	[kN]
Q_f	skin friction resistance	[kN]
Q_p	total end bearing	[kN]
f	unit skin friction capacity	[kPa]
A_s	side surface area of pile	[m^2]
q	unit end bearing capacity	[kPa]
A_p	gross end area of pile	[m^2]

In the simplification process of the plugged pile, it is assumed that the plug starts when the penetration to diameter ratio reaches 20. For a plugged pile, the outer shaft surface area and the bottom cross sectional area are used for the skin friction and end bearing capacity calculation. For an unplugged pile, the inner and outer shaft area and end annulus area are used for the skin friction and end bearing capacity calculation. The unit skin friction and end bearing capacity for the sand is given by:

$$\begin{aligned} f &= Kp_0 tan\delta \\ q &= p_0 N_q \end{aligned} \tag{4.34}$$

where,

K	coefficient of lateral earth pressure	[-]
p_0	effective overburden pressure	[Pa]
δ	friction angle between the soil and pile wall.	[deg]
N_q	bearing capacity factor	[-]

For an unplugged and plugged piles a value of K is taken as 0.8 and 1.0 respectively. The value of the bearing capacity factor depends upon the friction angle of the soil layer. Depending upon the density of the sand layer, maximum values of limiting skin friction and limiting unit end bearing values are listed in the API standard [6]. Values calculated from Eq. 4.34 are compared with API values and the lowest of the two is selected for the design. The ultimate bearing capacity of the structure is equated with the axial load of

the structure:

$$Q_d - f_z = 0 \tag{4.35}$$

where,

f_z	axial load	[kN]

4.7.2 Lateral stability

For the calculation of the lateral stability different soil models are studied. Most important are Brom, Blum, Non Dimensional Model (NDM) and FEM based models. Blum's method is widely used for the quick estimation of penetration length. In Blum's model the pile is considered to have zero displacement at the penetration length. This is allowed if the obtained penetration length is multiplied by 1.2. Blum's model is suitable for layered sandy soils. Brom's method is more suitable for clay soils. It has been expanded for cohesionless soils also. Brom's model overestimates the deflections and the model is conservative for cohesionless soils. It is not a reliable model for sandy soils. For NDM, the main assumption is that the stiffness of the soil increases linearly. In this method p-y curves have to be created manually and minimum two iterations have to be performed which makes it a time consuming process [72]. In addition, soil has to be homogeneous. The FEM model is the most reliable and accurate model but it increases the computation time considerably. Based on above findings Blum's model is selected for a quick calculation of the penetration length.

In Blum's model, the response of the soil is assumed to be elasto-plastic for lateral force. When the lateral force acts towards the right (Fig. 4.3), the soil on the right hand side is at passive earth pressure. The passive earth pressure occurs when soil is forced to its limiting strength in compression. On the other hand, soil on the left hand side is at active soil pressure, that is soil is at failure condition in extension.

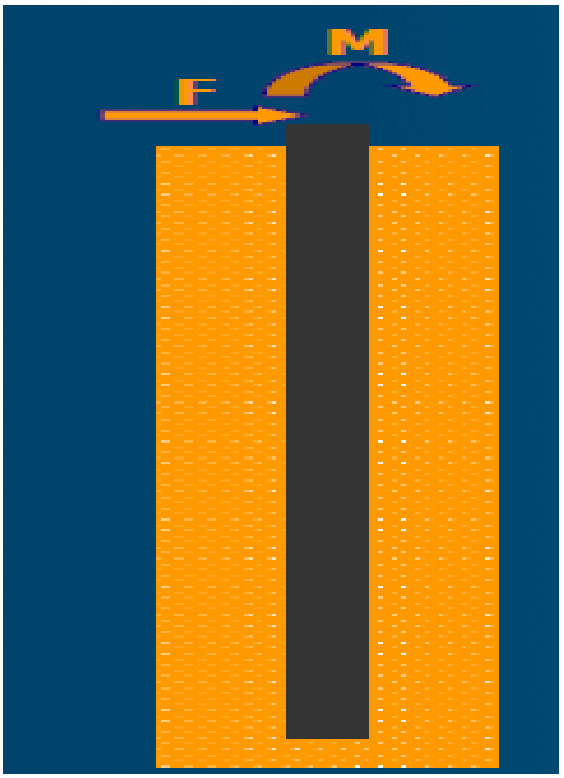

FIGURE 4.3: Force and moment on pile.

The penetration length is given by:

$$\begin{aligned} \sigma_0 p_l^2 - 6(F + \frac{M}{p_l}) &= 0.0 \\ \sigma_0 = \sum_0^n (K_{p_n} - K_{a_n}) D \gamma_n \frac{l_n}{p_l} & \\ K_{p_n} = \frac{1 + sin\delta}{1 - sin\delta} & \\ K_{a_n} = \frac{1 - sin\delta}{1 + sin\delta} & \end{aligned} \tag{4.36}$$

where,

σ_0	stress	[N/m^2]
p_l	penetration length	[m]
D	foundation diameter	[m]
γ	sub unit weight	[kg/m^3]
l_n	nth soil layer	[m]
F	force on pile top	[N]
M	moment on pile top	[N-m]
K_p, K_a	passive and active pressure coefficients	[-]

A detailed derivation of Blum's model can be read in [73].

4.8 Grout stability

As discussed in the section 2.12, the DNV has suggested to use cylindrical shape piles with shear keys or conical shape steel shells. The DNV has only proposed formulas for cylinders with shear keys. For this project simplification is carried out for cylindrical shape piles with shear keys. The shear stress in the grouted connection due to axial load and torque is given by:

$$\begin{aligned} \tau_{sa} &= \frac{P}{2R_p\pi L} \\ \tau_{st} &= \frac{M_z}{2R_p^2\pi L} \end{aligned} \tag{4.37}$$

where,

τ_{sa}	shear stress due to axial loading	[N/m^2]
P	axial loading	[N]
R_p	monopile radius	[m]
L	grout length	[m]
τ_{st}	shear stress due to torsion	[N/m^2]

The ultimate strength of grout due to friction and shear keys is given by:

$$\begin{aligned} \tau_{kf} &= \frac{\mu E \delta}{K R_p} \\ \tau_{ks} &= \frac{\mu E h f_{ck}^{0}.4\sqrt{\frac{t_p}{R_p}} sN}{21 sKL} \\ K &= \frac{R_p}{t_p} + \frac{E t_g}{E_g R_p} + \frac{R_s}{t_s} \\ s &= 2\sqrt{R_p t_p} \\ \frac{h}{s} &= 0.05 \\ N &= \frac{2L}{s} \\ \tau_{sa} &\leq \frac{\tau_{ks}}{\gamma_m} \\ \tau_{st} &\leq \frac{\tau_{kf}}{\gamma_m} \end{aligned} \tag{4.38}$$

where,

τ_{kf}	interface shear strength due to friction	[N/m^2]
μ	grout to steel interface coefficient of friction	[-]
δ	height of surface irregularities	[m]
K	stiffness factor	[-]
E	modulus of elasticity for steel	[N/m^2]
τ_{ks}	interface shear strength due to shear keys	[N/m^2]
h	shear key outstand	[m]
s	shear key spacing	[m]
f_{ck}	characteristic compressive cube strength of the grout	[Pa]
N	number of shear keys	[-]
t_p	wall thickness of pile	[m]
t_g	thickness of grout	[m]
E_g	modulus of elasticity for grout	[Pa]
t_s	transition piece thickness	[m]
R_s	transition piece radius	[m]

The selection of the spacing distance and shear outstand to spacing ratio is based on the experiment performed at the Leibniz University [50]. The ultimate capacity of grout is

given by:

$$\tau_{kg} = k f_{ck}^{0}.7(1 - e^{-2L/R_p}) \tag{4.39}$$

where,

τ_{kg}	characteristic shear strength of the grout	[N/m^2]
k	early age cycling reduction factor	[-]

To satisfy the structural requirements, the following condition should be met:

$$\sqrt{\tau_{st}^2 + \tau_{sa}^2} - \frac{\tau_{kg}}{\gamma_m} \leq 0.0 \tag{4.40}$$

where,

γ_m	material safety factor	[-]

The material safety factor of 3.0 is used.

Chapter 5

Verification of the simplified process

5.1 Introduction

The simplified design process and models are explained in Chapter 3 and 4. The case study assesses the validity of the simplified design process. In the case study simplified design process is applied to get the dimensions of support structures at new locations within an offshore wind farm. Next, the detailed design is carried out at new locations and then dimensions obtained from the simplified design and detailed design are compared. The design tool developed for this thesis is able to design for natural frequency and structural stability constraints. The structural stability constraint contains torsional, local, global buckling and yield checks. Therefore in the case study two scenarios are considered:

1. The monopile is subjected to the natural frequency constraint and thicknesses of the transition piece and turbine tower sections are subjected to structural stability constraint.
2. The monopile diameter and thicknesses of the transition piece and turbine tower sections are subjected to only the structural stability constraint.

Next, based on these two scenarios an application of the simplified design process for a wind farm is explained.

The actual input data of a wind farm was difficult to obtain therefore fictitious data is used for the case study. The input data is obtained from the civil department of Delft University of Technology. The data used for the case study is listed in Appendix A. The detailed design could not be carried out as described in the Chapter 2 because of the time constraints and complexity of the design. Some design aspects are neglected for the detailed design, which are listed down below:

- Vortex shedding frequency analysis is not performed
- Design of secondary steel materials and their impact on the structural stability is ignored
- C_m and C_d values are considered constant over the time scale of the project

For the detailed design, the natural frequency and penetration length are determined using Ansys software while loading on the structure is determined using Bladed software. The layout optimization is not carried out for the wind farm. Therefore the reference location for the detailed design is selected based on the water depth range. For the case study a 3.6MW turbine is used. The safety margin of 10% is applied on the natural frequency calculation. The desired natural frequency of the structure is kept at 0.29 Hz. The ULS load cases specified by the IEC are performed for the detailed design [54]. The DLC 6.1b (idling with yaw error of 8°) was found to be the dominant ULS with local buckling as the design driver for the turbine tower and transition piece thicknesses in both scenarios. The design driver value of 0.9 is kept for local buckling. For both scenarios the simplified design is carried out for the DLC 6.1b. Environmental parameters change from location to location within a wind farm and this affects the support structure dimensions. The effectiveness of the simplified design process to changes in environmental parameters is also studied. The environmental parameters for which the effectiveness of the simplified design is studied are soil, wave height, wave period, current speed, turbulence intensity and water depth. To study the effectiveness, each parameter is varied one by one and in the end all parameters are varied together. Results of the variations are presented in a tabular form. The simplified design term in table stands for the design tool output while final dimensions term stands for dimensions after application of the correction factors.

The case study is performed to check the effectiveness of the simplified process. However, the process can not give the same results as the detailed design. This is due to the basic assumption that correction factors obtained from the reference location can be applied even after varying the input parameters. The difference between results obtained from detailed and simplified process are carefully reviewed.

5.2 Reference design and correction factors

5.2.1 Scenario 1

In the first scenario both natural frequency and buckling constraints are applied. Table 5.1 gives the result of the detailed design, simplified design and corresponding correction factors.

TABLE 5.1: The comparison of detailed and simplified design and calculation of correction factors for scenario 1

20m water depth (Reference depth)			
Parameter	Detailed design	Simplified design	Correction factor
Monopile diameter (m)	5.6	5.9	0.94915
Penetration length (m)	38.0	42.5	0.89412
Transition piece diameter (m)	5.9	6.23	-
Transition piece thickness (mm)	67	62	1.0806
Turbine tower thickness in mm			
1	43.7	40.4	1.0817
2	41.8	39.5	1.058
3	39.3	37.5	1.048
4	37.3	35.4	1.053
5	33.1	31.1	1.064
6	26.8	25.3	1.0593

The monopile diameter is mainly dependent upon the natural frequency modeling. The natural frequency depends upon the length, stiffness, mass of the structure and top mass.

For the simplified and detailed design the top mass remains the same. The stiffness of the structure depends upon the structural and soil modelling. The largest uncertainty is involved in the soil modelling and soil-pile stiffness calculation. The penetration length of the simplified model is greater than the detailed design. As the transition piece and turbine tower have smaller thicknesses compared to the detailed design, this yields lower structural stiffness. The increase in structural diameter has more effect on the stiffness of the structure than on the mass in the natural frequency calculation. To achieve the natural frequency constraint the stiffness has to be increased. This can only be achieved by increasing the monopile diameter due to the design strategy. Therefore, the monopile diameter is larger in the simplified design than the detailed design. The transition piece and turbine tower base diameters depend upon the monopile diameter. These diameters are also larger than the detailed design diameters.

The buckling value of any section depends upon the diameter, thickness and loads acting on it. The buckling value increases with loads and decreases with diameter and thickness. The diameters of the transition piece and turbine tower sections are larger than the detailed design. The larger diameter offers equal bending resistance at lower thickness value. Therefore the buckling constraint is achieved at smaller thickness for the transition piece and turbine tower sections in simplified design than the detailed design process.

The penetration length obtained from the simplified design is larger than the detailed design. Among the axial and lateral stability, the lateral stability governs the penetration length calculation. The penetration length varies directly and indirectly with loads on pile top and soil-pile stiffness respectively. The loads are larger in the simplified model due to larger dimensions. The stiffness of the soil is directly dependent upon the accuracy of Blum model and diameter of the structure. The diameter of the foundation is greater in the simplified design than the detailed design. This leads to the higher soil-pile stiffness in the simplified model. But after multiplying penetration length obtained from Blum model by 1.2, it is greater than the detailed design.

For grout length, the DNV standard's suggestion of 1.5 times the monopile diameter governs the design.

5.2.2 Scenario 2

In the second case study, only the buckling constraint is applied on the support structure. Table 5.2 gives the result of the detailed and simplified design and corresponding correction factors.

The monopile diameter obtained from the simplified design is greater than the detailed design. As said in the earlier section 5.2.1, the buckling value increases with the loads and decreases with diameter. The simplified design slightly over predicts loads. Therefore the buckling value is satisfied at larger diameter than the detailed design.

The penetration length obtained from the simplified design is larger than the detailed design. The larger monopile diameter gives higher soil-pile stiffness but higher loads and multiplication factor of 1.2 in Blum model together leads to the overprediction of the penetration length. The transition piece and turbine tower thicknesses are under predicted due to the higher diameters.

In this scenario also penetration length is governed by the lateral stability and grout length by DNV standard's suggestion.

TABLE 5.2: The comparison of detailed and simplified design and calculation of correction factors for scenario 2

20m water depth (Reference depth)			
Parameter	Detailed design	Simplified design	Correction factor
Monopile diameter (m)	5.4	5.73	0.9425
Penetration length (m)	40.0	42.7	0.9368
Transition piece diameter(m)	5.7	6.06	-
Transition piece thickness (mm)	67	65	1.03
Turbine tower thickness in mm			
1	44.1	41.2	1.07
2	42.2	40.0	1.055
3	38.9	37.6	1.035
4	37.2	36.8	1.011
5	34.3	33.3	1.03
6	27.0	25.2	1.071

5.3 Effect of changes in water depth

After carrying out detailed and simplified design at the reference location, the effectiveness of the simplified design to changes in water depths is checked. For both scenarios water depth is varied from 10m to 40m in steps of 10m while other input values are kept constant.

5.3.1 Scenario 1

The results for the monopile diameter are given in Table 5.3. In this scenario, the monoile diameter is decided by the natural frequency constraint. The natural frequency value decreases when the length of the part of the structure above mudline increases. To compensate for this, the stiffness of the structure has to be increased to satisfy the natural frequency constraint. This leads to the larger monopile diameter for deeper water depths. As we move away from the reference design, the error in the detailed

design and simplified design with correction factors increases. For deeper water depths compared to the reference design, the simplified design after application of correction factors under predicts the monopile diameter.

TABLE 5.3: The response of the simplified design for monopile diameter to water depth variation for scenario 1

Monopile diameter comparison			
Water depth (m)	Detailed design (m)	Final dimensions (m)	Error (%)
10	5.3	5.24	1.13
20	5.6	5.6	0.0
30	6.0	6.0	0.0
40	6.5	6.45	0.704

The changes in the water depth affects the transition piece dimensions too. The results for transition piece diameter and thickness are given in Table 5.4 and 5.5 respectively. In the simplified transition piece design model, the transition piece base is kept above 6m from the water depth. The transition piece base value increases with the water depth. This leads to the higher moments and forces on the transition piece base. This increases the thickness of the transition piece. The transition piece diameter is dependent on the monopile diameter, grout and transition piece thickness. The grout thickness is kept constant due to installation constraints. The monopile diameter and transition piece thickness value increases with the water depth and this leads to the increased transition piece diameter with water depth.

TABLE 5.4: The response of the simplified design for transition piece diameter to water depth for scenario 1

Transition piece diameter comparison			
Water depth (m)	Detailed design (m)	Final dimensions (m)	Error (%)
10	5.6	5.53	1.25
20	5.9	5.9	0
30	6.4	6.3	1.45
40	6.9	6.77	1.86

TABLE 5.5: The response of the simplified design for transition piece thickness to water depth for scenario 1

Transition piece thickness comparison			
Water depth (m)	Detailed design (mm)	Final dimensions (mm)	Error (%)
10	59	61.6	-4.4
20	67	67	0
30	75	75.64	-0.86
40	81	83.2	-2.278

The result for the penetration length is given in Table 5.6. As discussed in section 5.2.1, the penetration length depends upon the loads and soil-pile stiffness of the support structure. The effect of increased loads with water depth is nullified by the increased diameter of the structure. The penetration length is slightly increased with water depth. However, for 10m water depth, the support structure experiences the breaking wave loads. The magnitude of breaking wave force is almost equal the magnitude of combined inertia and drag force. This resulted in the increased penetration length for lower water depth.

TABLE 5.6: The response of the simplified design for penetration depth to water depth for scenario 1

Penetration length vs Water depth			
Water depth (m)	Detailed design (m)	Final dimensions (m)	Error (%)
10	39	41.12	-5.4
20	38	38.0	0
30	39	39.16	-0.41
40	40	40.23	-0.588

The turbine tower base diameter is kept equal to the transition piece diameter. Therefore, the turbine tower diameter has increased with the water depth. The drag load on the structure increases with increased diameter. But the magnitude of drag load is relatively smaller than the hub load. The resistance to loading can be achieved at

lower thickness values for larger diameters. The result for the turbine tower thickness is given in Table 5.7. The number 1 section corresponds to the tower section closest to the transition piece. The turbine tower section thickness decreases with increasing water depth.

TABLE 5.7: The response of the simplified design for turbine tower section thickness to water depth for scenario 1

Turbine tower section thickness comparison			
Turbine tower section	Detailed design (mm)	Final dimensions (mm)	Error (%)
for 10m water depth			
1	47.1	47.81	-1.5
2	46.2	46.52	-0.69
3	44.3	43.6	1.5
4	41.1	41.2	-0.243
5	35.5	36.7	-3.9
6	27.3	27.9	-2.04
for 30m water depth			
1	40.7	40.67	0.07
2	37.8	38.5	-1.9
3	36.3	37.62	-3.65
4	34.8	36.45	-4.76
5	31.1	32.35	-4.03
6	26.3	27.22	-3.51
for 40m water depth			
1	36.9	37.75	-2.3
2	35.1	35.97	-2.5
3	34.2	35.21	-2.96
4	32.8	34.34	-4.72
5	29.7	31.92	-7.5
6	25.2	26.37	-4.66

The error in the design process is increasing as design moves in deeper or shallower

water depths than the reference location. In the simplified design, except for turbulence intensity, hub load is kept independent of environmental variation. But in reality load-structure interaction has an effect on the hub load. It is observed that the hub load is lowered by 2-3% for 30m and 40m water depths while for 10m water depth the hub load was same. This resulted in lower penetration length and transition piece thickness compared to the simplified design with correction factors. For deeper water depths, the monopile and transition piece diameters are under predicted while penetration length, transition piece and turbine tower thickness are over predicted.

For shallower water depth similar trend is observed. High error in penetration length and transition piece thickness is due to the consideration of breaking wave loads in the simplified design model. Bladed software does not calculate loads due to breaking waves and this has resulted in the lower estimation of penetration length and transition piece thickness for the detailed design.

5.3.2 Scenario 2

The result for the monopile diameter for the detailed design and simplified design with correction factor is given in Table 5.8. The monopile diameter has increased with water depth. As water depth increases, buckling length of the support structure, hydrodynamic and aerodynamic loading and lever arm increase with it. For monopile only diameter is the design variable. As thickness value is linked to the diameter using the API [6] formula. The monopile diameter is increased to increase the resistance to loading and satisfy the design driver constraint. For shallower and deeper water depths the simplified design with correction factors over and under predicts the monopile diameter respectively.

The explanation of the transition piece dimensions, turbine tower thickness and penetration length variation with water depth can be explained on the same line as explained in previous section. Table 5.9, 5.10, 5.11 and Table 5.12 shows the variation in the support structure dimensions with water depth.

The error pattern observed is same as scenario one. The SCF is not applied for the monopile diameter calculation. This has led to the lower monopile thickness (Eq. 3.2)

than the transition piece thickness despite of experiencing higher loads and having lower resistance to the loading than the transition piece.

TABLE 5.8: The response of the simplified design for monopile diameter to water depth for scenario 2

Monopile diameter comparison			
Water depth (m)	Detailed design (m)	Final dimensions (m)	Error (%)
10	4.8	5.0	-4.253
20	5.4	5.4	0.0
30	5.8	5.86	-1.03
40	6.3	6.32	-0.317

TABLE 5.9: The response of the simplified design for transition piece diameter to water depth for scenario 2

Transition piece diameter comparison			
Water depth (m)	Detailed design (m)	Final dimensions (m)	Error (%)
10	5.1	5.29	-3.83
20	5.7	5.7	0
30	6.2	6.23	-0.483
40	6.7	6.72	-0.298

TABLE 5.10: The response of the simplified design for transition piece thickness to water depth for scenario 2

Transition piece thickness comparison			
Water depth (m)	Detailed design (mm)	Final dimensions(mm)	Error (%)
10	58	60.81	-4.84
20	67	67	0
30	83	85.55	-3.07
40	95	97.92	-3.07

TABLE 5.11: The response of the simplified design for penetration depth to water depth for scenario 2

Penetration length vs Water depth			
Water depth (m)	Detailed design (m)	Final dimensions (m)	Error (%)
10	41	43.46	-6.05
20	40	40.0	0
30	40	41.12	-2.81
40	42	42.24	-0.59

TABLE 5.12: The response of the simplified design for turbine tower section thickness to water depth for scenario 2

Turbine tower section thickness comparison			
Turbine tower section	Detailed design (mm)	Final dimensions (mm)	Error (%)
for 10m water depth			
1	49.8	49.23	1.12
2	48.3	47.86	1.27
3	46.2	44.8	3.03
4	42.3	40.5	4.17
5	38.9	36.3	6.5
6	29.3	30.21	-3.12
for 30m water depth			
1	41.7	40.56	2.71
2	39.2	38.71	1.22
3	38.1	37.45	1.7
4	35.3	34.36	2.63
5	31.8	31.3	1.53
6	26.5	26.67	-0.67
for 40m water depth			
1	37.9	37.46	1.15
2	36.3	36.01	0.603
3	35.4	34.97	1.21
4	34.1	33.15	2.76
5	30.7	31.31	-1.99
6	26.0	26.78	-3.02

5.4 Effect of changes in soil properties

The soil properties change from location to location within a wind farm. This has an effect on the support structure dimensions. In this section, the effectiveness of the

simplified design to changes in soil properties is checked. The soil layer values are kept constant.

For scenario one, first soil properties are changed slightly to represent the variation within a wind farm. The lateral stability of the penetration length depends upon the submerged unit weight and friction angle. These two parameters are slightly varied. Next, to check the limit of applicability of the simplified process, soil is made very stiff and very soft. The stiff soil is achieved by increasing the submerged unit weight and friction angle. Input parameters for soil properties are listed in Appendix A.2.

In scenario two, the monopile diameter is determined by the buckling constraint. As already said, the buckling constraint depends upon the loading, structural length and resistance to the loading. Soil properties do not play any role in the buckling criteria. Therefore changes in soil properties only leads to the penetration length variation. Therefore for scenario two, the effectiveness of penetration length modelling to friction angle and submerged unit weight is checked. For this analysis friction angle and submerged unit weight values are increased and decreased separately in all soil layers. The value by which friction angle and submerged unit weight are changed compared to the reference value is given in the result tables.

5.4.1 Scenario 1

The slight variation in soil properties has almost a negligible effect on the support structure dimensions. But when soil properties are made very stiff or very soft dimensions of the support structure are changed considerably. Table 5.13 and 5.14 shows the results for very stiff and very soft soil respectively.

TABLE 5.13: The response of the simplified design to very stiff soil for scenario 1

20m water depth (Reference depth)			
Parameter	Detailed design	Final dimensions	Error (%)
Monopile diameter	5.2	5.15	0.8865
Penetration length	26.8	25.12	6.25
Transition piece diameter	5.54	5.46	1.365
Transition piece thickness	70	72.4	-3.43
Turbine tower thickness			
1	45.8	46.07	-0.61
2	43.1	43.49	-0.91
3	41.3	42.09	-1.75
4	37.9	38.67	-2.03
5	33.7	34.48	-2.325
6	27.3	26.7	2.219

TABLE 5.14: The response of the simplified design to soft soil for scenario 1

20m water depth (Reference depth)			
Parameter	Detail design	Final dimensions	Error (%)
Monopile diameter	5.9	5.98	-1.151
Penetration length	52	50.16	3.53
Transition piece diameter	6.2	6.26	-0.79
Transition piece thickness	63	62.8	0.307
Turbine tower thickness			
1	41.7	41.0	1.68
2	39.8	38.83	2.41
3	38.3	37.93	0.94
4	36.3	35.71	1.59
5	32.1	32.46	-1.12
6	26.2	26.37	-0.67

The soil-pile stiffness increases with increase in the submerged unit weight and friction angle of the soil. The natural frequency of the structure depends upon the stiffness of the structure and soil and mass of the structure. Qualitatively speaking, natural frequency is directly related to the stiffness of soil and structure and inversely to the top mass, length and mass of the structure. With increase in the soil stiffness less structural stiffness is required to satisfy the natural frequency constraint. The stiffness of the structure decreases with decrease in the monopile diameter. Therefore the monopile diameter decreases with increase in soil properties values.

The effect of change in monopile diameter on the other dimensions of the support structures is already explained the section 5.2.1. The error for slight variation and very soft soil is not very large. On the other hand the error in penetration length obtained for very stiff soil is quite large compared to the very soft soil and slight variation. The high error in penetration length may be because of the difference in Blum model and FEM soil model used by Ansys.

5.4.2 Scenario 2

The Table 5.15 shows the effect of submerged unit weight on the penetration length. The penetration length decreases with increase in submerged unit weight of sand. The increase in the submerged unit weight increases the effective stresses in the sand. This increases the lateral pressure exerted by sand on the foundation, which gives shorter penetration lengths.

Table 5.16 shows the effect of friction angle on the penetration length. The friction angle is a measure of the shear strength of sand. The shear strength is a measure of resistance to deformations or sliding. The shear strength increases with the friction angle. It is evident from the table that the penetration length decreases with increase in friction angle.

The error in the penetration length given by the simplified design process increases as soil becomes stiffer or softer. Especially for stiffer soil the error is higher. The reason could be the the differences in soil models implemented in the simplified design and Ansys.

TABLE 5.15: The response of the simplified design for penetration depth to submerged unit weight for scenario 2

Penetration length vs submerged unit weight			
Submerged unit weight	Detailed design (m)	Final dimensions (m)	Error (%)
Decreased by 6	55.0	57.42	-4.22
Decreased by 4	49.0	48.52	0.9797
Decreased by 2	44.0	43.46	1.228
Original	40.0	40.0	0.0
Increased by 1	38.0	38.68	-1.77
Increased by 2	36.0	37.47	-3.925
Increased by 4	32.0	33.8	-5.37

TABLE 5.16: The response of the simplified design for penetration depth to friction angle for scenario 2

Penetration length vs friction angle			
Friction angle	Detailed design	Final dimensions (m)	Error (%)
Decreased by 10	50.0	48.25	3.51
Decreased by 5	45.0	43.75	2.781
Original	40.0	40.0	0.0
Increased by 5	35.0	36.81	-5.18
Increased by 10	31.0	33.72	-8.78

5.5 Effect of changes in turbulence intensity

For DLC 6.2b, 50 year extreme wind velocity is considered for the support structure design. During idling situation turbulence intensity variation within a wind farm is low. Therefore first the support structure design is carried out for small variation in the turbulence intensity. Next, extreme variation is considered to check the applicability limit of simplified design process.

5.5.1 Scenario 1

From Eq. 4.16 and Fig. 5.1 it is evident that aerodynamic load increases with the turbulence intensity. Table 5.17, 5.18, 5.19, 5.20, 5.21 gives the result for the turbulence intensity variation on the support structure dimensions. The thickness of the turbine tower and transition piece is calculated from the buckling constraint. As the loading on the turbine tower and transition piece increases the resistance to loading is increased by increasing the thickness. The increased transition piece thickness results in increased transition piece diameter. The monopile diameter is dependent upon the natural frequency constraint. An increase in turbine tower thickness has more effect on the mass component of the natural frequency, which leads to decrease in the natural frequency. An increase in transition piece thickness has more effect on the stiffness component of the natural frequency which leads to increase in the natural frequency. Also increase in loading increases the penetration length which in turns increases the stiffness of the structure. Therefore the change in monopile diameter is not very large.

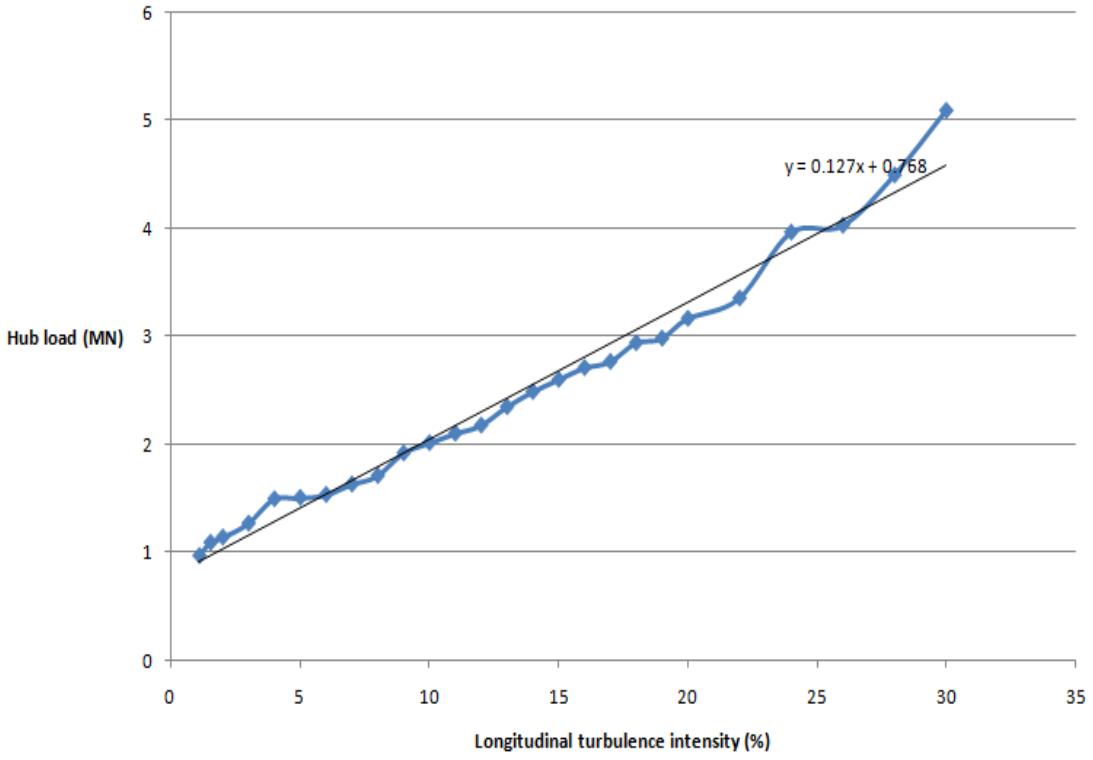

FIGURE 5.1: Hub load vs Turbulence intensity for extreme wind speed

TABLE 5.17: The response of the simplified design for monopile diameter to turbulence intensity for scenario 1

Monopile diameter comparison			
Turbulence intensity (%)	Detailed design (m)	Final dimensions (m)	Error (%)
5	5.6	5.6	0.0
10	5.6	5.6	0.0
15	5.7	5.61	1.57
20	5.8	5.66	2.41

TABLE 5.18: The response of the simplified design for transition piece diameter to turbulence intensity for scenario 1

Transition piece diameter comparison			
Turbulence intensity (%)	Detailed design	Final dimensions (m)	Error (%)
5	5.9	5.89	0.169
10	5.9	5.9	0
15	6.0	5.93	1.03
20	6.1	5.99	1.72

TABLE 5.19: The response of the simplified design for transition piece thickness to turbulence intensity for scenario 1

Transition piece thickness comparison			
Turbulence intensity (%)	Detailed design (mm)	Final dimensions(mm)	Error (%)
5	59	58.35	1.09
10	67	67	0
15	76	77.8	-2.37
20	85	87.53	-2.97

TABLE 5.20: The response of the simplified design for penetration depth to turbulence intensity for scenario 1

Penetration length vs Turbulence intensity			
Turbulence intensity (%)	Detailed design (m)	Final dimensions (m)	Error (%)
5	36	34.84	3.13
10	40	40.0	0
15	40	40.59	-1.48
20	42	42.91	-2.18

TABLE 5.21: The response of the simplified design for turbine tower thickness to Turbulence intensity for scenario 1

Turbine tower section thickness comparison			
Turbine tower section	Detail design (mm)	Final dimensions (mm)	Error (%)
for 5% turbulence intensity			
1	35.1	34.39	2.0
2	33.3	33.44	-0.42
3	31.1	31.44	-1.09
4	28.2	30.34	-7.6
5	27.1	27.35	-0.93
6	22.3	21.92	1.67
for 15% turbulence intensity			
1	47.9	50.08	-4.55
2	46.1	49.41	-7.22
3	42.2	46.12	-9.27
4	41.2	44.14	-7.15
5	37.3	40.23	-7.85
6	32.0	31.56	1.35
for 20% turbulence intensity			
1	54.2	56.57	-4.37
2	52.1	55.02	-5.61
3	50.9	53.86	-5.82
4	48.1	50.36	-4.71
5	43.0	45.97	-6.92
6	37.8	37.92	-2.5

The error in turbine tower thickness for 15% and 20% of turbulence intensity is large due to the overprediction of the hub load. In Fig. 5.1, the force calculated using the equation of straight line is higher compared to the actual force at 15% and 20% turbulence intensity. This results into higher moments on the structure. For 5% turbulence intensity the loads are under predicted which leads to the lower penetration length and transition piece thickness. To compensate for reduced stiffness the monopile given by

the simplified design method is larger than detailed design. Therefore the error is positive for penetration length and transition piece thickness and negative for monopile and transition piece diameter.

5.5.2 Scenario 2

Table 5.22, 5.23, 5.24, 5.25, 5.26 give the results for the scenario two. For scenario 2, the monopile diameter, turbine tower and transition piece thicknesses depend on the buckling constraint. As loading on the support structure increases the support structure dimensions are also increased to satisfy the buckling constraint. The error in the results for scenario two can be explained on similar line as described in scenario one.

TABLE 5.22: The response of the simplified design for monopile diameter to turbulence intensity for scenario 2

Monopile diameter comparison			
Turbulence intensity (%)	Detailed design (m)	Final dimensions (m)	Error (%)
5	4.9	4.79	2.1
10	5.4	5.4	0.0
15	5.6	5.84	-4.33
20	6.0	6.22	-3.82

TABLE 5.23: The response of the simplified design for transition piece diameter to turbulence intensity for scenario 2

Transition piece diameter comparison			
Turbulence intensity (%)	Detailed design	Final dimensions (m)	Error (%)
5	5.2	5.08	2.14
10	5.7	5.7	0
15	5.9	6.15	-4.26
20	6.36	6.53	-2.78

TABLE 5.24: The response of the simplified design for transition piece thickness to turbulence intensity for scenario 2

Transition piece thickness comparison			
Turbulence intensity (%)	Detailed design (mm)	Final dimensions (mm)	Error (%)
5	58	60.81	-4.85
10	67	57	0
15	73	71.12	2.57
20	80	75.24	5.94

TABLE 5.25: The response of the simplified design for penetration depth to turbulence intensity for scenario 2

Penetration length comparison			
Turbulence intensity (%)	Detailed design (m)	Final dimensions (m)	Error (%)
5	36	37.28	-3.56
10	40	40.0	0
15	41	42.24	-3.04
20	45	44.02	2.15

TABLE 5.26: The response of the simplified design for Turbine tower section thickness to turbulence intensity for scenario 2

Turbine tower section thickness comparison			
Turbine tower section	Detailed design (mm)	Final dimensions (mm)	Error (%)
for 5% turbulence intensity			
1	38.1	39.39	-3.38
2	37.2	37.98	-2.09
3	35.1	34.45	1.84
4	29.8	30.83	-3.46
5	27.2	27.6	-1.48
6	23.1	22.6	2.13
for 15% turbulence intensity			
1	49.2	48.48	1.44
2	47.1	46.2	1.89
3	44.3	47.07	-6.25
4	41.8	40.63	2.78
5	39.1	37.9	3.05
6	34	31.28	7.98
for 20% turbulence intensity			
1	53.1	52.12	1.83
2	50.9	49.47	2.79
3	48.2	47.38	1.69
4	45.2	45.08	0.254
5	43.4	43.26	0.319
6	36.0	36.21	-0.59

5.6 Effect of changes in wave height, wave period and current speed

Wave heights, wave period and current speed changes from location to location within a wind farm. The data obtained for the case study has not given the variation within

the wind farm. Therefore the met ocean study performed by E.On and EMU Ltd for Rampion wind farm is used as a rough estimate for the variation of wave height, wave period and current speed. The met ocean study showed the variation of upto 13% in wave height, 10% in wave period and 5% in current speed [74]. Therefore, the wave height, wave period and current speed are also varied within the mentioned range. For this study the wind generated current speed is kept constant.

5.6.1 Scenario 1

The current speed term comes into the drag load calculation. The KC number gives the idea whether hydrodynamic loading is inertia dominant or drag dominant or combination of both. The hydrodynamic load is said to be inertia dominant for KC value less than 5 and drag dominant for KC value greater than 45 in between it is combination of both. The KC value at any section is given by:

$$KC = \frac{(U_c + u_{max})T_{app}}{D} \tag{5.1}$$

where,

U_c	extreme current speed	[m/s]
T_{app}	apparent wave period	[s]
u_{max}	maximum wave particle velocity	[m/s]
D	section diameter	[m]

The wave velocity (Eq. 4.3) and current speed (Eq. 4.5 and 4.6) decreases with the water depth so does the KC number. The KC number is calculated at the highest water level. For current speed of 1.04m/s, wave period of 10s and diameter of 5.9m the KC number is 5.2. This clearly shows that hydrodynamic load is inertia dominant. Therefore changing the current value did not alter the structure dimensions. The penetration length obtained from the simplified design is increased by 0.1m. For the detailed design the change in penetration length is nil.

The increase in wave height increases the hydrodynamic loading on the structure. The total load on the structure comprises of aerodynamic and hydrodynamic loading. The

contribution of hydrodynamic load to the total load decides the effect of wave height changes on the support structure dimensions. The aerodynamic moment experienced by the support structure is 10x times the hydrodynamic moment. Therefore changes in wave height has very low impact on the support structure dimensions. The change in wave height affects the buckling criteria. The transition piece thickness is increased by 2mm for increase in wave height and decreased by 1mm for decrease in wave height. The monopile diameter is decided by the natural frequency constraint, small change in transition piece thickness did not have much effect on the monopile diameter. The change of transition piece diameter due to change in thickness did not yield any change in turbine tower thickness. The penetration length is increased by 0.3m for increase in wave height and decreased by 0.2m for decreased in wave height for the simplified design. For the detailed design 13% change in wave height did not have any significant impact.

A change in wave period also affects the hydrodynamic loading. For constant water depth, the inertia force decreases and drag force increases with wave period. This is due to the elongation of elliptical orbits for longer waves which increases the horizontal particle velocity more rapidly than horizontal particle acceleration [75]. However, 10% change in a wave period resulted in minute changes in the transition piece thickness and penetration length in the simplified design. The detailed design did not get affected by changes in the wave period.

5.6.2 Scenario 2

In this scenario, the monopile diameter is determined based on the buckling constraint. As discussed in the previous section, the changes in wave height, wave period and current speed affect the hydrodynamic loading and so does the buckling constraint. The direction of change in hydrodynamic loading with the mentioned parameters is already explained in the previous section.

The monopile diameter is not affected by the changes in current speed due to the inertia dominant hydrodynamic loading. The results for the changes in wave height are given in Table 5.27, 5.28, 5.29, 5.30, 5.31. To satisfy the buckling constraint for increased wave loading due to increase in wave height, the monopile diameter is slightly increased. For the transition piece thickness and penetration length, increase in wave loading and

monopile diameter negates the effect of each other. This resulted in the almost constant transition piece thickness and penetration length for changes in wave height. The dimensions of the support structuer are not affected by the changed in wave period.

TABLE 5.27: The response of the simplified design for monopile diameter to wave height for scenario 2

Monopile diameter comparison			
Wave height (m)	Detailed design (m)	Final dimensions (m)	Error (%)
6.7	5.2	5.26	-1.3
8.8	5.4	5.4	0.0
9.7	5.5	5.41	1.64

TABLE 5.28: The response of the simplified design for transition piece diameter to wave height for scenario 2

Transition piece diameter comparison			
Wave height (m)	Detailed design (m)	Final dimensions (m)	Error (%)
6.7	5.4	5.56	-2.41
8.8	5.7	5.7	0
9.7	6.07	5.7	2.16

TABLE 5.29: The response of the simplified design for transition piece thickness to wave height for scenario 2

Transition piece thickness comparison			
Wave height (m)	Detailed design (mm)	Final dimensions (mm)	Error (%)
6.7	66	65.96	0.04
8.8	67	67	0
9.7	68	67.0	1.47

TABLE 5.30: The response of the simplified design for penetration depth to wave height for scenario 2

Penetration length vs Water depth			
Wave height (m)	Detailed design (m)	After application of correction factor (m)	Error (%)
6.7	40	39.43	1.4
8.8	40	40.0	0
9.7	42	40.28	4.09

TABLE 5.31: The response of the simplified design for penetration depth to wave height for scenario 2

Turbine tower section thickness comparison			
Turbine tower section	Detailed design (mm)	Final dimensions (mm)	Error (%)
for 6.7m water depth			
1	44.9	43.99	2.02
2	43.3	41.98	3.02
3	39.7	38.9	2.01
4	38.8	37.3	3.86
5	34.9	34.09	2.3
6	26.7	27.0	-1.12
for 9.7m water depth			
1	43.8	44.0	-0.43
2	41.7	41.98	-0.68
3	38.4	38.9	-1.28
4	36.8	37.3	-1.34
5	34.0	34.09	-0.275
6	26.6	27.0	-1.48

For 6.7m wave height, the error obtained is low and absolute difference between detailed design and simplified design is almost same. For 9.7m wave height despite increase in loads, the monopile diameter given by simplified model did not change compared to the

reference design. This resulted in higher error for 9.7m wave height. The increase of wave height to 9.7m resulted in only 10% and 20% increase in inertia and drag loads. As already stated, the hydrodynamic loading contribution to the total loading is only 10%, therefore such a small increase in loads did not result in large increase in support structure dimensions. On the other hand reduction of wave height to 6.7m reduced the inertia and drag loads by almost 25% and 50% respectively. Therefore changes in support structure dimensions for 6.7m are larger than the 9.7m wave height.

5.7 Effect of variation of all parameters

In real wind farms a single variation of environmental parameter is rarely experienced. Mostly all environmental parameters change from location to location. For this study, the turbulence intensity, soil properties are slightly decreased while wave height, current speed are slightly increased compared to the reference location parameters. Soil layers values are also varied in this study. Input values used for the analysis are given in Appendix A.3.

5.7.1 Scenario 1

Table 5.32 gives the result for scenario one. The lower turbulence intensity and increased monopile diameter has given lower penetration length and turbine tower thickness. The decrease in soil properties and penetration length has resulted in decreased soil-pile stiffness. The monopile diameter is increased to compensate for this. The combine effect of lower turbulence intensity and increased wave height, current speed and monopile diameter has resulted in almost negligible change in transition piece thickness.

TABLE 5.32: The comparison of detailed and simplified design and calculation of correction factors for scenario 1

Parameter	Detailed design	Final dimensions	Error (%)
Monopile diameter (m)	5.9	5.82	1.223
Penetration length (m)	38.0	37.3	1.88
Transition piece diameter (m)	6.3	6.12	2.74
Transition piece thickness (mm)	67	69.16	-3.22
Turbine tower thickness in mm			
1	36.1	37.42	-3.63
2	34.9	36.4	-4.3
3	34.2	35.42	-3.57
4	31.7	33.5	-5.69
5	29.3	30.8	-5.34
6	25.2	24.57	2.47

5.7.2 Scenario 2

Table 5.33 gives the result for scenario two. The magnitude of increase in hydrodynamic loading compared to decrease in aerodynamic loading is higher. This has resulted in slight increase in monopile diameter and transition piece thickness. Due to the increased diameter the penetration length is slightly decreased. The turbine tower thickness is decreased due to the lower aerodynamic loading.

TABLE 5.33: The comparison of detailed and simplified design and calculation of correction factors for scenario 2

Parameter	Detailed design	Final dimensions	Error(%)
Monopile diameter (m)	5.6	5.45	2.56
Penetration length (m)	40.0	39.43	1.4
Transition piece diameter (m)	6.0	5.75	4.05
Transition piece thickness (mm)	65	68.03	-4.66
Turbine tower thickness in mm			
1	38.9	39.4	-1.2
2	38.1	38.5	-1.06
3	36.2	36.4	-0.599
4	33.2	32.85	1.04
5	29.7	29.9	-0.57
6	24.0	25.4	-5.8

5.8 Analysis of application of the simplified design process

As explained in section 3.2, at the reference location main design driver constraint should be identified. After comparing the dimensions of support structures from two scenarios (section 5.2) at the reference location, it is evident that the natural frequency is the dominant constraint for the monopile and local buckling for the transition piece and turbine tower thickness. According to the principle of the simplified design process, the support structure should be designed using the same design drivers at other locations within a wind farm. If we compare the results of both scenarios for variation in environmental properties, the stated principle holds valid. But when the variation is extreme like making soil very stiff or very soft (section 5.4), increasing turbulence intensity by 100% (increase from 10% to 20%, section 5.5)the buckling constraint becomes dominant for the monopile. In such circumstances simplfied design process will not hold good. It is very unlikely that such extreme variation in soil properties will be experienced in the wind farm. Even the extreme turbulence intensity variation is highly unlikely during the extreme wind speed scenario. But if the dominant load case is during power production

then the variation of 10% to 20% turbulence intensity within a wind farm is possible. In such circumstances an engineering judgment should be made before applying the simplified design process principle.

5.9 Validation of aerodynamic simplified models

From the case study, the response of the design tool to the variation in input parameters is studied. During the case study, the proposed aerodynamic simplified method (4.2.3.2) is verified for idling condition (DLC 6.1b) only. The applicability of the proposed simplified method for other wind models is checked in this section. The main purpose of the validation is to check the nature of the graphs between hub load and torque vs. turbulence intensity.

A number of simulations are performed to verify the simplified aerodynamic models. The structural dimensions obtained from the detailed design during the case study are used for the simulations. Due to the time constraint the simulations are only performed for the rated wind speed for all design situations except for parked/idling conditions. For parked/idling conditions, the wind speed is selected based on the DLC. An appropriate wave height, current speed and water levels are selected based on the DLC. For EOG, the gust speed is taken equal to 10m/s.

For DLC 1.3 and 1.1 only turbulence intensity value differs other parameters are same. As simulations are performed for the turbulence intensity variation, no separate simulations are performed for DLC 1.3 and 1.1. Out of DLC 2.1 and 2.2, only DLC 2.1 is performed to check the validity during the fault condition. For parked/idling condition DLC 6.1b, 6.1c and performed to check the EWM and RWM models. The DLC 6.2b and 6.3b are performed to check the applicability during the fault condition and extreme yaw misalignment respectively. The inputs and graphs of the simulations are given in Appendix B.

From simulations it is observed that only for the EWS, hub load vs.turbulence intensity follows a polynomial curve, others follow a straight line. In EWS model, for first 12 seconds the transient wind speed is used after that the normal wind shear profile (Eq. 4.13)is followed. The transient wind speed difference between top and bottom of the rotor increases with turbulence intensity. The hub load is proportional to square of the

wind speed. The increase in the transient wind speed with turbulence intensity makes the hub load vs turbulence intensity a polynomial curve of degree two.

For EDC, the IEC has specified the relation between direction change magnitude and turbulence intensity value [32]. Fig. 5.2 and 5.3 shows the results of the simulation when specified relation is used. The proposed method fails if the specified relation is used.

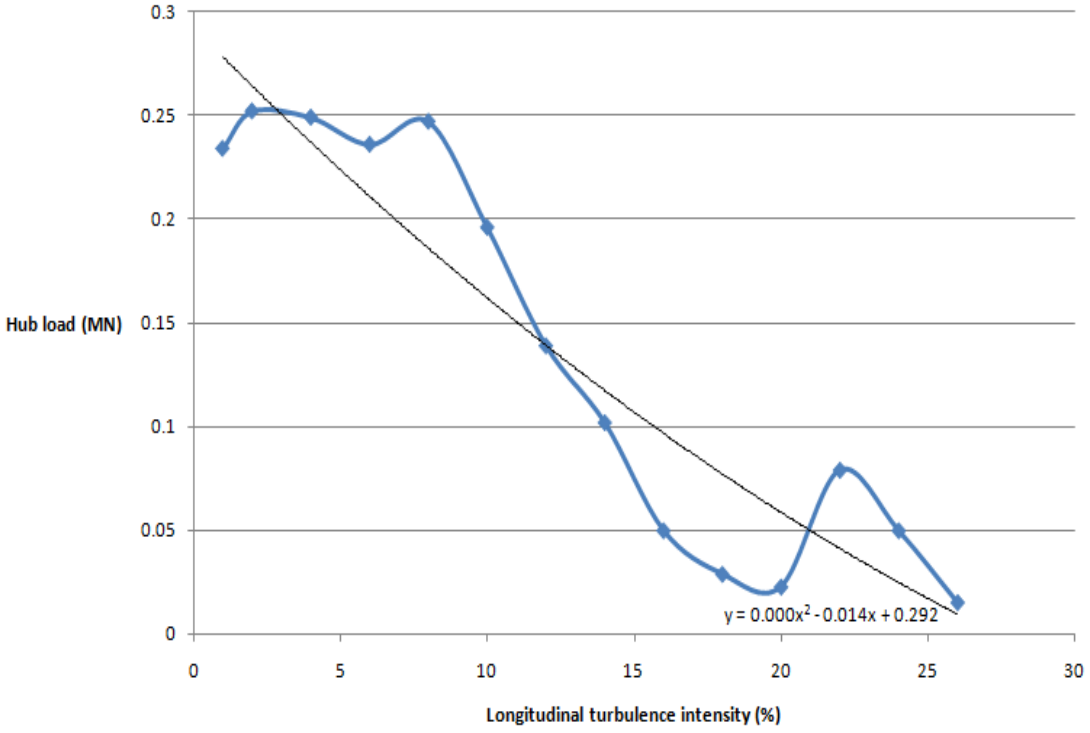

FIGURE 5.2: Hub load vs longitudinal turbulence intensity for DLC 3.3 with the use of specified IEC relation between direction change magnitude and turbulence intensity value.

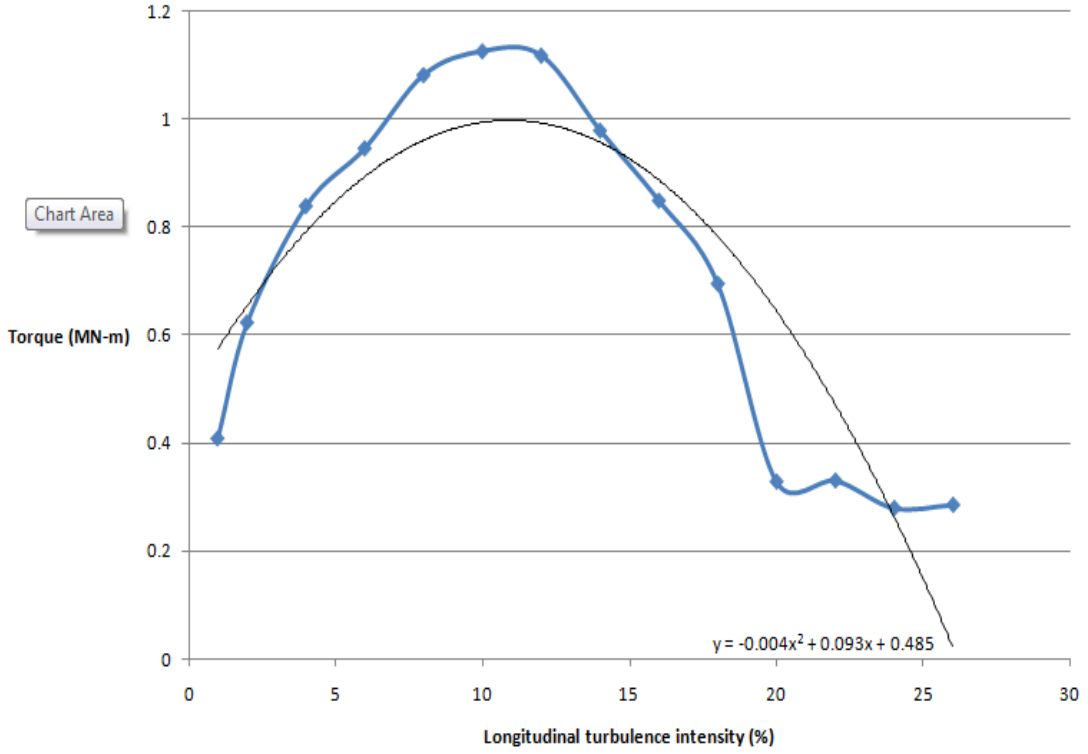

FIGURE 5.3: Torque vs longitudinal turbulence intensity for DLC 3.3 with the use of specified IEC relation between direction change magnitude and turbulence intensity value.

The DLC 3.3 uses the EDC model. The reason of failure is in the EDC model and DLC itself. The EDC model specifies to use the transient direction change for the first 6 seconds, starting from 0 degrees till the extreme direction change magnitude. After that, the direction change value remains constant for the rest of the time. The DLC 3.3 is for loads arising during the start up phase. For the transient situation during the start up, the loads depend upon the control system response to the wind speed direction change. The magnitude of direction change per second increases with turbulence intensity. This leads to lesser time for control system to adjust to new varying condition. The deviation from the ideal angle of attack increases with extreme direction change magnitude. This leads to lesser capture of energy and loads. The lateral force (hub load) is also related to cosine of the incoming flow angle. The cosine of the force decreases with increase in the extreme direction change. This results into the lower of hub loads with increased extreme direction change. The torque depends upon the lateral force and lateral turbulence intensity. The lateral force decreases and lateral turbulence intensity increases with the longitudinal turbulence intensity. During

the initial period, the effect of turbulence intensity is greater than the lateral force but later, the decrease of lateral force dominated the torque outcome. For the EDC model, the extreme direction change magnitude should be kept constant so as to apply the proposed simplified method.

For EOG, the IEC has specified a relation between the gust speed and turbulence intensity [32]. The proposed method does not address the simplification for the variation in the gust speed. The proposed method is applicable as long as the gust speed is equal between the reference location and new location.

For ECD, the IEC does not consider the variation in the turbulence in tensity. For ECD and EOG models, a designer has to give turbulence intensity value equal to zero in the design tool and y-intercept equal to the reference location load.

Chapter 6

Conclusion and Recommendations

6.1 Conclusion

The aim of the thesis is to develop a simplified design method to design multiple support structures tailored to their local environment within a wind farm by using data of the detailed design of the reference location. For this study an existing Python based design tool is improved. Previous work [15] is used as a reference and starting point. This tool designs the support structure based on the natural frequency, yielding and buckling constraints. The design tool has integrated the hydrodynamic, aerodynamic, soil and structural stability models based on GL, IEC, API and DNV design standards.

The hub load, torque, correction factors and dominant design drivers and their values are obtained from the reference location design. The tool calculates the dimensions of the support structure for the dominant design drivers using simplified models. The dimensions are then multiplied by correction factors to get the final dimensions of the support structures. The case study is performed to check the validity of the the simplified design process. In the case study various environmental parameters are varied. From the case study it is observed that for offshore wind support structures natural frequency and local buckling are the main design drivers. The lateral stability governs the penetration length calculation. The grout length is decided by the DNV standard suggestion. Among various environmental parameters the turbulence intensity, water

depth and soil properties have the most dominating impact on the support structure dimensions variation within a wind farm.

The proposed simplified method to design multiple support structures within an offshore wind farm is useful and feasible. The implemented simplified models and use of correction factor method are acceptable. The support structure design process can be separated based on design divers, natural frequency, yielding, torsional, local and global buckling. The support structure need not to be checked for each design driver. Depending on the design driver at the reference location, other support structures within a wind farm can safely be designed using only the same dominant design drivers without posing any risk to the structural integrity. However for wind farms with extreme variation in environmental parameters such as soil properties or turbulence intensity this approach may not yield successful results. The best reference location is a site with an intermediate water depth, soil properties and turbulence intensity. If such site does not exist then an engineering judgment should be used to decide which one among the water depth, turbulence intensity and soil properties variation would have the major impact on the support structure dimensions variation and based on that a reference site should be selected.

A designer should be careful while applying the simplified method for Extreme direction change (EDC) and Extreme operating gust (EOG). For EDC, the variation in extreme direction change with turbulence intensity is not considered. For EOG, the gust speed variation is not considered. Therefore the simplified method is applicable as long as the gust speed and extreme direction change is equal between the reference and new design location.

The accuracy of the results of the simplified design process are sufficient to support the principle of the simplified design process. The absolute accuracy of the simplified design process is in the range of 0-6%. The response of the simplified design process to changes in the environmental parameters is in accordance with expectations. Several environmental parameters have clear effect on the support structure dimensions. The magnitude of this effect depends on how these parameters affect the design drivers and correction factors. The wave height, current speed and wave period variation within a wind farm has very negligible effect on the support structure dimensions. There is no need to design support structure tailored to local wave height, current speed and wave

period if the natural frequency is the design driver for the monopile diameter. Within a wind farm, a combination of wave height, current and wave period should be selected which yields extreme loading and all support structures should be designed using this combination.

The simplified design process has various limitations. The clay model, fatigue constraint, Serviceability Limit State (SLS) and Accidental Limit State (ALS) are not implemented in this process. These limitations might hamper the applicability of the simplified design process. Further study is required to implement and analyze the effect of these methods on the the simplified design process. The error, this process might give when applied for the design of real support structures is still unknown. The accuracy of breaking wave loads on the structure is not validated.

6.2 Recommendations

By implementation of the efficient support structure design, it was shown that multiple support structures for the wind farm can be designed. However due to the time constrain a number of assumptions are made. To compensate for this a number of recommendations are made. The recommendations are divided into modelling and constraints.

Modelling:

- A simplified soil model for clay should be implemented [1]
- The future trend is towards deeper water depths for offshore wind farms. For deeper water depths multimember structures like jacket, tripod etc. starts to become more viable. These support structures should also be included in the design
- For this study optimization is not carried out for the whole structure. Optimization can further reduce the mass of the support structure
- The developed design tool can be applied in other support structures applications too [2]

[1] Author has already implemented clay model for natural frequency and axial stability calculation only lateral stability calculation needs to be improved.

[2] Author has already extended the use of the design tool for offshore substation and onshore wind support structures design.

Constraints:

- This thesis recommends to design and employ support structures based on a location within a wind farm to reduce the LPC. But the effect of single versus multiple assembly line on the cost of manufacturing, installation and transportation was not studied. It is important to include cost analysis as the objective function
- For this study the fatigue damage constraint is not included. Fatigue can influence the dimensions of the support structure
- The natural frequency constraint should be improved to include the effect of vortex formation and its effect on structural stability

Appendix A

Inputs for case study

A.1 Wind farm data for reference design

Environmental parameters		
parameter	value	unit
Reference wind speed height	74	[m]
Gust speed	10.0	[m/s]
50 year extreme wind speed	25.2	[m/s]
alpha	0.14	[-]
Turbulence intensity	10	[%]
DLC	6.12	[-]
Water depth	20.0	[m]
HAT	2.14	[m]
LAT	-1.78	[m]
positive storm surge	1.93	[m]
negative storm surge	-1.16	[m]
50 year extreme wave height	8.8	[m]
Wave period	10.0	[s]
Current speed	0.8	[m/s]
Angle between wave and lateral direction	30.0	[degree]
slope of Fx vs TI	0.127	[-]
slope of Mz vs TI	0.752	[-]
Y intercept of Fx	0.768	[MN]
Y intercept of Mz	3.663	[MN]

Soil parameters					
Soil layer	Submerged unit weight (kN/m^3)	Friction angle	flim (kPa)	qlim (MPa)	Nq
2.0	7.5	20.0	67.0	1.9	8
13.0	8.5	25.0	81.3	4.8	20
35.0	9.5	30.0	95.7	9.6	40
1000.0	9.5	35.0	114.8	12	50

A.2 Soil variation

A.2.1 Slight variation

Soil layer	Submerged unit weight (kN/m^3)	Friction angle	flim (kPa)	qlim (MPa)	Nq
2.0	8.5	25.0	81.3	4.8	20
13.0	7.5	28.0	88.5	7.2	30
35.0	9.0	25.0	81.3	4.8	20
1000.0	9.0	30.0	95.7	9.6	40

A.2.2 Very stiff

Soil layer	Submerged unit weight (kN/m^3)	Friction angle	flim (kPa)	qlim (MPa)	Nq
2.0	12.0	35.0	114.8	12.0	50
13.0	15.0	38.0	114.8	12.0	50
35.0	20.0	40.0	114.8	12.0	50
1000.0	22.0	40.0	114.8	12.0	50

A.2.3 Very soft

Soil layer	Submerged unit weight (kN/m^3)	Friction angle	flim (kPa)	qlim (MPa)	Nq
2.0	5.0	20.0	67.0	1.9	8
13.0	5.5	22.0	114.8	12.0	50
35.0	6.0	22.0	114.8	12.0	50
1000.0	6.5	25.0	81.3	4.8	20

A.3 Everything change

Environmental parameters		
parameter	value	unit
Turbulence intensity	8	[%]
DLC	6.12	[-]
Water depth	25.0	[m]
50 year extreme wave height	9.3	[m]
Wave period	10.7	[s]
Current speed	0.86	[m/s]

Soil parameters					
Soil layer	Submerged unit weight (kN/m^3)	Friction angle	flim (kPa)	qlim (MPa)	Nq
2.0	8.0	22.0	67.0	1.9	8
8.0	8.8	27.0	88.5	7.2	30
24.0	9.3	26.0	81.3	4.8	20
1000.0	9.7	32.0	105.2	10.8	45

Appendix B

Simulation results

B.1 Power production

B.1.1 DLC 1.1 and 1.3

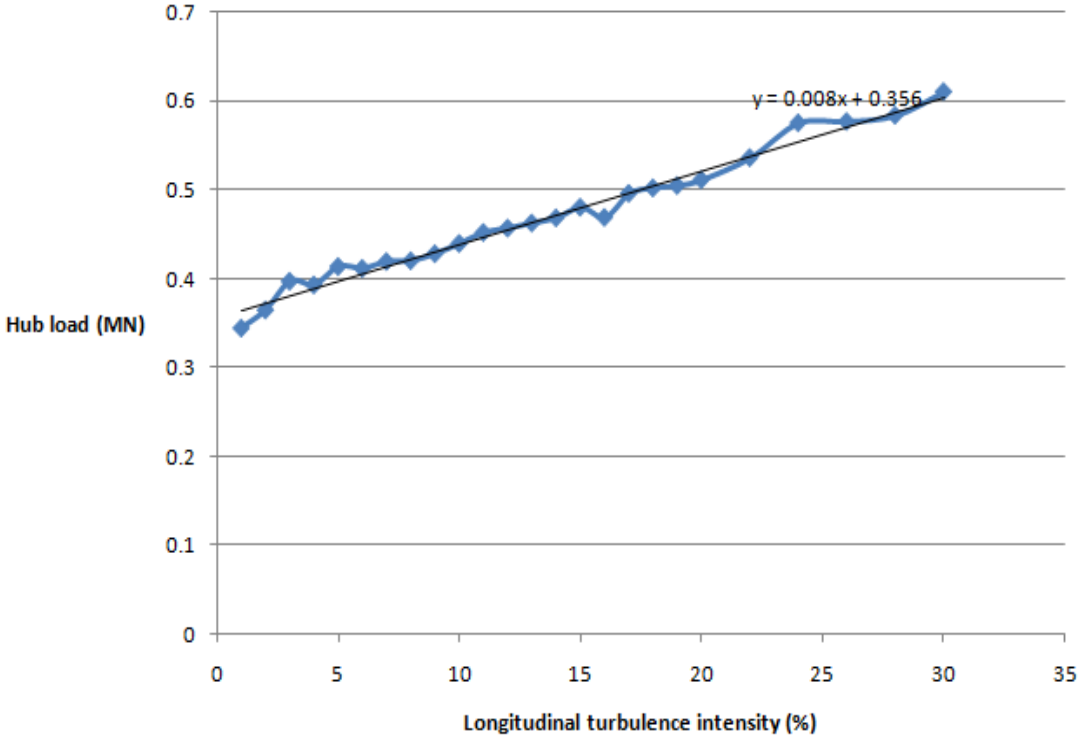

FIGURE B.1: Hub load vs longitudinal turbulence intensity for 20m water depth for DLC 1.1 and 1.3.

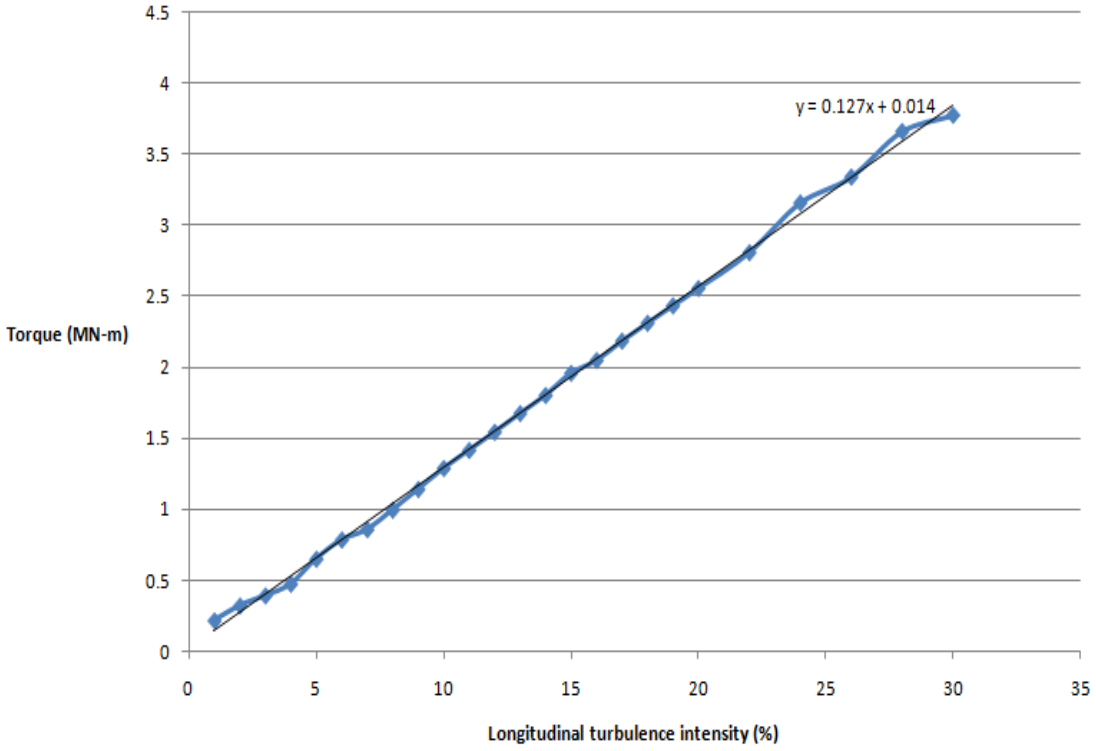

FIGURE B.2: Torque vs longitudinal turbulence intensity measured at hub height for 20m water depth for DLC 1.1 and 1.3.

B.1.2 DLC 1.4

TABLE B.1: The hub and torque load measured at hub height for DLC 1.4 (ECD model).

Parameter	10m	20m (reference location)	30m	40m
Hub load (MN)	0.401	0.403	0.397	0.398
Torque (MN-m)	1.638	1.632	1.632	1.641

B.1.3 DLC 1.5

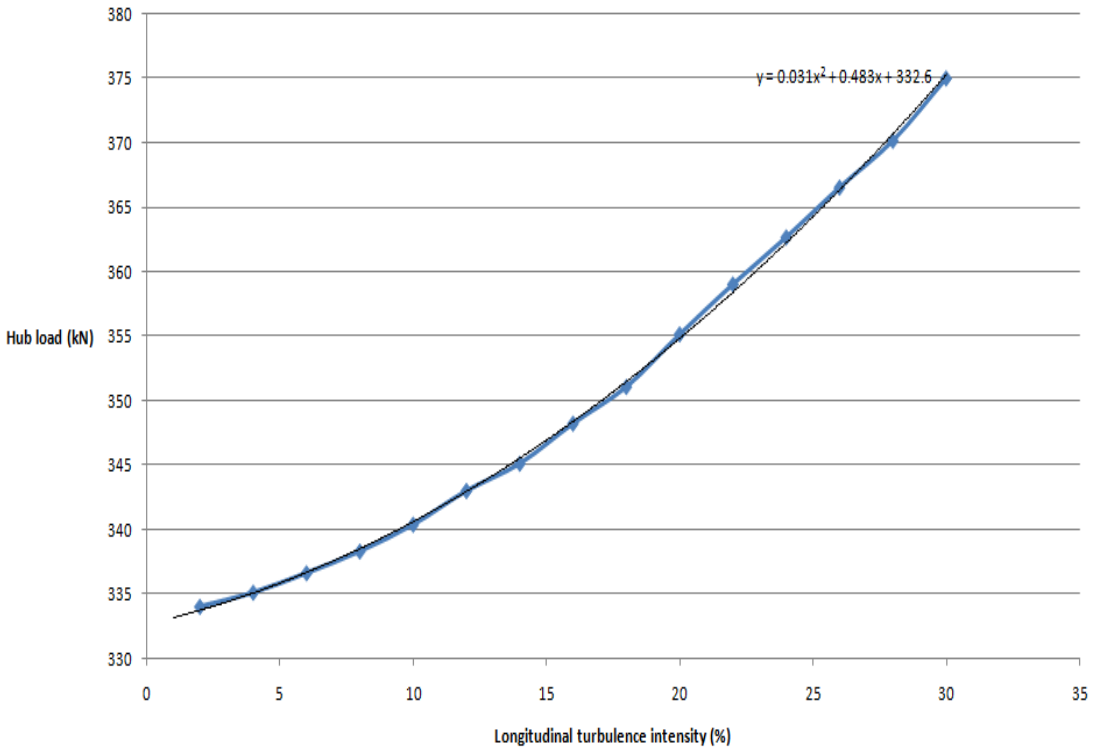

FIGURE B.3: Hub load vs longitudinal turbulence intensity for 20m water depth for DLC 1.5 (EWS model).

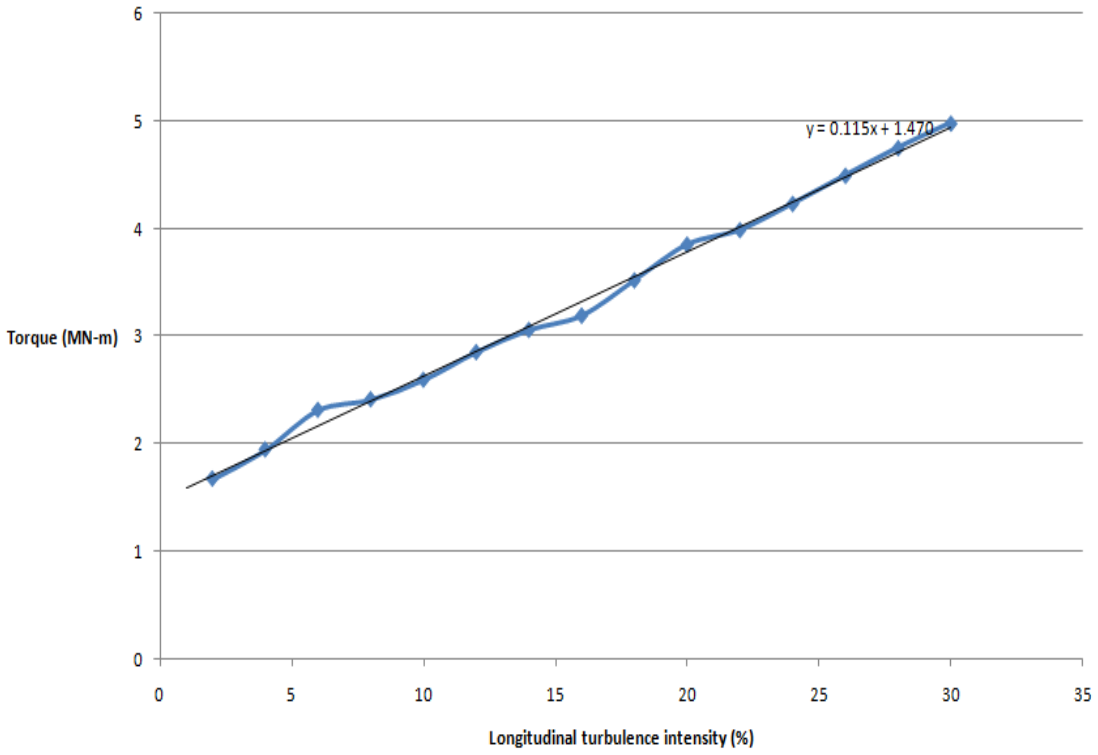

FIGURE B.4: Torque vs longitudinal turbulence intensity measured at hub height for 20m water depth during for DLC 1.5 (EWS model).

B.1.4 DLC 1.6b

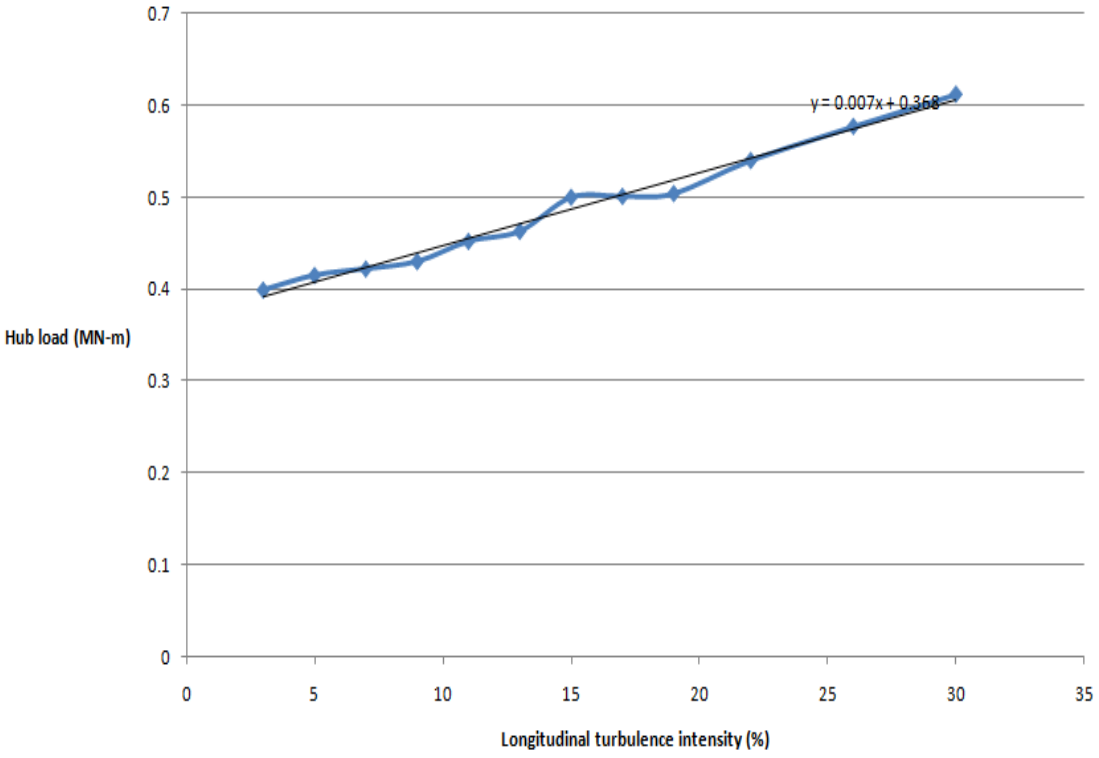

FIGURE B.5: Hub load vs longitudinal turbulence intensity for 20m water depth for DLC 1.6b.

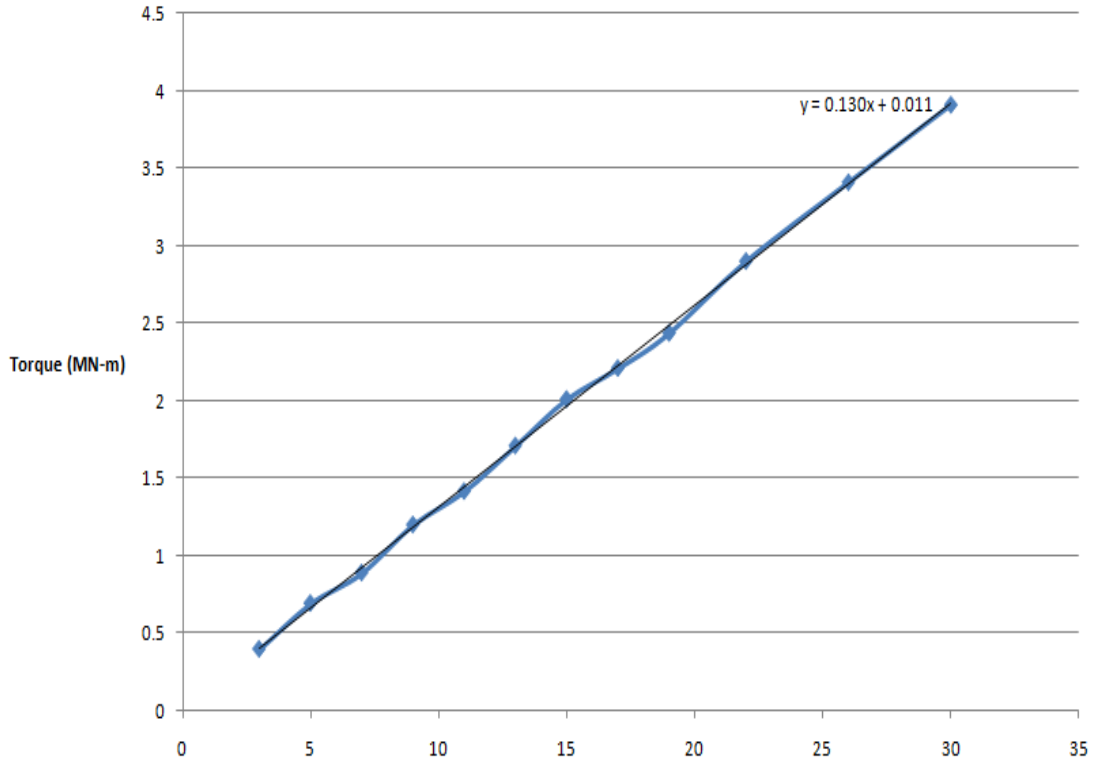

FIGURE B.6: Torque vs longitudinal turbulence intensity measured at hub height for 20m water depth for DLC 1.6b.

B.2 Power production plus occurrence of fault

B.2.1 DLC 2.1

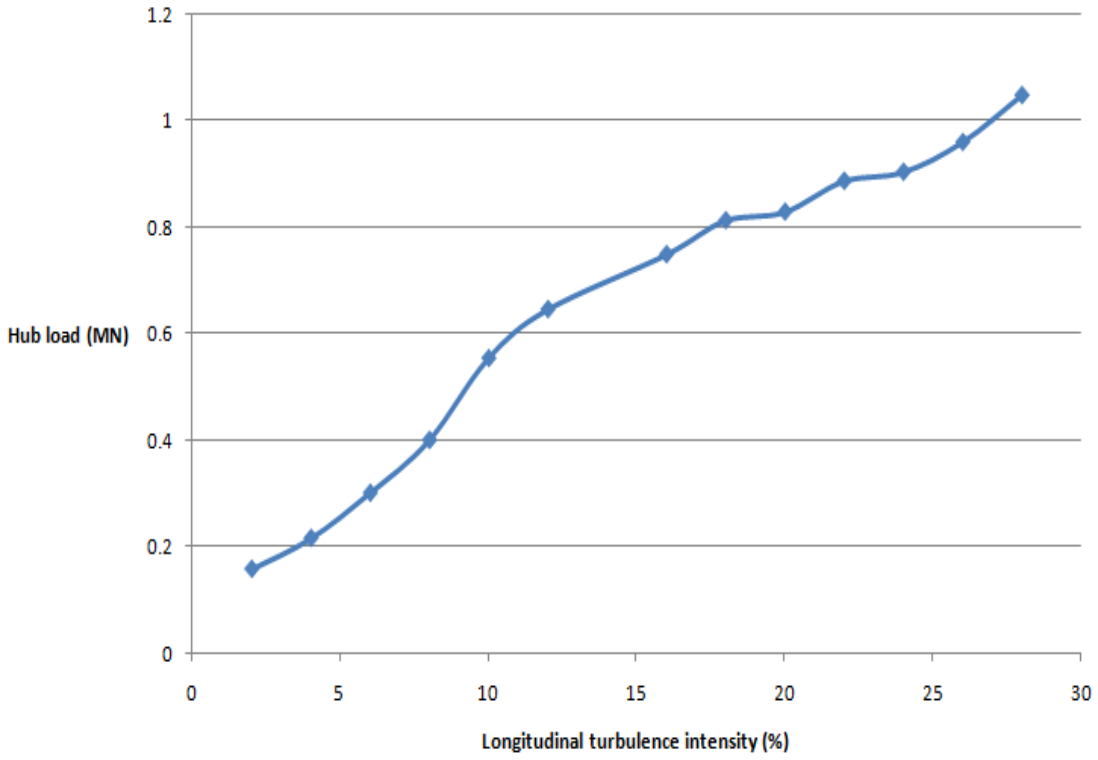

FIGURE B.7: Hub load vs longitudinal turbulence intensity for 20m water depth for DLC 2.1.

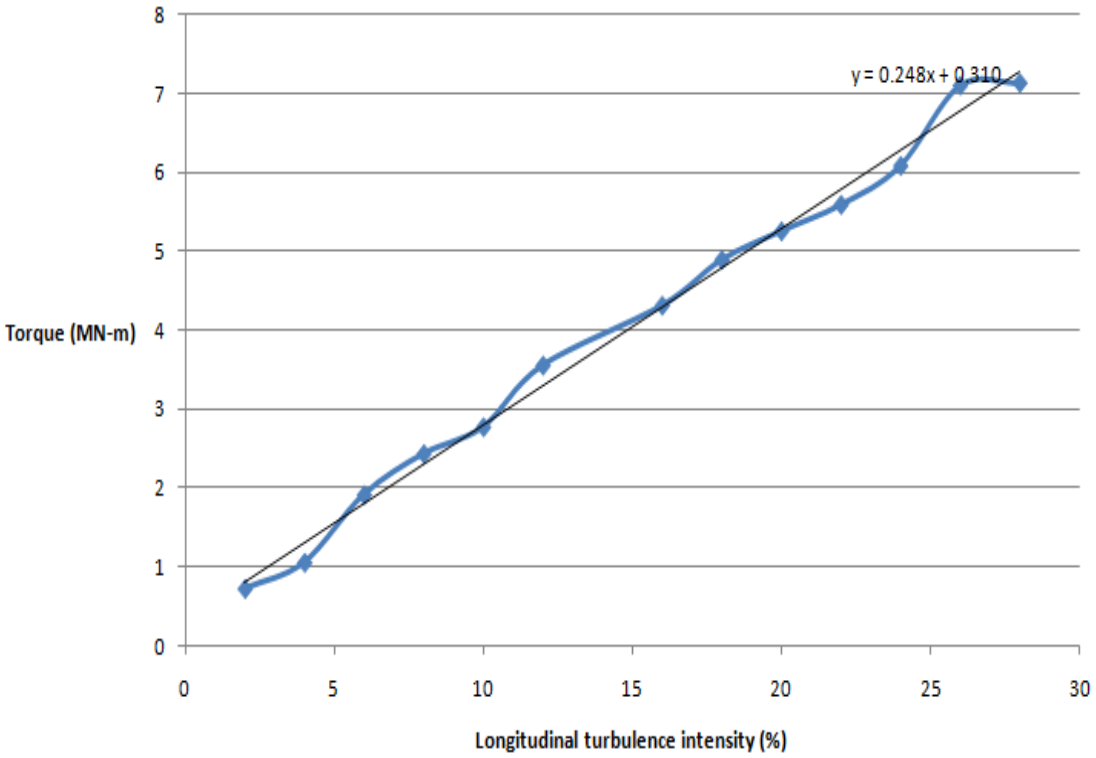

FIGURE B.8: Torque vs longitudinal turbulence intensity measured at hub height for 20m water depth for DLC 2.1.

B.2.2 DLC 2.3

TABLE B.2: The hub and torque load measured at hub height for DLC 2.3 (EOG model).

Parameter	10m	20m (reference location)	30m	40m
Hub load (MN)	0.86603	0.86604	0.86616	0.86620
Torque (MN-m)	0.9	0.9	0.89	0.89

B.3 Start up

B.3.1 DLC 3.2

TABLE B.3: The hub and torque load measured at hub height for DLC 3.2 (EOG model).

Parameter	10m	20m (reference location)	30m	40m
Hub load (MN)	0.501	0.498	0.495	0.496
Torque (MN-m)	0.301	0.302	0.303	0.303

B.4 Normal shut down

B.4.1 DLC 4.2

TABLE B.4: The hub and torque load measured at hub height for DLC 4.2 (EOG model).

Parameter	10m	20m (reference location)	30m	40m
Hub load (MN)	0.581	0.583	0.581	0.583
Torque (MN-m)	0.409	0.408	0.408	0.408

B.5 Emergency shut down

B.5.1 DLC 5.1b

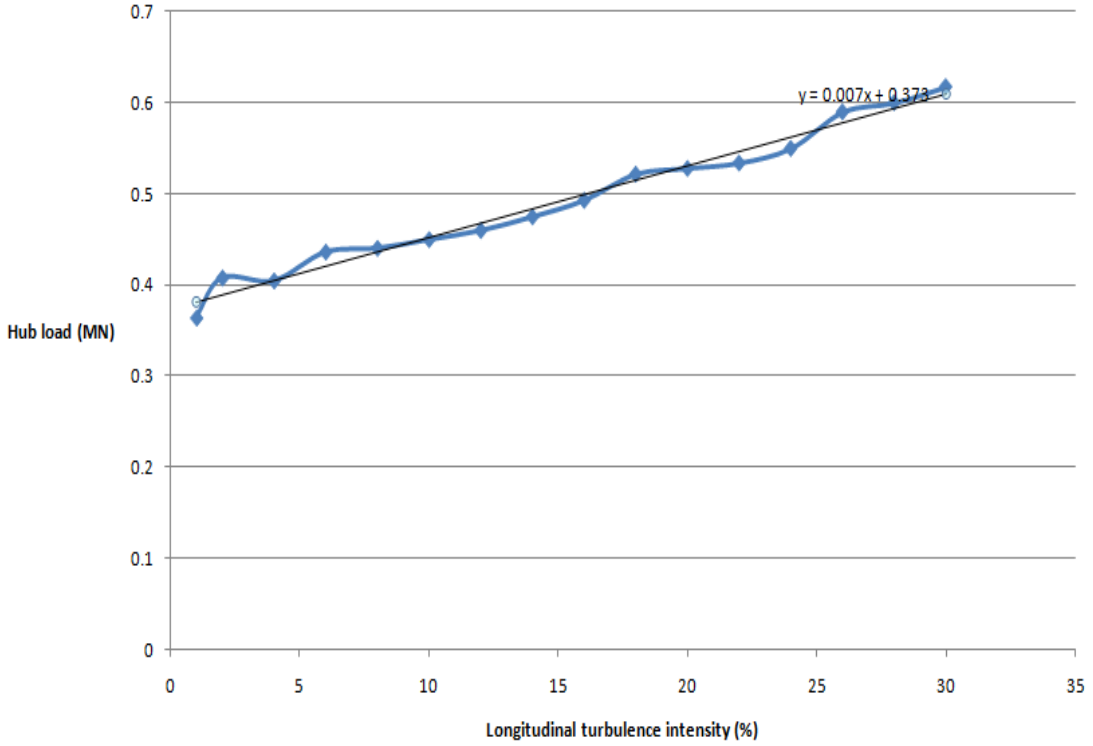

FIGURE B.9: Hub load vs longitudinal turbulence intensity for 20m water depth for DLC 5.1.

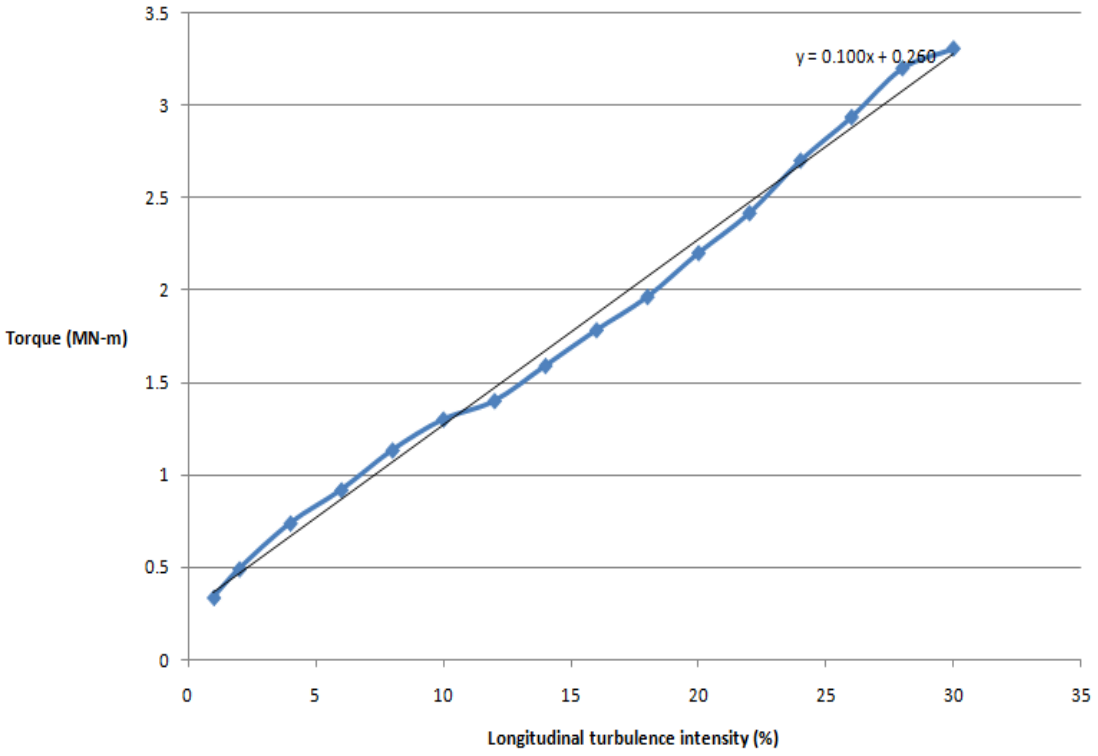

FIGURE B.10: Torque vs longitudinal turbulence intensity measured at hub height for 20m water depth for DLC 5.1.

B.6 Parked or idling

B.6.1 DLC 6.1b

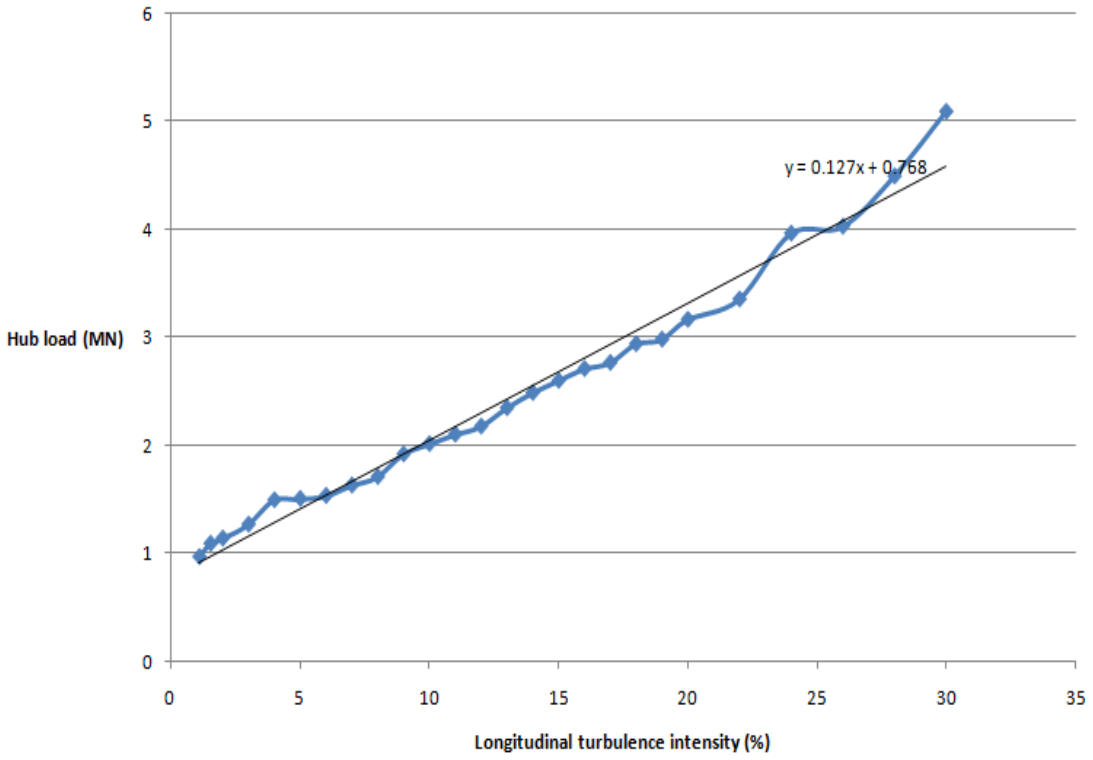

FIGURE B.11: Hub load vs longitudinal turbulence intensity for 20m water depth for DLC 6.1b.

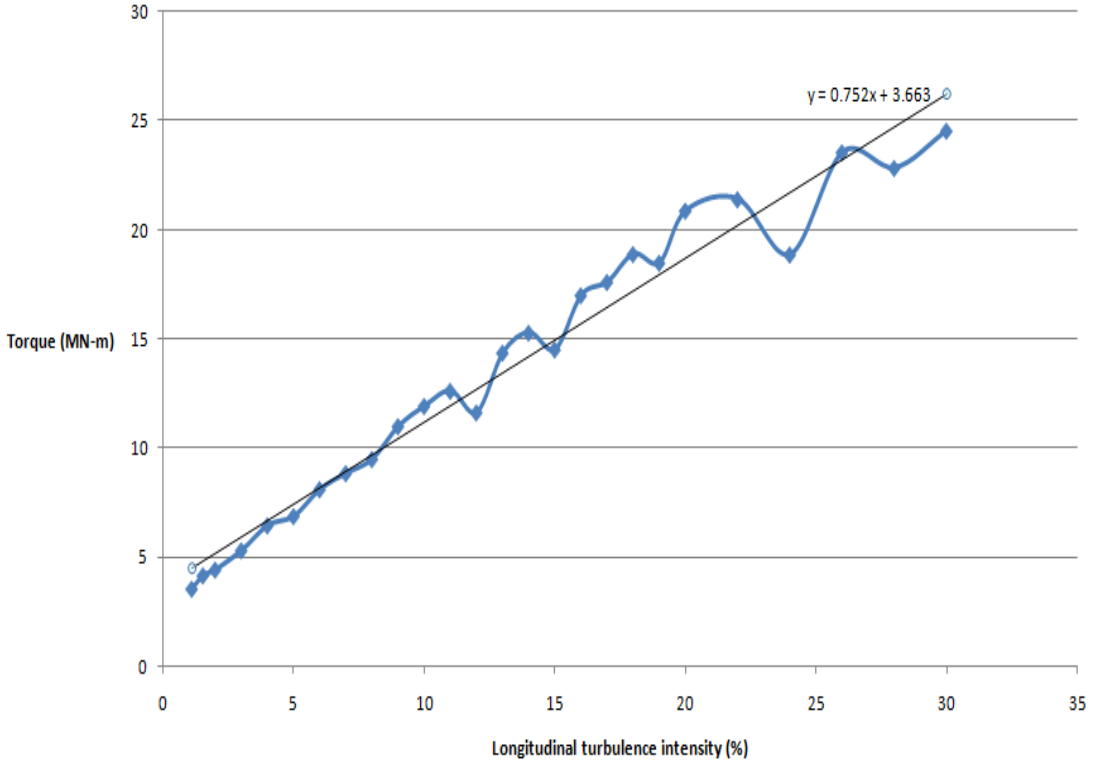

FIGURE B.12: Torque vs longitudinal turbulence intensity measured at hub height for 20m water depth for DLC 6.1b.

B.6.2 DLC 6.1c

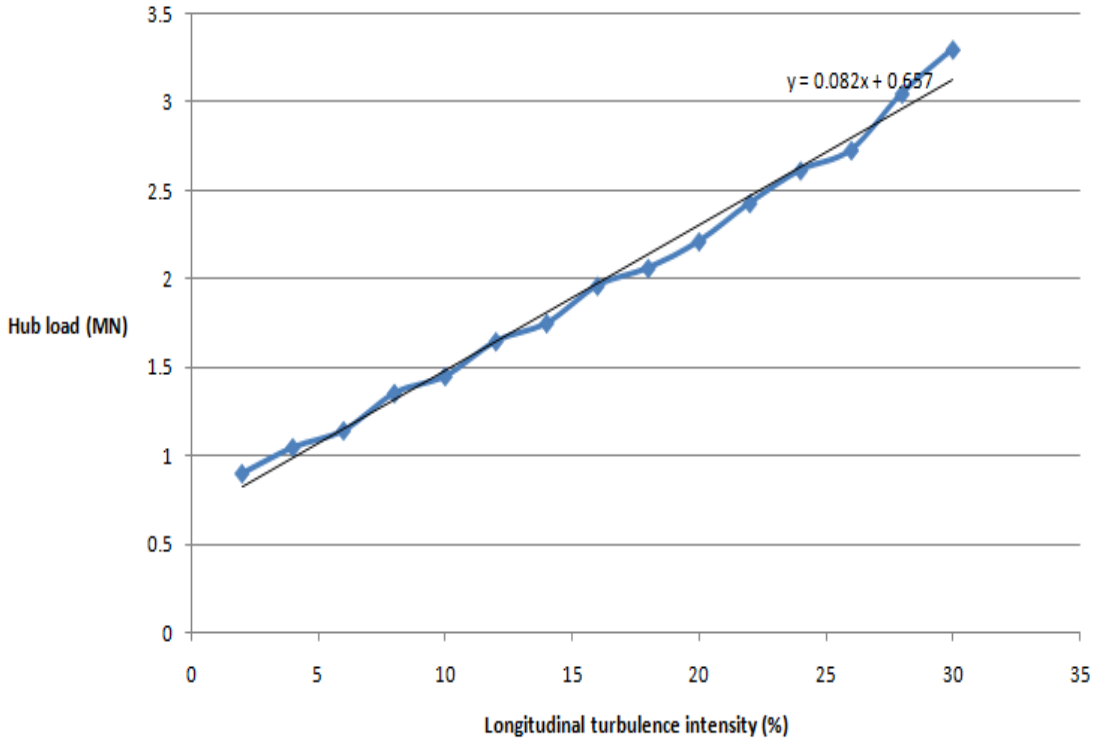

FIGURE B.13: Hub load vs longitudinal turbulence intensity for 20m water depth for DLC 6.1c.

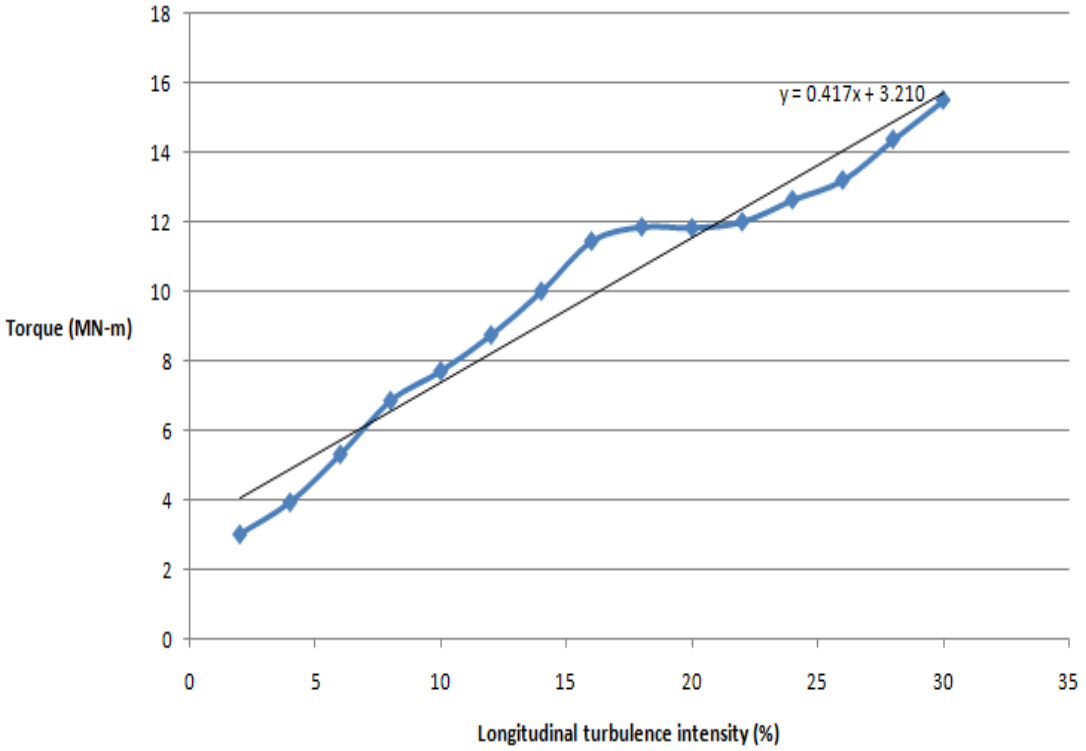

FIGURE B.14: Torque vs longitudinal turbulence intensity measured at hub height for 20m water depth for DLC 6.1c.

B.6.3 DLC 6.2b

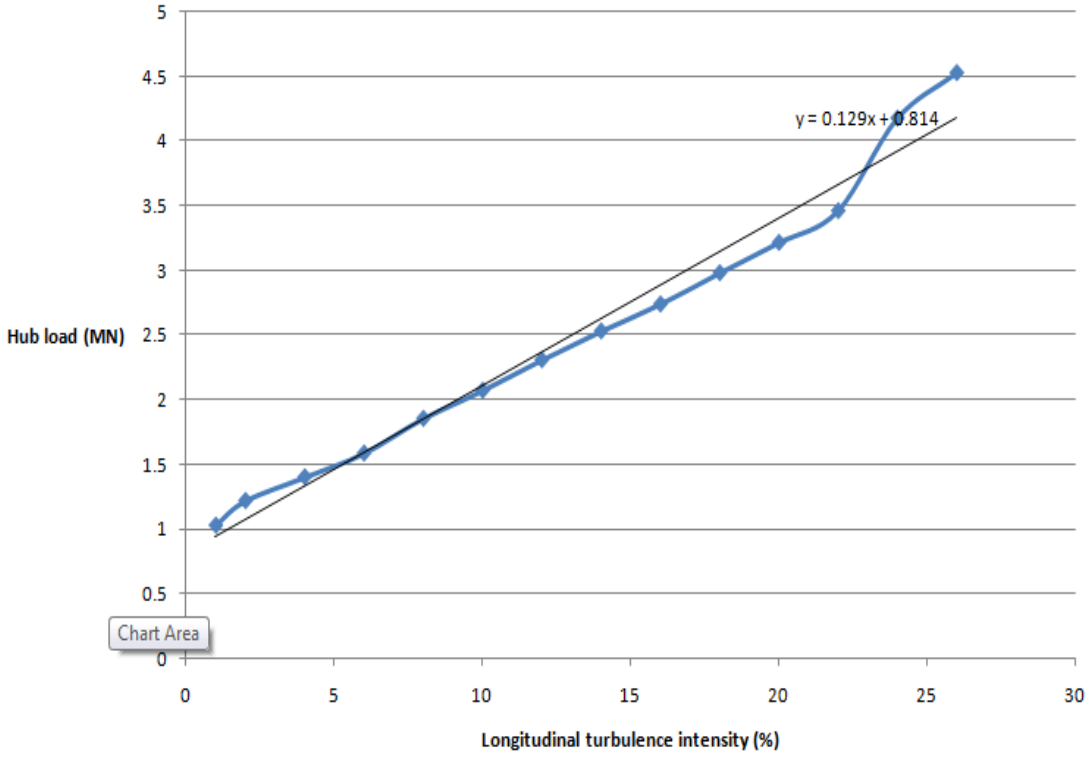

FIGURE B.15: Hub load vs longitudinal turbulence intensity for 20m water depth for DLC 6.2b.

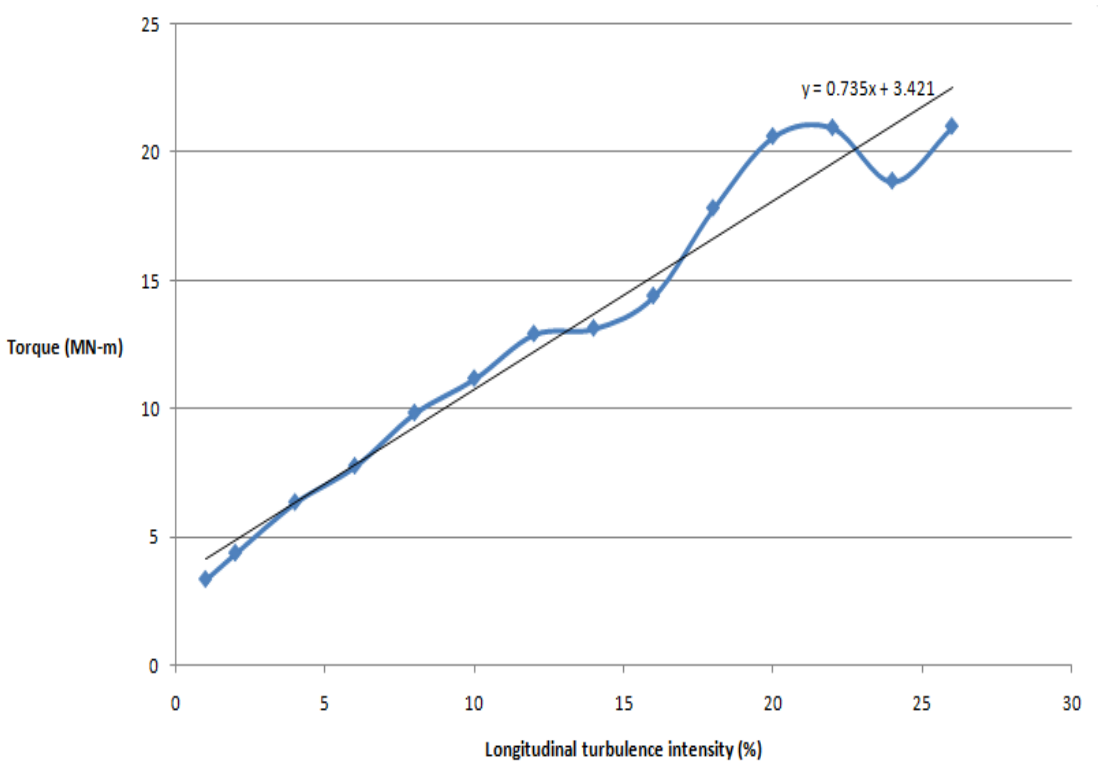

FIGURE B.16: Torque vs longitudinal turbulence intensity measured at hub height for 20m water depth for DLC 6.2b.

B.6.4 DLC 6.3b

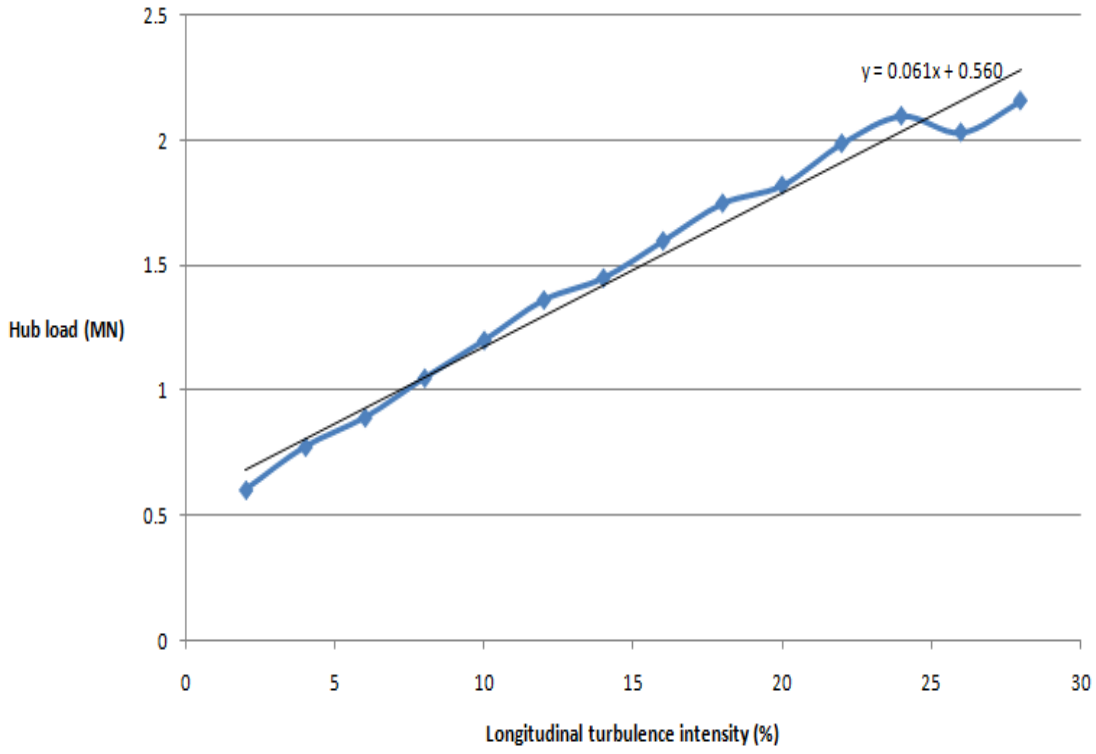

FIGURE B.17: Hub load vs longitudinal turbulence intensity for 20m water depth for DLC 6.3b

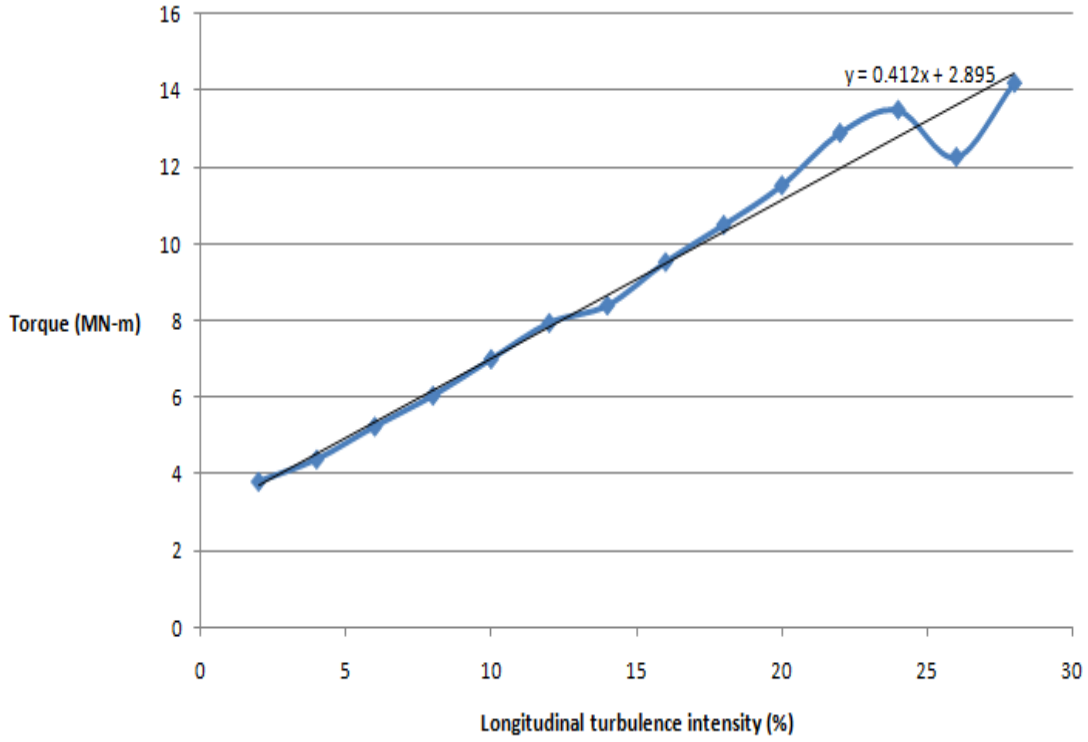

FIGURE B.18: Torque vs longitudinal turbulence intensity measured at hub height for 20m water depth for DLC 6.3b.

Bibliography

[1] European Wind Energy Association. *Wind in our Sails, The coming of Europe's offshore wind energy industry.* EWEA, Brussels, Belgium, 2011.

[2] Antonio Jarquin Laguna. Offshore wind farm design, 2013. Lecture notes.

[3] UK EnergyResearch Centre. *Great Expectations: The cost of offshore wind in UK waters understanding the past and projecting the future.* UK EnergyResearch Centre (UKERC), London, United Kingdom, 2010.

[4] Jan Van Der Tempel. Design of support structures for offshore wind turbines. Phd thesis, Delft University of Technology, 2006.

[5] Maxim Segeren. Offshore wind support structures, 2013. Lecture notes.

[6] American Petroleum Institute. Recommended Practice for Planning, Designing and Constructing Fixed Offshore Platforms—Working Stress Design, 2002. API RECOMMENDED PRACTICE 2A-WSD (RP 2A-WSD).

[7] Rad Haghi. Integrated design and optimization of an offshore wind turbine monosile support structure. Master thesis, Delft University of Technology, April 2011.

[8] World Coal Association. Fossil fuels reserves. http://www.worldcoal.org/coal/where-is-coal-found/, 2014. [Online; accessed 13-March-2014].

[9] USA office of energy efficiency and renewable energy. History of wind enegry. http://energy.gov/eere/wind/history-wind-energy, 2014. [Online; accessed 13-March-2014].

[10] Global Wind Energy Council. *Global Wind Report.* GWEC, Brussels, Belgium, 2012.

[11] European Wind Energy Association. *Pure Power Wind energy targets for 2020 and 2030.* EWEA, Brussels, Belgium, 2011.

[12] European Wind Energy Association. *Deep Water: The next step for offshore wind energy.* EWEA, Brussels, Belgium, 2013.

[13] Germanischer Lloyd. Rules and Guidelines: Guideline for the Certification of Offshore Wind Turbines , July 2004.

[14] 4Coffshore. http://www.4coffshore.com/index.html. Last visited 13/6/2014.

[15] M.B. Zaaijer. "Great expectations for offshore wind turbines. Emulation of wind farm design to anticipate their value for customers" PhD Thesis. Delft University of Technology.

[16] W.E. de Vries and V.D. Krolis. Effects of deep water on monopile support structures for offshore wind turbines, 2007. Proceedings of the European Wind Energy Conference and Exhibition.

[17] J. Wolfram. The Effect of Marine Growth on Vortex Shedding and Fatigue Life of Tubular Members. International Offshore and Polar Engineering Conference, Edinburgh, U.K., 1991.

[18] Jan van der Tempel and David-Pieter Molenaar. Wind Turbine Structural Dynamics – A Review of the Principles for Modern Power Generation, onshore and Offshore, 2002. Wind Engineering volume 26, No. 4, pp211-220.

[19] Nando Timmer and Michiel Zaayer. Introduction to Wind Energy, 2012. Lecture notes.

[20] Patrick Holmes. Coastal Infrastructure Design, Constructuion and Maintenance. Imperial College London.

[21] J.M.J. Journee and W.W. Massie. Offshore Hydromechanics First edition, January 2001. Delft University of Technology.

[22] Anders Wedel Nielsen, Jacob V. Tornfeldt Sørensen, Flemming Schlütter, Henrik Bredmose. WAVE LOADS ON A MONOPILE IN 3D WAVES.Proceedings of the ASME 2012 31st International Conference on Ocean, Offshore and Arctic Engineering OMAE2012 July 1-6, 2012, Rio de Janeiro, Brazil.

[23] Prof. P. Schaumann, C. Böker, ForWind – Center for Wind Energy Research Institute for Steel Construction, Leibniz University of Hannover. Influence of Wave Spreading in Short-term Sea States on the Fatigue of Offshore Support Structures at the Example of the FINO1-Research Platform.

[24] International Organization for Standardization. ISO (19901-1) Petroleum and natural gas industries — Specific requirements for offshore structures — Part 1: Metocean design and operating considerations International Organization for Standardization, Geneva, Switzerland , 2005.

[25] Ove T. Gudmestad and Geir Moe. "Hydrodynamic Coefficients for Calculation of Hydrodynamic Loads on Offshore Truss Structures." Marine Structures 9 (1996) 745-758, 0951 -8339(95)00023-2. Statoil A/S, Forus, N-4035, Stavanger, Norway NTH, Trondheim, Norway.

[26] . J. D. Fenton. Nonlinear Wave Theories. Department of Civil Engineering, University of Auckland, Private Bag, Auckland, New Zealand. The Sea, Vol.9: Ocean Engineering Science.

[27] V. Magar, M.S. Gross, D. Mouaze. Laboratory-Scale Environmental Impact Assessment of a Monopile Foundation under Different Wave Conditions. University of Le Havre, France, University of Cambridge, UK.

[28] M.B. Zaaijer, J. van der Tempel and H. Subroto. "The effects of Scour on the design of Offshore Wind Turbines". Delft University of Technology.

[29] Wim Bierbooms. Site conditions for wind turbine design, 2013. Lecture notes.

[30] V. Terzija F. Gonzalez-Longatt, P.Wall. Wake effect in wind farm performance: Steady-state and dynamic behaviour, 2011. School of Electrical and Electronic Engineering, The University of Manchester .

[31] Carlos Simao Ferreira Gerard van Bussel. Rotor Aerodynamics, 2013. Lecture notes .

[32] International Electrotechnical Commission. IEC 61400-1: Wind turbines part 1: Design Requirements, August 2006.

[33] E A Bossanyi. GH Bladed Theory Manual, September 2007.

[34] Ismail B. Celik. Introductory Turbulence Modeling, December 1999.

[35] Tao Han. The assesment of dynamic wake effects on loading. Master thesis, Delft University of Technology, Novemberl 2011.

[36] Budynas and Nisbett. Shigley's Mechanical Engineering Design, 8th edition 2007. McGraw Hill Education, ISBN: 0-390-76487-6.

[37] Chai H. Yoo and Sung C Lee. Stability of Structures Principles and applications. ISBN: 978-0-12-385122-2.

[38] Raines, R. D., Ugaz, O., and O'Neill, M. (1992). "Driving characteristics of open toe piles in sand." J. Geotech. Eng., 118(1), 72–88.

[39] Feng Yu, Jun Yang. "Base Capacity of Open-Ended Steel Pipe Piles in Sand." DOI: 10.1061/(ASCE)GT.1943-5606.0000667. © 2012 American Society of Civil Engineers.

[40] Paikowsky, S. G., and Whitman, R. V. (1990). "The effect of plugging on pile performance and design." Can. Geotech. J., 27(4), 429–440.

[41] . DNV. JOINT INDUSTRY PROJECT. SUMMARY REPORT FROM THE JIP ON THE CAPACITY OF GROUTED CONNECTIONS IN OFFSHORE WIND TURBINE STRUCTURES. REPORT NO. 2010-1053 REVISION NO. 05.

[42] . Marcus Klose, Marc Mittelstaedt andAmol Mulve. Grouted Connections – Offshore Standards Driven by the Wind Industry. Germanischer Lloyd Industrial Services GmbH - Competence Centre Renewables Certification, Hamburg, Germany.

[43] Dick Veldkamp. Chances in wind energy, a probabilistic approach to wind turbine fatigue design. Phd thesis, Delft University of Technology, 2006.

[44] . Richard Pijpers. Fatigue, lecture notes, 2014. Delft University of Technology.

[45] . René Alderliesten. Fatigue of Structures and Materials, lecture notes, 2013. Delft University of Technology.

[46] Jaap Schijive. Fatigue of Structures and Materials, 2nd edition 2001. Kluwer academic publishers, ISBN-0-7923-7013-9.

[47] . Brent method python application. "http://docs.scipy.org/doc/scipy/reference/generated/scipy.optimize.brentq.html". Last visited 22 March 2014.

[48] . Brent theory. "http://www.uam.es/personal_pdi/ciencias/ppou/CNC/TEMA6/f10.pdf". Last visited 22 March 2014.

[49] . Brent method. "http://users.wpi.edu/~walker/MA3257/HANDOUTS/brents_algm.pdf". Last visited 22 March 2014.

[50] . Peter Schaumann, Fabian Wilke, Stephan Lochte-Holtgreven. "Nonlinear Structural Dynamics of Offshore Wind Energy Converters with Grouted Transition Piece." Leibniz Universität Hannover.

[51] . R. L. WIEGEL. "A presentation of cnoidal wave theory for practical application." Department of Engineering, University of California, Berkeley.

[52] . John D. Fenton. "The Cnoidal Theory of Water Waves." Chapter 2 of Developments in Offshore Engineering.

[53] Harald E. Krogstad and Øivind A. Arntsen. Linear wave theory Part A, February 2000. Norwegian University Science and Technology, Tronndheim.

[54] International Electrotechnical Commission. IEC 61400-3: Wind Turbines Part 3: Design requirements for offshore wind turbines , July 2007.

[55] Rene Huijsmans Peter Naaijen and Sape Miedema. Offshore Hydrodynamics, 2014. Lecture notes.

[56] Jan Westphalen Extreme Wave Loading on Offshore Wave Energy Devices using CFD. PhD Thesis University of Plymouth June 2011.

[57] PM. Breaking waves Hagemeijer and wave forces in shallow water: a review Koninklijke/Shell Exploratie en Produktie Laboratorium 1985.

[58] . KAI IRSCHIK, UWE SPARBOOM, HOCINE OUMERACI. "BREAKING WAVE LOADS ON A SLENDER PILE IN SHALLOW WATER." Proc. 29th Int. Conf. Coastal Eng. (ICCE 2004), ASCE, Lisbon.

[59] Giovanni Cuomo, William Allsop, Tom Bruce, Jonathan Pearson. Breaking wave loads at vertical seawalls and breakwaters. Published in Coastal Engineering, 57 (4), (2010).

[60] . Thomas Lykke Andersen and Peter Frigaard. "LECTURE NOTES FOR THE COURSE IN WATER WAVE MECHANICS." Aalborg University Department of Civil Engineering Water and Soil.

[61] . P.K. Stansby, L.C. Devaney, T.J. Stallard. "Breaking wave loads on monopiles for offshore wind turbines and estimation of extreme overturning moment." IET Journal of Renewable Power Generation 2013, 7(5), 514-520.

[62] . J. Wienke, H. Oumeraci. "Breaking wave impact force on a vertical and inclined slender pile—theoretical and large-scale model investigations." Coastal Engineering 52 (2005) 435– 462.

[63] DNV-OS-J101. Dsign of offshore wind turbine structures, October 2007.

[64] A. Labuschagne, N.F.J. van Rensburg and A.J. van der Merwe. Comparison of linear beam theories. Mathematical and Computer Modelling Volume 49, Issues 1–2, January 2009, Pages 20–30.

[65] Prof. Devdas Menon. Lecture notes of Advanced Structural Analysis. Department of Civil Engineering, Indian Institute of Technology, Madras.

[66] . Suleyman Kocak and Yalcin Mengi. A simple soil-structure interaction model. Applied Mathematical Modelling 24, December 1999 pp 607-635.

[67] . H.J. Everts, A.Frits van Tol. Soil Structure Interaction, lecture notes, 2013. Delft University of Technology.

[68] . CASELUNGHE ARON and ERIKSSON JONAS. "Structural Element Approaches for Soil-Structure Interaction." Master Thesis CHALMERS UNIVERSITY OF TECHNOLOGY.

[69] . M. H. El Naggar and M. Novak. Nonlinear lateral interaction in pile dynamics.Soil Dynamics and Earthquake Engineering, 14(2), 1995.

[70] . Kerstin Lesny. Foundations for Offshore Wind Turbines Tools for Planning and Design. VGE, 2010.

[71] Daniel J. Rixen. Numerical methods in engineering dynamics, wb1416 lecture notes, 2011-2012. Delft University of Technology, Faculty 3mE.

[72] . J.A.T. Ruigrok. "Laterally Loaded Piles Models and Measurements." Master Thesis Delft University of Technology.

[73] Arnold Verruijt. "Laterally Loaded pile." Delft University of Technology.

[74] E.ON and EMU Ltd. Rampion Offshore Wind Farm Metocean Survey and Assessment, ES Section 6 – Physical Environment Appendix 6.2, December 2012.

[75] J.H. Vugts, J. van der Tempel and E.A. Schrama. HYDRODYNAMIC LOADING ON MONOTOWER SUPPORT STRUCTURES FOR PRELIMINARY DESIGN. Delft University of Technology.